The influence of vimentin on actin dynamics and force generation in RPE1 cells

Dissertation
zur Erlangung des Grades

des Doktors der Naturwissenschaften

der Naturwissenschaftlich-Technischen Fakultät
der Universität des Saarlandes

von

Zahra Mostajeran

Saarbrücken

2021

Tag des Kolloquiums:	30.04.2021
Dekan:	Prof. F. Lautenschläger
Berichterstatter:	Jun. Prof. L. Aradillazapata
Vorsitz:	Prof. Dr. A. Ott
Akad. Mitarbeiter:	Dr. I. Dahmke

Declaration of original authorship

I hereby declare that this dissertation is my own original work except where otherwise indicated. All data or concepts drawn directly or indirectly from other sources have been correctly acknowledged. This dissertation has not been submitted in its present or similar form to any other academic institution either in Germany or abroad for the award of any other degree.

---------- ----------

Place, Date Signature

ای نسخه ی نامه ی الهی که توئی وی آینه ی جمال شاهی که توئی

بیرون ز تو نیست هر چه در عالم هست در خود بطلب هر آنچه خواهی که توئی

(مولانا)

The universe is not outside of you, to achieve anything you want, seek inside yourself. Everything that you want you already are! (Molavi)

Abstract

The cytoskeleton is a network of filaments in cells, it consists of actin filaments, intermediate filaments and microtubules. It is very dynamic and plays a key role in many biological processes such as cell migration and cell division. Actin stress fibers are involved in force generation, cell retraction and cell protrusion during migration. The polymerization and depolymerization of actin filaments regulate cell migration and are influenced by the activity of actin binding proteins. Even though no motor molecules bind to vimentin, and it does not generate forces, its role is important in the regulation of cell migration. To better understand the mechanism of cell migration, it is important to understand how cytoskeleton filaments interplay. Therefore, understanding the role of vimentin on actin dynamics, and its implication in actin force generation are the two main interests of my Ph.D. thesis.

I first measure actin dynamics in vimentin depleted cells using fluorescence recovery after photobleaching. I show that silencing of vimentin expression slows down actin dynamics but does not affect the fraction of actin monomers that participate. In addition, I show that plectin as a vimentin-actin cross-linker protein does not have the same effect.

Finally, I study actin force generation using traction force microscopy. I show that silencing of vimentin disarranges the distribution of traction forces and adhesion sites but does not impact the magnitude of traction forces.

Kurzfassung

Das Zytoskelett ist ein Filamentnetzwerk in Zellen; es besteht aus Aktinfilamenten, Intermediärfilamenten und Mikrotubules. Es ist sehr dynamisch und spielt eine Schlüsselrolle in vielen biologischen Prozessen, wie Zellmigration und Zellteilung. Aktin-Stressfasern sind an der Krafterzeugung, Zell-Retraktion und Zell-Protrusion bei der Migration beteiligt. Die (De-)Polymerisierung von Aktinfilamenten reguliert die Zellmigration und wird durch die Aktivität von Aktin-Bindungsproteinen beeinflusst. Obwohl keine molekularen Motoren an Vimentin binden und es keine Kräfte erzeugt, spielt es eine wichtige Rolle für die Zellmigration. Um den Mechanismus der Zellmigration besser zu verstehen, ist es wichtig die Wechselwirkung zytoskelettaler Filamente zu verstehen. Daher sind die zwei Forschungsschwerpunkte dieser Abschlussarbeit das Verständnis der Rolle von Vimentin für die Aktin-Dynamik und deren Implikation für die Aktin-Krafterzeugung.

Zuerst untersuche ich daher die Aktin-Dynamik in vimentin-dezimierten Zellen mittels „FRAP“. Ich zeige, dass die Geninaktivierung von Vimentin die Aktin-Dynamik reduziert, aber der beteiligte Aktinmonomer-Anteil nicht beeinflusst wird. Zusätzlich zeige ich, dass Plektin, als Vimentin-Aktin Bindungsprotein, nicht den gleichen Effekt hat.

Schließlich untersuche ich die Aktin-Krafterzeugung mittels „TFM“. Ich zeige, dass die Geninaktivierung von Vimentin die Verteilung der Zugkräfte und Adhäsionsflächen reguliert, jedoch nicht die Größe der Zugkräfte.

Acknowledgements

I would like to thank the following people for helping with this research project: First of all, I would like to express my sincere gratitude to Saarland University and the Leibniz institute for new materials (INM) for letting me be part of this adventure.
I would like to thank Prof. Dr. Franziska Lautenschläger for providing guidance and feedback throughout this project. Thank you, Franziska, for all your supervision and supports. I would like to thank Prof. Dr. Albrecht Ott, Jun. Prof. Dr. Laura Aradillazapata, and Dr. Indra Dahmke for accepting to take part in my thesis committee. I would like to thank Dr. Emanuel Terriac for the thoughtful comments, recommendations, and discussions on this dissertation. Further, I would like to express my gratitude and appreciation for Dr. Doriane Vesperini whose guidance, support, and encouragement have been incredibly precious throughout writing this dissertation. Doriane, I am extremely grateful for our friendly discussions during running and walking close to the Saar river and your support in my academic and my private life. From the bottom of my heart, I would like to say a big thank you to all the group members for their energy, understanding, and help throughout my project, special thanks to Daniel, Doriane, Divyendu, Luci, Galia, Carsten, and also Manu, Luiza, and Kevin Thank you all, I never face Monday morning blues, because of nice colleagues like you. Special thanks to the administrations of the group, Mrs. Elke Huschens, Mrs. Martina Bonnard, and Mrs. Christine Jörg. I would also like to thank Dr. Essak Khan for supporting and instructing me in laboratories, dear Essak, without your help and guidance this project would have not been the same. I would like to extend my sincere thanks to Dr. Indra Dahmke (Navina) for supporting me scientifically and reviewing this thesis.
I also would like to say special thanks to Mrs. Silke Kiefer and Dr. Mitchell Han for teaching me professional skills in the laboratory. I would like to thank the Saarland University staff, special thanks to Mrs. Sina Kraus, all the staff in “Mensa” and in “ZIS”, you all assisted me to have nice moments at the Saarland University. I would like to thank all people in the INM, special thanks to Mr. Bernd Rus, Mrs. Sabine Müller, Mrs. Miriam Badziong, Mr. Ralf Muth, the IT service group, people who provide coffee in the kitchen**,** Mrs. Brigita Hafner at the reception who welcomes me every morning at work with her nice smile, people at the reception who let me have access to the INM in the weekends and all people who in the lengthy corridor gave me a nice smile and greeting me with

“guten Tag”. I would like to express my deepest appreciation to Dr. Yousefi, my psychologist in Iran, for supporting me emotionally and mentally. He taught me: “how to give myself a break after running a long and rough distance”. I would like to thank all my friends, special thanks to Dr. Tayebeh Khanjani for being always available, a head-to-toe listener friend, Zahra Kafrashian for supporting me with her positive feelings, Mohammad Torkamanzadeh for all kindness and for the food that he provided for me when I was writing my thesis, and Dr. Mohammad Jilavi for his advice and information. Special thanks to Dr. Zahra Abooali in Canada for our friendly chats and Skypes at the weekends, in early mornings and late evenings, thank you for your supportive advice and for letting me share all my feelings and thoughts with you. I’m deeply indebted to my mother, who always brings hope and light to my life with her beautiful smile and her supportive words. I cannot forget to thank my brothers and my family for all the unconditional support in all these academic years.

Table of contents

List of Figures

List of Tables

List of abbreviations

AA	Acrylic acid
AAm	Acrylamide
ABD	Actin binding domain
ABP	Actin binding protein
ADF	Actin depolymerizing factor
ADP	Adenosine diphosphate
ARP2/3	Actin-Related Proteins
ATP	Adenosine triphosphate
bis-AAm	N,N'-methylene-bis-acrylamide
BSA	Bovine Serum Albumin
CARMIL2	Capping Protein, ARP2/3, myosin I linker 2
Cc	Critical concentration
cDNA	Complementary DNA
CLSM	Confocal laser scanning microscopy
CNS	Central nervous system
CP	Capping Protein
C-terminus	Carboxyl terminus
DAPI	4′,6-diamidino-2-phenylindole
DMEM/F-12	Dulbecco´s Modified Eagle Medium
DMSO	Dimethylsulfoxide
DPBS	Dulbecco's phosphatebuffered saline
ECM	Extracellular Matrix
EDTA	Ethylenediaminetetraacetic acid
ELC	Essential light chain
EMT	Epithelial to mesenchymal transition
FA	Focal adhesion
F-actin	Filamentous actin
FBS	Fetal bovine serum
FCS	Fluorescence correlation spectroscopy
FLAP	Fluorescence loss after photoactivation

FRAP	Fluorescence recovery after photobleaching
FTTC	Fourier transform traction cytometry
FWTM	Full width at tenth of maximum
G-actin	Globular actin
GAPDH	Glyceraldehyde 3-phosphate dehydrogenase
GEF	Guanine nucleotide exchange factor
GFAP	Glial fibrillary acidic protein
GFP	Green fluorescence protein
HA-VSMCs	human aortic vascular smooth muscle cells
HFF	Human foreskin fibroblast
IF	Intermediate filament
iFRAP	Inverse FRAP
KD	Knock down
KO	Knock out
LIMK	Lim Kinase
LSM	Laser scanning microscopy
MEF	Mouse embryonic fibroblast
MHC	Myosin heavy chains
MIIA	Myosin II A
MIIB	Myosin II B
MIIC	Myosin II C
miRNA	Micro-RNA
MLC	Myosin light chains
MLCK	Myosin light chain kinases
mRNA	Messenger RNA
MT	Microtubule
MTOC	Microtubule organizing center
n.s.	Not significant
NA	Numerical aperture
NBC	Nucleotide-binding cleft
nCtrl	Negative control
N-terminus	Amino terminus
PAAm	Polyacrylamide

PBS	Phosphate buffered saline
Pi	Orthophosphate
PIV	Particle image velocimetry
PLL-g-PEG	Polylysine grafted polyethyleneglycol
PPC	Particles per cell
PRD	Plectin repeat domains
qPCR	Quantitative polymerase chain reaction
RFP	Red fluorescent protein
RLC	Regulatory light chain
ROCK	Rho-associated kinase
ROI	Region of interest
RPE1	Retinal pigmented epithelial
SDS-PAGE	Sodium Dodecyl Sulfate-Polyacrylamide Gel Electrophoresis
SF	Stress fiber
siRNA	Small (short) interfering RNA
SNR	Signal to noise ratio
TBS	Tris-buffered saline
TBST	Tris-buffered saline Tween
TFM	Traction force microscopy
ULF	Unit length of filament
WB	Western blot
WGA	Wheat germ agglutinin
WT	Wild type

1 Introduction

The cells are composed of three main compartments: the cell membrane, the nucleus and the cytoplasm. The cytoplasm comprises all the components within a cell beside the nucleus and surrounded by the cell membrane. The word “cytoplasm” is derived from two separated words: “cyto” means cell and “plasm” means stuff, thus cytoplasm means “cell stuff”. The cytoplasm consists of the cytosol, a solution of water, salts, various proteins and cytoskeleton filaments, and all the organelles. The proteins associate with each other and are involved in cellular processes, such as molecular transport, diffusion, energy conversion, cell migration and cell division. The network of protein filaments extends through the cytoplasm composes the cytoskeleton.

The cytoskeleton maintains the cell shape and plays major roles in cell migration and cell division. Three types of filaments build up the cytoskeleton: microfilaments (actin filaments), intermediate filaments (IFs) and microtubules (MTs) (Figure 1.1).

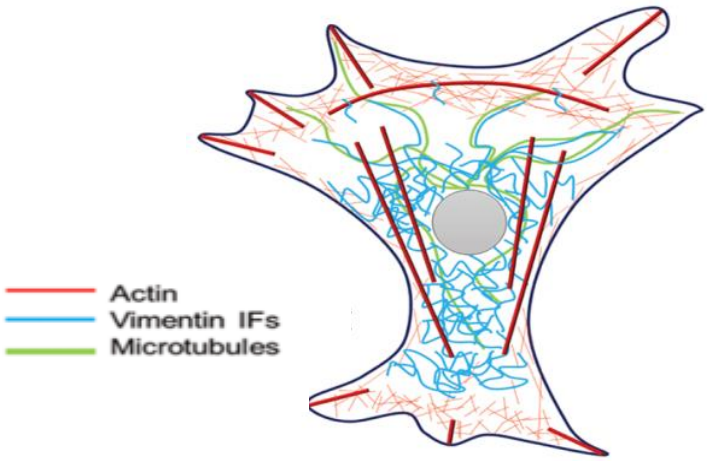

Figure 1.1 Cytoskeleton filaments

Sketch of the cytoskeleton of an adhered cell. Actin in red, microtubules in green and vimentin IF in blue. (Adapted from [1]).

The actin cytoskeleton is composed of a linear polymer microfilament called filamentous actin (F-actin) and actin binding proteins (ABPs). Depending on the ABPs involved in actin filament assembly, actin filaments have different shapes, such as actin networks (i.e., lamellipodium and cortex) and actin bundles (i.e., stress fibers (SFs)). Actin stress fibers are composed of actin filaments, myosin motor molecules and protein cross-linkers,

which connect to the focal adhesions at both ends of the filament and transfer forces from migrating cells to the extracellular matrix.

Cell migration is essential to develop and maintain many biological processes within tissues and organs. It is sensitive to external signals and occurs during progress such as wound healing, immune responses, and procreation. The fundamental mechanisms are almost known even though adherent cells (e.g., fibroblasts) and suspended cells (e.g., immune cells) behave differently. In adherent cells, migration follows four successive steps: 1) Cell polarization: actin filaments polymerize at the front edge of the cell and form protrusions (i.e., lamellipodia and filopodia); 2) Cell adhesion: formation of new focal adhesion in the direction of cell migration; 3) Cell contraction: the SF bundles contract at the cell rear to assist the contraction of the cell body; 4) Cell retraction: the old focal adhesions detach and the cell rear retracts to push the cell body toward the direction of migration (Figure 1.2). Actin SFs are involved in cell force generation, cell retraction and cell protrusion during the migration of adherent cells.

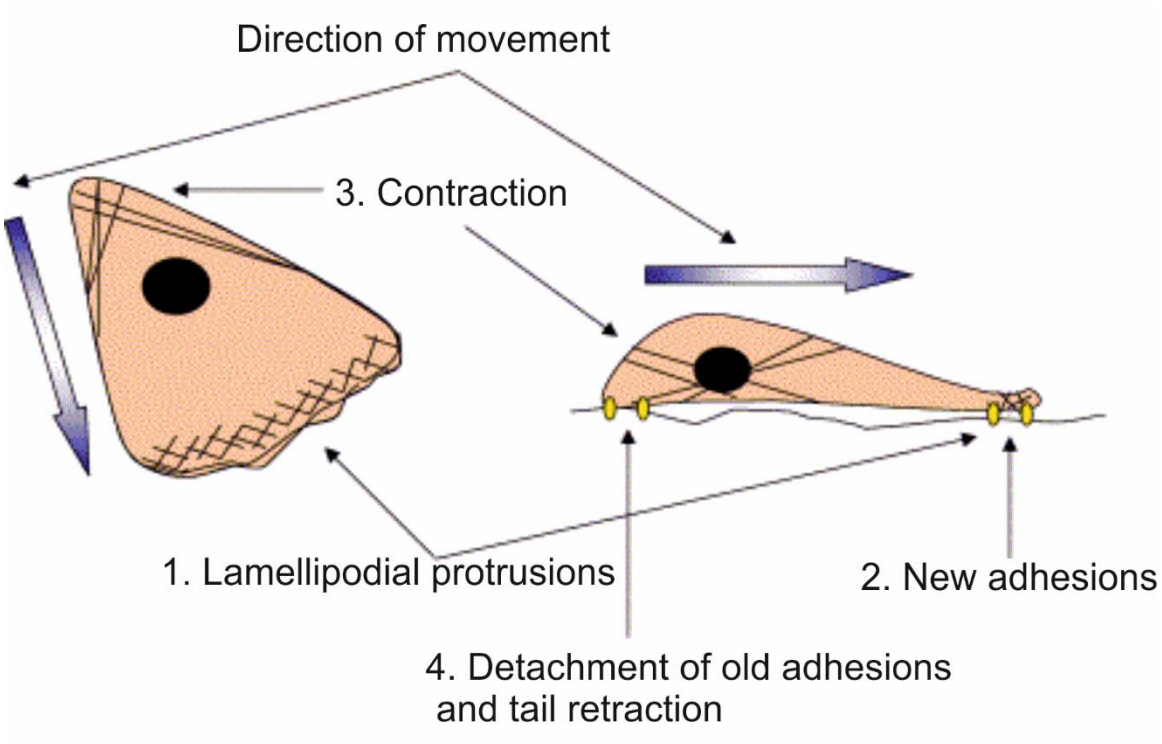

Figure 1.2 Cell migration mechanism in the adherent state.

Schematic drawing of four successive steps of cell migration. 1) polymerization of actin filaments at the front edge of the cell to form protrusions; 2) formation of new focal adhesion in the direction of cell migration; 3) contraction of the SF bundles at the cell rear; 4) detachment of the old focal adhesions and retraction of the cell rear to push the cell body toward the direction of migration (Adapted from [2])

The polymerization and depolymerization of actin filaments (i.e., actin dynamics) regulate the rate of cell migration and are influenced by the activity of proteins, such as myosin and tropomyosin [3]. Furthermore, the role of other cytoskeleton components (i.e., microtubules and intermediate filaments) is important in cell motility and cell migration. Vimentin is a subgroup of intermediate filaments, no motor molecules bind to it and it does not generate forces to be involved in cell migration; however, it is known as a cell migration regulator [4, 5]. It was shown that a lack of vimentin decreases cell migration velocity due to a reduction of cell stiffness [5]. A defect in cell migration might lead to serious disorders such as invasion and in consequence an increased risk of cancer metastasis. Several evidences show that vimentin plays a major role in the progression and invasion of the cancer cells [6]. First, vimentin is overexpressed in various cancers (e.g. prostate cancer, central nervous system (CNS) tumors, lung cancer and breast cancer [7]) which has been shown to be correlated with the enhancement of invasion of cancerous cells and tumor growth [7]. Moreover, it has been shown that vimentin is necessary for metastasis in human lung adenocarcinoma [8]. Secondly, the overexpression of vimentin results in elevation of cell motility and wound healing [9]. Understanding how vimentin and actin filaments interplay to carry out cell migration might help to find a solution to prevent metastasis.

In the presented project I investigate the interplay between vimentin and actin filaments. Even though no motor molecules bind to vimentin filaments and it does not generate forces to directly assist cell migration I hypothesized whether this intermediate filament influences actin dynamics and regulates cell migration.

First, I studied the influence of vimentin on actin dynamics in stress fibers. I used the fluorescence recovery after photobleaching (FRAP) technique to measure F-actin dynamics in vimentin depleted and control cells. FRAP data were modeled with a first-order exponential function to obtain two parameters that signify the recovery time and the rate of actin monomers that are involved in recovery to define actin dynamics. I silenced vimentin filaments via siRNA transfection method as described in chapter 3.2.1. Knocking down (silencing) the expression of an individual protein in living cells enables studying its role in cell mechanisms and its interactions with the other cell components. The amount of silenced vimentin was measured via the western blot (WB) technique and is explained in the methodology section (3.5) and the appendix and protocol section (11.2).

Secondly, I studied the effect of actin bundles thickness on actin dynamics in stress fibers via evaluating the actin bundle thicknesses as detailed in chapter 3.7. In chapter 3.9 vimentin depleted and negative control cells were seeded on crossbow micropatterned in order to keep cell shape, cell size, and the position of the stress fibers [10]. Actin dynamics in stress fibers in crossbow micropatterned cells was assessed and compared to previous results on nonpatterned cells.

Thirdly, I measured actin dynamics in stress fibers of plectin depleted and negative control cells to study whether actin turnover rate is influenced by inhibiting the indirect interaction of vimentin and actin, mediated by plectin. Plectin is known as a vimentin-actin cross-linker [11], and overexpression of plectin elevates migration and invasion of cancer cells [12]. To have a deeper understanding of actin dynamics, I studied specifically cytoplasmic actin dynamics of vimentin depleted and negative control cells.

Finally, I measured traction force on vimentin depleted and negative control cells to understand the link between the lack of vimentin to either up-regulation or down-regulation of cell traction forces.

In brief, the following chapter presents the background related to cell cytoskeleton, the interaction between cytoskeleton, and the techniques used in this study. Chapter 3 is an overview of the technical skills used for the experiments. Chapters 4 and 5 present the results of my Ph.D. mainly on actin dynamics and traction force in vimentin and plectin depleted cells. First, I showed that the labeling method to probe the actin monomer proteins and the FRAP technique are the proper applications to measure actin dynamics. I then found that there is interplay between vimentin and actin SFs, however, vimentin does not influence cytoplasmic actin dynamics. I then, showed that plectin plays a key role in the amount of actin monomers that are involved in actin dynamics. Next, I indicated how the traction force generated via actin bundles is influenced by vimentin. Finally, chapter 6 gives a summary of the main conclusions of my study.

2 Background

2.1 Cell

Cells are the basic unit of any living organism. Any cell that consists of a nucleus surrounded by a nuclear membrane is called a eukaryote cell. The cells that do not contain nuclear membrane and lack any other organelles that have a membrane in eukaryote cells are called prokaryote cells. Eukaryote cells are composed of a highly complex system of biopolymers, but in general, all mammalian cells consist of the cell membrane, the cytoplasm and the nucleus. However, there are some exceptions, e.g., red blood cells do not contain the nucleus. Eukaryote cells also contain organelles such as Golgi apparatus, mitochondria, endoplasmic reticulum and lysosome. Figure 2.1 shows a drawing of an animal cell with its organelles. Some organelles do not exist in all cell types.

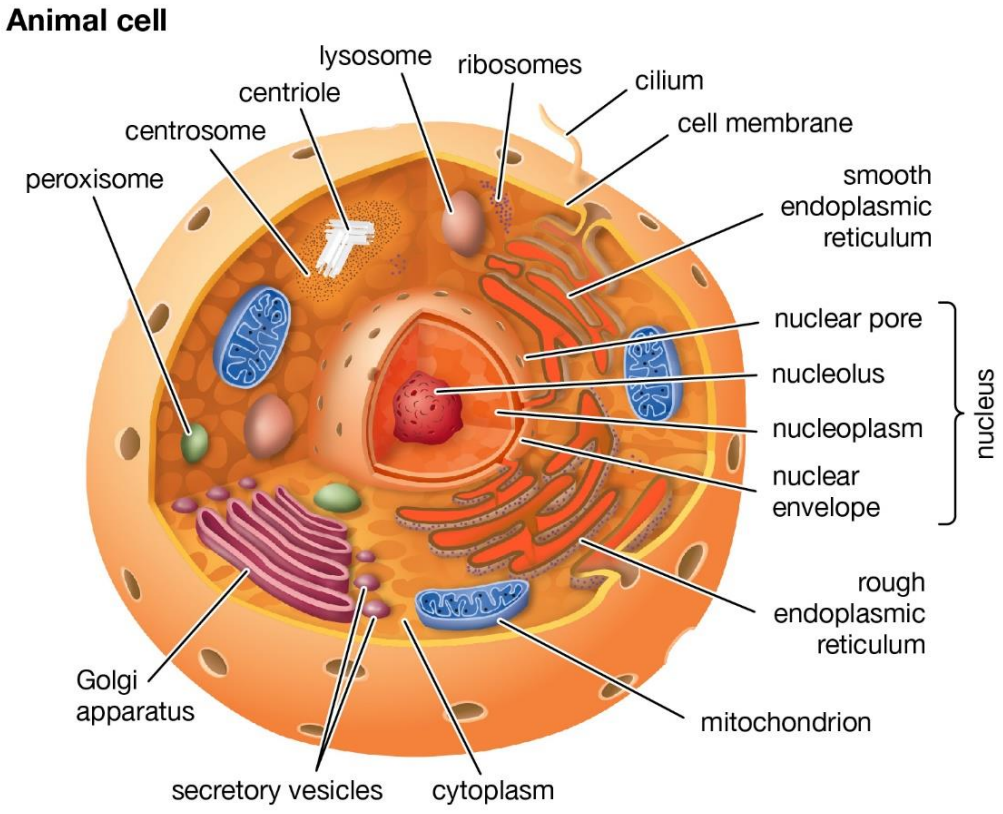

Figure 2.1 Animal cell

Principle structure of an animal cell and its organelles. It indicates three main compartments of the animal cells: the nucleus, the cytoplasm and the cell membrane and also other organelles such as mitochondria, Golgi apparatus, lysosome and endoplasmic reticulum. (From [13]).

Understanding the cell behavior and cell function might help to answer the deep root questions such as the physiology of tissues and organisms in nanoscale and changes in cellular behavior and cellular function during disease progress in cell biology and medical research. However, due to the complexity of the cell properties, it is not possible to understand the whole behavior of the cells. To study the cells, a bottom-up approach is often used, investigating one aspect of the cell functions and the cell properties, and finding the interaction between them. In this project, I focused on the interplay between two individual subgroups of the cytoskeleton: actin and vimentin.

2.2 Cytoskeleton

In cells, the cytoplasm contains water, salts and biomolecules such as proteins. Between the nucleus and the cell membrane in the cytoplasm and also in the nucleus there is a network of biopolymers known as the cytoskeleton. The cytoskeleton extends inside the cytoplasm, maintains the cell shape, and provides cell mechanical properties. Furthermore, it is a highly dynamic network that facilitates the cell to deform and migrate. The cytoskeleton stabilizes cell-cell interaction via the extracellular matrix (ECM) and is involved in cell division [14, 15], cell signaling pathway and intracellular (signaling) transport [16]. The cytoskeleton network is composed of three main types of filaments: microtubules (MTs), actin filaments, and intermediate filaments (IFs) [17] (Figure 1.1). Binding proteins, such as plectin and myosin motor molecules crosslink proteins to each other, contribute to the cell mechanics [18] and regulate filaments nucleation and elongation.

2.2.1 Microtubules

Microtubules (MTs) are polar, hollow tubes with a diameter of 24 nm and are the largest cytoskeleton components. MTs consist of an alternation of α- and β-tubulin monomers assembly all along the tube starting from the MT organizing center (MTOC) also called centrosome (Figure 2.2). The centrosome stabilizes MT minus end. The plus ends elongate towards the cell edge. MTs polymerize in both plus and minus ends even though at the plus ends it is faster [19].

MTs are involved in several cellular mechanisms such as vesicle transfer [20], cell migration [21], and cell adhesion by interacting with ABPs.

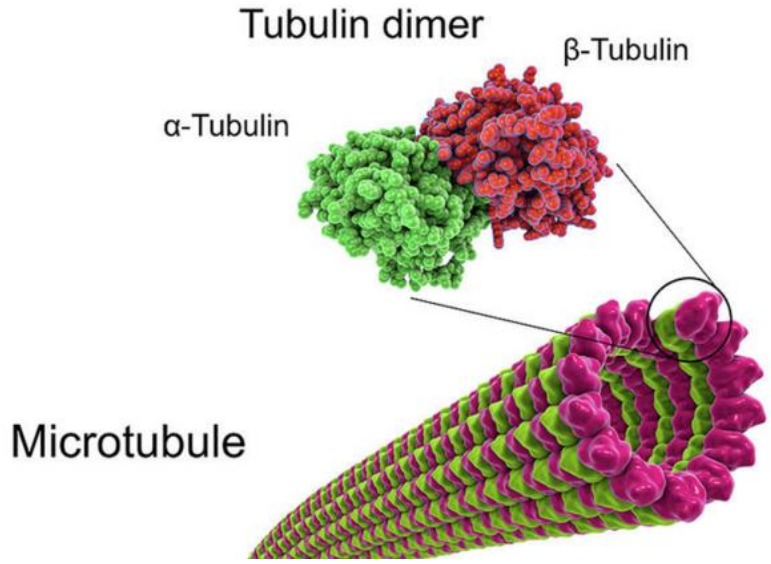

Figure 2.2 Structure of an MT.

An MT fiber consists of the assembly of tubulin dimers composed of two subunits, the α- and the ß-tubulin. (From [22])

2.2.2 Actin

Since actin was discovered in 1942 by Straub[23], it has been always the object of many biological and biophysical studies. It plays a main role in cell motility and cell division. During these years many attempts have been dedicated to model the actin structure. Models were generated from optical diffraction of actin paracrystals, e.g. the Heidelberg model, ribbon-to-helix transition models, and the Hegelman-Padron model are a few models that were generated to solve the actin filaments structure [24].

Actin monomer

Monomeric actin (also called globular actin or G-actin) built up double-strand helical filaments [25] called actin filaments (also called filamentous actin or F-actin). The G-actin is composed of two specific parts called the pointed end or minus (-)-end and barbed end or plus (+)-end. It consists of two major domains that are known as the outer and the inner domains [26] (referring to their orientation in filaments) or the small and the large domains (referring to their size). These two major domains are divided into four subdomains (named from 1 to 4) and binding sites. Two clefts, one between subdomains 1 and 3, one between subdomains 2 and 4 are formed and consist of binding sites for other proteins. Subdomain 1 contains two termini; N, amino terminus, and C, carboxyl terminus also called N-terminus and C-terminus. The cleft between subdomains 1 and 3 (refers to as patch or groove) is mainly hydrophobic and consists of actin binding sites for

ABPs such as myosin motor molecules. The other cleft called nucleotide-binding cleft (NBC) binds either to adenosine triphosphate (ATP) or to adenosine diphosphate (ADP) nucleotides. Figure 2.3 (a) presents a Ribbon diagram of the actin monomer with the four subdomains, ATP and N- and C-termini. Figure 2.3 (b) displays a space-filling model of actin monomer with nucleotide-binding cleft and barbed-end groove.

G-actin has approximately a size of 55 * 55 * 35 Å with a mass of roughly 41.7 kDa[1]. The crystal structure of G-actin contains 375 amino acid residues [23] and actin isoforms vary only in a few amino acids mainly in the N-terminal. In total three main actin isoforms have been identified, α-actin is found in skeletal, cardiac and smooth muscle cells ($\alpha_{skeletal}$-actin, $\alpha_{cardiac}$-actin, and α_{smooth}-actin), β-cytoplasmic actin is found in all muscle cells (β_{cyto}-actin) and ɣ-actin is expressed in all or only smooth muscle cells (γ_{cyto}-actin and γ_{smooth}-actin, respectively). β- and ɣ-actin are found in most of the mammalian cell types where they have different cellular functions and localization [27]. ABPs distinguish between actin monomer isoforms and have a preferred interaction partner [28]. As a result actin monomer isoforms are not distributed homogeneously in cells [27]. There are several studies about the actin isoform localization in cells. Some studies suggest that β-actin and ɣ-actin are completely colocalized in actin filaments [29]. In contrast, several studies have shown a low colocalization and found that β-actin localized at the leading edge of the cells and in lamellipodia [30], whereas ɣ-actin was preferentially located in actin filaments within the cytoplasm [31, 32]. On the contrary other studies have shown that β-actin is located in actin stress fibers (SFs) [33] and ɣ-actin is enriched in actin arcs [31]. Therefore, the exact localization of β-actin and ɣ-actin remains an interesting open question but is not the focus of this study.

[1] Kilodalton (1 kDa ≈$1.66 * 10^{-15}$ µg).

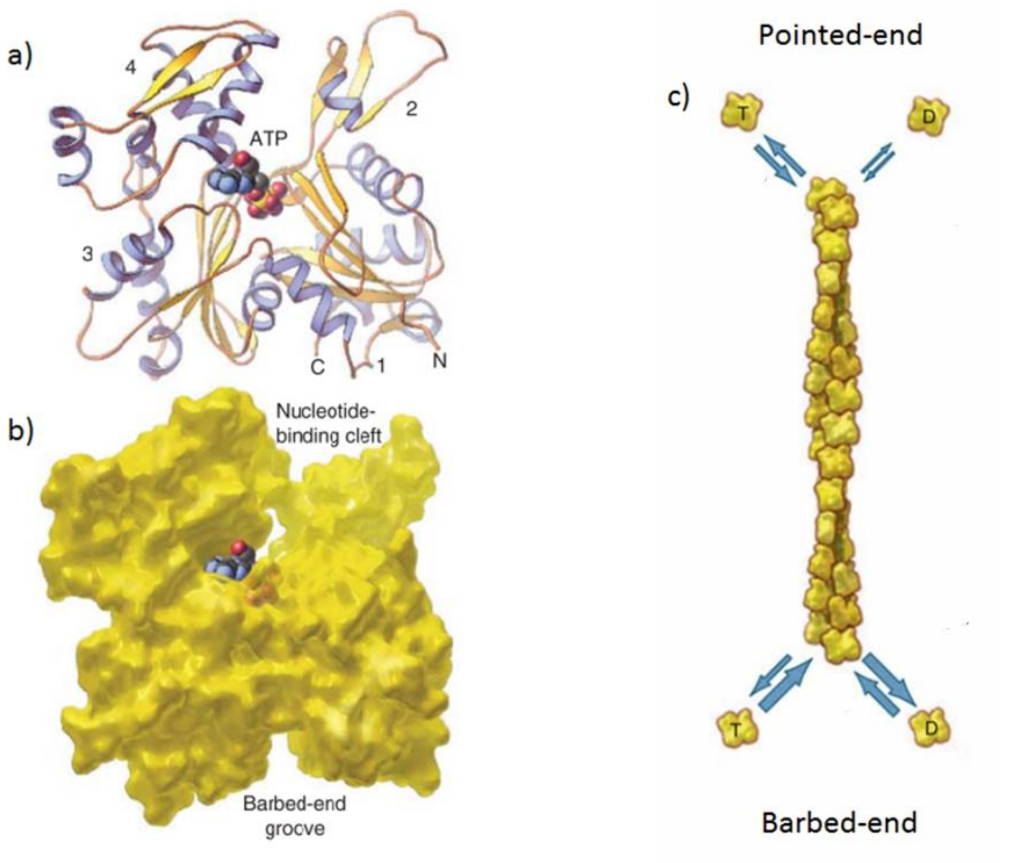

Figure 2.3 Structure of G-actin and F-actin.

a) Ribbon diagram of the actin monomer with the 4 subunits, N- and C- termini and ATP. b) Space-filling model of actin monomer with a nucleotide-binding cleft, barbed-end groove and ATP (in red and blue into the cleft). c) Scheme for a double-strand form of an actin filament with pointed-end and barbed-end. The arrows in the pointed end and barbed end with different thicknesses show the association and dissociation rate of G-actin. (Adapted from [34].)

Filamentous actin

Actin filaments are double-strand helical filaments that consist of G-actin assemblies (Figure 2.3 (c)). F-actin has a persistence length of 17 μm [35] and a thickness of about 7 nm. Actin filaments are highly dynamics polymer microfilaments that are essential for the contraction and mobility of the cells. Actin polymerization elongates actin filaments and allows the cells to produce forces, and causes the cell membrane protrusion at the cell edge [36]. Understanding the polymerization and depolymerization dynamics of actin monomers in actin filaments investigates how these biopolymers contribute to cell motility and cell contraction [37]. G-actins bind to each other from the (+)-end the (-)-end to polymerize into F-actin. The F-actin growing side is called barbed (+)-end. G-actins depolymerize mainly on the pointed (-)-end. G-actin is not a symmetrical molecule and after polymerization and assembly, it results in the polarity of the F-actin. Polymerization

requires a minimum concentration of G-actin called critical concentration (Cc) and hydrolyzation of ATP. The Cc depends on the temperature, the pH, and the ion concentration [38] and differs at the two ends of F-actin. The ratio of the dissociation rate constant (with the unit of 1/s) against the association rate constant (with the unit of 1/μM.s) defines Cc (with the unit of μM). The Cc at the pointed (-)-end and the barbed (+)-end sides are approximately 0.7 μM and 0.1 μM according to [39]. F-actin nucleation is initiated by hydrolyzing ATP at the barbed (+)-end (ATP + H2O= ADP + Pi + free energy), where Pi is an orthophosphate (inorganic phosphate group)) in a rate of 0.3 1/s [39]. At the minus (pointed)-end, the phosphorylation of the ADP initiates F-actin depolymerization. The ATP hydrolysis is faster than ADP phosphorylation; these procedures also result in the polarity of the actin filaments. In the presence of ATP Actin filaments possess different critical polymerization constants at both ends. Within a certain concentration range of actin monomers one end of the actin filament may grow while the other depolymerizes. Growing F-actin only on one side leads to treadmilling [39]. Treadmilling is known as converting ATP to ADP by hydrolyzation and in consequence phosphorylation of actin ADP to ATP [39].

The actin cytoskeleton is a complex of actin filaments, ABPs, and actin cross-linking proteins. In the cytoskeleton depending on the ABPs involved in actin filament assembly, actin filaments form three shapes: actin networks (in lamellipodium and cortex), actin bundles (such as SFs) and actin rings. Remodeling of the actin structure in the cytoskeleton modifies the cell shape, functions and mechanisms. **Error! Reference source not found.** presents different structures of actin filaments, such as antiparallel contractile structure in actin SFs, branched and cross-linked network in the lamellipodium, parallel bundles in filopodium and cross-linked network in actin cortex.

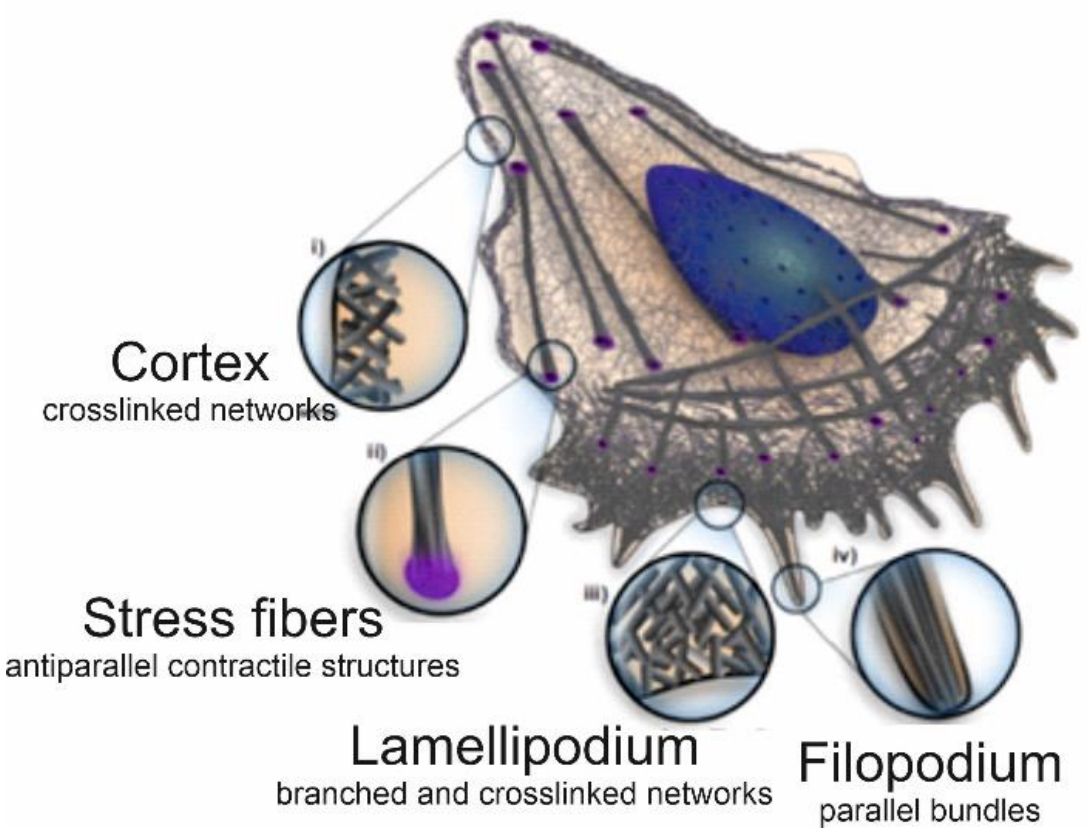

Figure 2.4 Different structures of actin filament.

The cortex, the lamellipodia, the filopodia and the SFs. The actin cortex forms a dense cross-linked network, while in SFs the actin polymerizes into antiparallel contractile structures. (Adapted from [36])

Actin filament structure and dynamics in different systems (e.g. actin cortex, lamellipodia, filopodia, and SF bundle), also depend on ABPs. In the following paragraph, the main ABPs and also focal adhesions and plectin as a vimentin-actin cross-linker protein which have interplay with actin, are described.

2.2.2.1 Actin binding proteins

Actin binding proteins mainly provide a large number of actin monomers to polymerize actin filaments, initiate new actin filaments nucleation, promote actin filaments elongation, cap ends of the filaments to prohibit elongation, link filaments to each other and cut filaments to monomers. Figure 2.5 presents the interactions of ABPs with actin filaments in order to assemble actin monomers as an actin filament structure. Regarding actin SF bundles and measuring actin dynamics in SFs myosin II, α-actinin, and focal adhesions are the most important ABPs that are considered here.

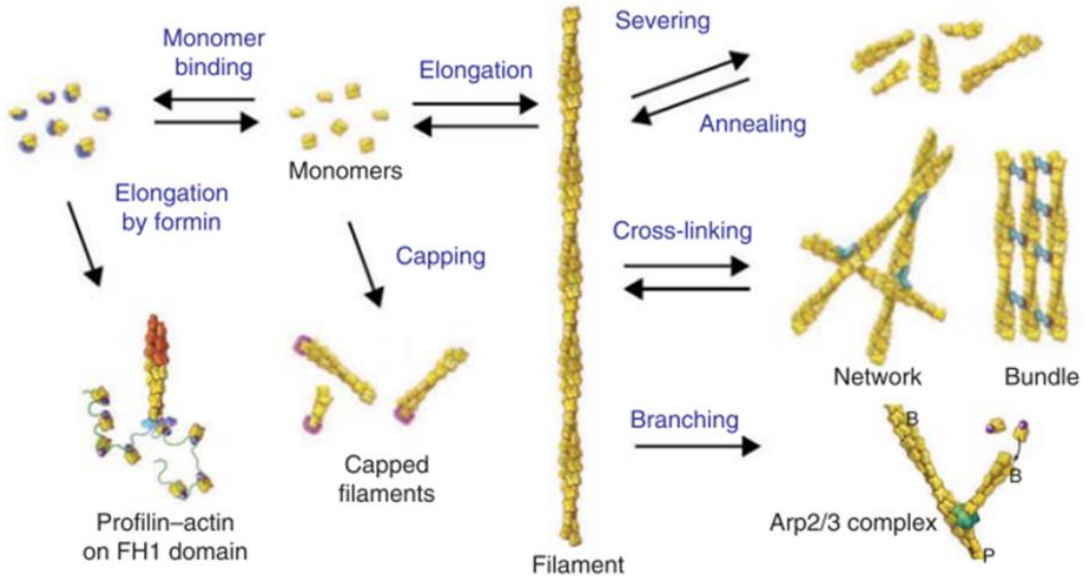

Figure 2.5 Different aspects of actin assembly.

ABPs and their contribution to actin filaments assembly and disassembly, such as branching, nucleation, elongation, severing. (From [34])

- **Myosin II**

Myosin II molecules are large with a size of 500 kDa and consist of two myosin heavy chains (MHCs); each contains a head domain also called a motor domain (N-terminal), a tail domain (C-terminal), and a neck domain that connects the head and tail domains. The head domain binds to the sides of the actin filaments and the tail domain interacts either with the cargo molecules or the tail domain of another myosin. Each heavy chain is connected to two myosin light chains (MLCs), which bind in the neck region of the MHC (Figure 2.6). MLCs are known as the essential light chain (ELC) with a size of 25 kDa, and the regulatory light chain (RLC) with a size of 19 kDa. RLC is phosphorylated by MLC kinases (MLCK). RLC phosphorylation acts as a mediator and modulates actomyosin contraction. RLC dephosphorylation is catalyzed by MLC phosphatase.

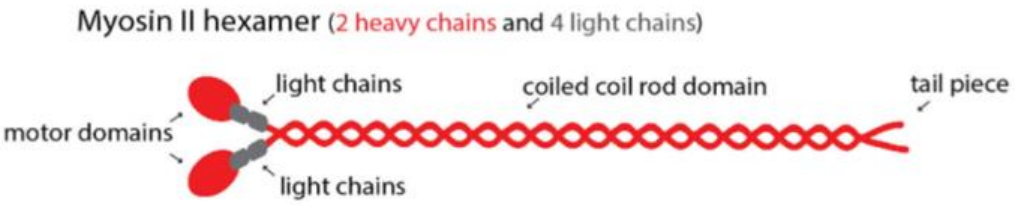

Figure 2.6 Scheme of a Myosin II molecule.

Myosin II consists of two heavy chains (red); each chain contains a motor domain, a tail domain, and a neck domain which connects head and tail domains. Each heavy chain is connected to two myosin light chains (grey). (From [40].)

Myosin II "walks" along actin filaments and which generates forces and provides cell migration regulates membrane protrusions, cell polarization, and cell adhesion dynamics [41]. Myosin II has three isoforms: myosin II-A (MIIA), myosin II-B (MIIB), and myosin II-C (MIIC). MII-A and -B are mostly localized either in the cell center and cell front or cell edge and cell rear during the cell migration. MII-A and -B contribute together in organizing actin SFs assembly and have an important role in regulating traction force during cell migration [42]. Myosin II in non-muscle cells generates contraction force and contributes to cell adhesion, cell motility, cell migration directionality, and tissue morphogenesis [43].

- **α-actinin**

α-actinin is a cross-linking protein that belongs to the spectrin[2] family that binds to actin filaments and connects actin filaments to each other. α-actinin furthermore, associates with signaling proteins and acts as an actin-regulator. It also interacts with focal adhesion proteins such as vinculin and links actin SF bundles and divers signaling pathways [44].

- **Actin-related proteins 2/3 complex**

The actin-related proteins 2/3 (ARP2/3) complex is composed of nucleation proteins and binds to the actin filaments (mother filament) side. Branches of actin filaments (daughter filaments) nucleate and elongate from ARP2/3 complexes on the actin filaments (mother filaments).

[2] Spectrin is a protein that has a main role as a scaffold in cytoskeleton and plasma membrane.

- **Formin proteins**

Formin proteins (Formins) interact with the barbed end of the actin filaments and both initiate and inhibit actin filaments elongation.

Focal adhesions

Focal adhesions are large multiprotein complexes that engage integrin[3] to link the cytoskeleton to the ECM. Focal adhesions are known as intracellular signaling complexes which transmit cell signals between the cytoskeleton and ECM [45]. Under the steady situation focal adhesions anchor actin SFs to the ECM, but during the cell migration, they constantly disassemble and assemble to contribute to the cell migration process.

Plectin

Plectin is a large cytolinker protein (500 kDa) with a multi-domain structure and more than 4000 amino acids. Plectin contains one actin binding domain (ABD) and a plakin domain in the N terminal, a central coiled-coil rod domain, and a C terminal domain which consists of six plectin repeat domains (PRDs) [46, 47] (Figure 2.7).

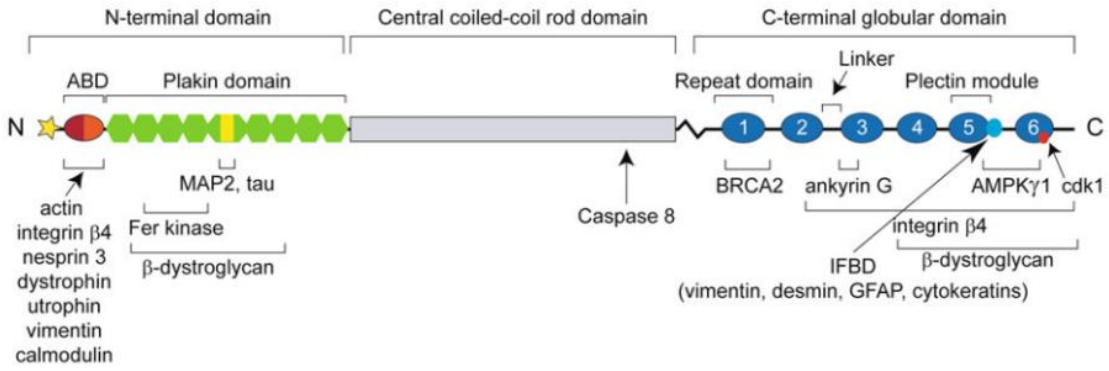

Figure 2.7 A Schematic representation of plectin protein

Schematic drawing of plectin: the N-terminal containing ABD and plakin domain, the central rod domain, and the C-terminal domain consisting of six plectin repeat domain (blue). The model represents the position of the binding regions to intermediate filaments and other cell components. (From [48].)

The ABD in plectin has a multifunctional structure. Plectin binds to actin, integrin, nesprin[4] and vimentin via ABD. Plectin has eight isoforms. Most of them differ in small sequence in their N-terminal. Plectin is expressed in the majority of the cell lines and tissues [48]. It has multiple functional domains and associates with various proteins [48].

[3] Integrins are the receptors localized on the cell surface and mediate cell-extracellular matrix and cell-cell adhesion.
[4] Nesprins are a family of the proteins that associate the nuclear membrane to the cytoskeleton.

Plectin plays the main role to organize the cytoskeleton structure and influences the mechanical and dynamical properties of the cytoskeleton. Furthermore, it interacts with MT associated proteins, links intermediate filaments and MTs, and associates with focal adhesions. Plectin binds to intermediate filaments via its plectin repeat domains in its C-terminal and also via its N-terminal. It has interplay with intermediate filaments and is required for their formation and their directional movement toward [49-52] the cell periphery [53]. Actin and vimentin filaments interact indirectly by plectin [50] as plectin connects vimentin filaments to each other and to actin filaments [50, 54].

2.2.2.2 Cortex

The actin cortex is composed of actin filaments, ABPs such as formin proteins, ARP2/3 [55] and myosin motor molecules that form a mesh size underneath the membrane and link to the membrane via the ezrin[5] cross-linker protein [56]. It assists the cells to deform their shape during cell migration and cell motion by generating mechanical forces, and furthermore, withstands mechanical forces applied to the cell. In the motile state of the cell, the cortical proteins make the actin cortex attach and detach from the actin meshwork.

2.2.2.3 Stress Fibers

Stress fibers (SFs) are contractile bundles of 10 to 30 parallel (in nonmotile cells) or antiparallel actin filaments (in motile cells) [57]. They consist of ABPs such as myosin motor molecules, α-actinin cross-linker protein, tropomyosin[6] [58], actin-depolymerizing factor (ADF)/cofilin [59], and titin[7] [60].

In the cell migration process actin SFs form different structures of certain morphology, and are classified into four types [61]: dorsal SFs, transverse arcs, ventral SFs, and perinuclear actin caps [62, 63] (Figure 2.8). Dorsal SFs extend from the ventral to the basal side of the cell and associate from the ventral cell surface to focal adhesions. The Dia1 formin protein promotes the nucleation of the dorsal SFs throughout the center cell [64]. Dorsal SFs are connected perpendicularly to the transverse arcs from their second end. Commonly dorsal SFs do not contain myosin motor molecules and they do not

[5] Ezrin is one of the proteins from the ezrin, radixin and moesin (ERM) family that connect actin cortex to the membrane.
[6] Tropomyosin binds to the sides of the actin filaments to cover and connect six to seven actin subunits. It regulates the access of the actin-binding proteins, such as cofilin, to actin filaments to prevent actin depolymerization.
[7] Titin is a long protein and is responsible for the passive state of the muscle cells.

contract. Transverse arcs are curved actomyosin bundles [65] that associate with dorsal SFs. Transverse arcs and dorsal SFs interaction forms the actin flow (called retrograde flow) which moves toward the cell center in migrating cells.

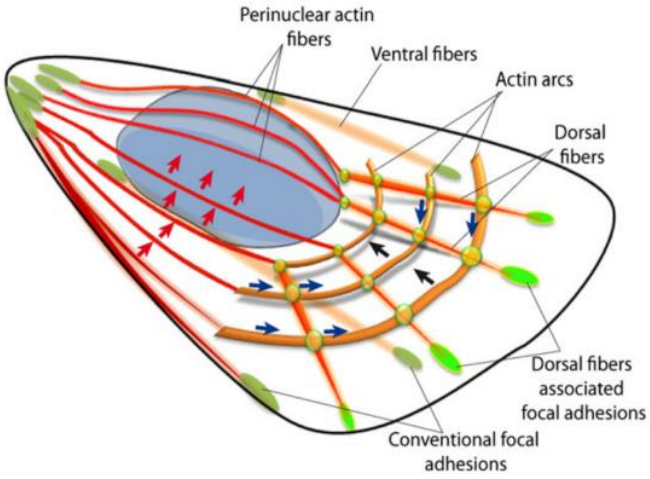

Figure 2.8 The four types of actin SFs.

Actin arc, perinuclear actin fibers, dorsal fibers and ventral fibers. SFs connect to focal adhesion (in green) and α-actinin (in yellow) which participate in cell mechanics. (From [62]).

Ventral SFs are formed by the retrograde flow. In contractile ventral SFs, α-actinin cross-linking proteins link actin filaments to each other and are called actin bundles. The actin bundles are linked via myosin motor molecules from the side and anchor to the focal adhesions at both ends and usually elongate toward the cell migration direction [62]. Ventral SFs are the main subject of this project in the fluorescence recovery after photobleaching (FRAP) measurements. Figure 2.9 displays a scheme of a ventral SF bundle and its component.

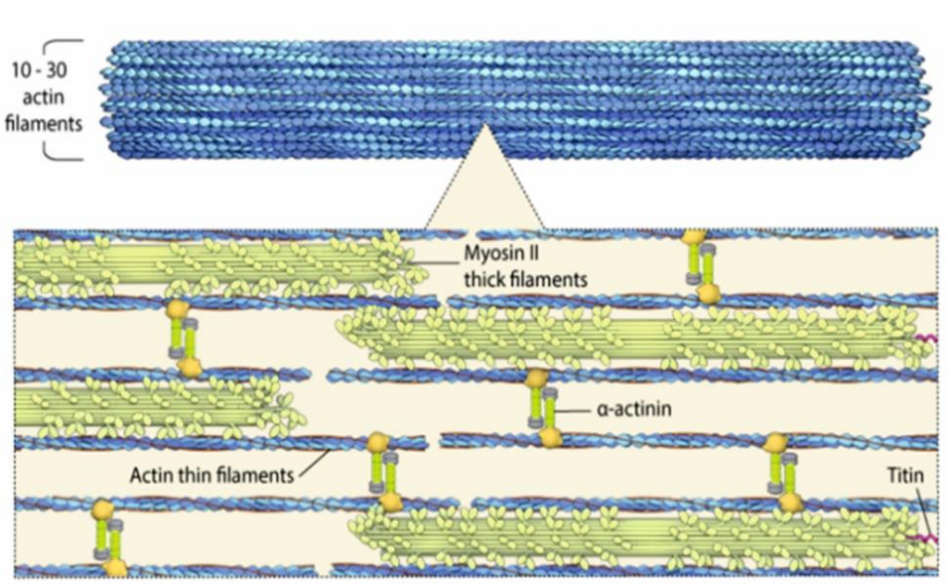

Figure 2.9 A schematic representation of the ventral SF bundle.

Actin SF bundle consists of actin filaments, myosin II filaments, α-actinin, titin and tropomyosin filaments (red). Actin filaments in ventral SFs are involved in cell contraction and cell migration by linking to myosin filaments and α-actinin from the sides and anchoring to the FAs at both ends. (Adapted from [66])

Perinuclear actin caps are SFs that are localized on top of the nucleus. One of the main roles of perinuclear actin caps is to regulate the shape of the nucleus [63].

Typically in motile cells, SFs are thin and highly dynamic [67]. Early studies suggested that myosin motor molecules generate SFs contraction that promotes cell migration [68, 69]. Alternatively, other researchers suggested that SFs are inhibiting cell migration via generating contraction forces [70]. Besides, SFs play the main role in focal adhesion maturation and regulate focal adhesion dynamics by generating contractile forces. The force contraction generated by SFs is necessary to spontaneously strengthen focal adhesions and also the turnover of the adhesion [71]. So, on one hand low contractility would prevent the adhesion turnover at the cell rear and inhibit the tail retraction. On the other hand, high contractility would either enhance the adhesion at the cell front or sever the adhesion at both ends. Therefore, an optimal balance between contractility and adhesion is required for efficient motility.

The main role of the actin filaments in cells is generating forces for cellular processes such as cell migration, cell division, morphogenesis, and endocytosis. Actin filaments are involved in cell force generation by two discrete mechanisms. First, according to actin polymerization regulated by ABPs. Second: according to the force generation via the movement of myosin motor molecules along actin filaments.

Activation of RhoA (a subgroup of the Rho[8] family) through the Guanine nucleotide exchange factor (GEF-H1) stimulates actin polymerization and F-actin stabilization. Transforming protein RhoA is part of the hydrolase enzyme GTPases[9]-protein family. Rho proteins are involved in cell signaling and activation of the Rho family. Rho-associated kinase (ROCK) I and II are serine/threonine kinases. ROCK is known as a downstream effector of the Rho family that is activated by RhoA. Rho effectors such as mDia[10] [72] and ROCK control and regulate actin SFs formation. Despite the effect of Rho proteins on actin SFs regulation, actin SFs as such regulate biochemical and signaling pathways via generating forces [73]. ROCK also activates myosin II phosphorylation and stimulates cell contraction and force generation.

2.2.3 Intermediate filaments

Intermediate filaments (IFs) are one of the three major cytoskeletal structures. IFs have a coiled-coil structure with a diameter of 10 nm that is smaller than MT filaments and larger than actin filaments. IFs in contrast to MTs and actin filaments are nonpolar and assemble the same way in both ends of the filament. The formation of IF proteins into filaments does not require nucleotide hydrolysis [74], and their assembly is not similar to the assembly of other cytoskeletal filaments. Unlike MTs and actin filaments, IFs do not have treadmilling and no molecular motors binding to them, but they are still dynamic. IFs are classified into six subgroups that are widely dissimilar in sequences and have different ranges of molecular weight [74]. Table 2.1 shows the six classes of the IFs. The type of IFs expressed in cells are related to their physiological functions and except vimentin which is expressed in most of the cell types the rest of IFs families are cell-specific [75]. IFs due to their mode of assembly can subdivide into three groups: keratin, vimentin-like assembly and lamins.

[8] Rho ≡ ρ
[9] GTPases are the hydrolase enzyme GTPases-protein family that hydrolyzes guanosine triphosphate (GTP) to guanosine diphosaphate (GDP).
[10] mDia is a member of formin proteins family and play a main role on actin filaments elongation and SFs formation.

Table 2.1 Types of IFs.
Six subgroups of IFs and their cellular distribution. *vimentin can be expressed in most of the cell types. **have not been classified yet. (Adapted from [75].)

IFs	Class	Cell type
Acid cytokeratins	I	Epithelial cells
Neutral-basic cytokeratins	II	Epithelial cells
Vimentin*		Mesenchymal cells
Glial fibrillary acidic protein (GFAP)		Astroglial cells
Desmin	III	Muscle cells
Synemin		Skeletal muscle cells
Peripherin		Neurons
Nestin		CNS and muscle precursor cells
Neurofilaments	IV	Neurons
Internexin		Neurons
Lamins	V	Ubiquitous
Filensin, phakinin	N.C.**	Lens
Transitin	N.C.	Ubiquitous

The persistence length l_p of IFs is directly correlated to their bending stiffness (κ) ($\kappa=k_BTl_p$) where k_B is Boltzmann constant and T is the temperature in Kelvin. The persistence length of IFs reaches values from 0.3 to 1 μm [76-78] which is small compared to actin (3-20 μm [76, 79]) and MT persistence length (1-8 mm [76, 80]). When the persistence length is in the range of the filament length, the filament is semi-flexible. IFs can be considered as flexible filaments (i.e, their length is much longer than the persistent length) and actin filaments have a semi-flexible structure. IFs have the least stiffness among all the cytoskeletal components and due to their flexible structure can elongate several times their initial length [77]. The flexibility of the IFs network and its stiffness behavior make vimentin an excellent component to protect the cells against deformation [81, 82]. IFs provide mechanical support for cell integrity and affect cellular properties. IFs functions include: to participate in cell growth, to promote wound healing, and to provide cell migration [52], cell adhesion [52] and cell division [14, 15]. Their main role in cell mechanics can lead to impaired functions in case of IFs mutations and might lead to diseases [77] such as skin disorders (keratin mutations) [79], cardiomyopathy and muscular dystrophy diseases (mutations in desmin, lamin A and vimentin) [83, 84], Alexander disease (mutations in glial fibrillary acidic protein (GFAP))

[85] and cancer (mutations in vimentin) [51]. The link between IFs mutations and the different diseases is still largely unknown.

In this project, I concentrated on actin-vimentin interactions and do not study other types of IFs.

Vimentin

Vimentin similar to all of the proteins in the family of IFs has a common three-domain structure; a central α-helical rod with two non-helical domains: a head domain (Amino terminal or N-terminal) and a tail domain (Carboxy terminal or C-terminal) [86]. The basic form of vimentin is a two-strand parallel coiled-coil of monomers that compose a dimer. Two antiparallel dimers assemble laterally and form a tetramer. A fully assemble filament is composed of a lateral association of eight tetramers and form the unit length of filaments (ULFs) with a length of 60 nm [79] (Figure 2.10). As a consequence of the antiparallel assembly of polar dimers, tetramers are symmetric and form nonpolar filaments (i.e. vimentin filaments are polymerizing the same way in both ends). To assemble into higher order structures, ULFs can either elongate the head or the tail. The end-to-end annealing of ULFs forms mature filaments that are also nonpolar.

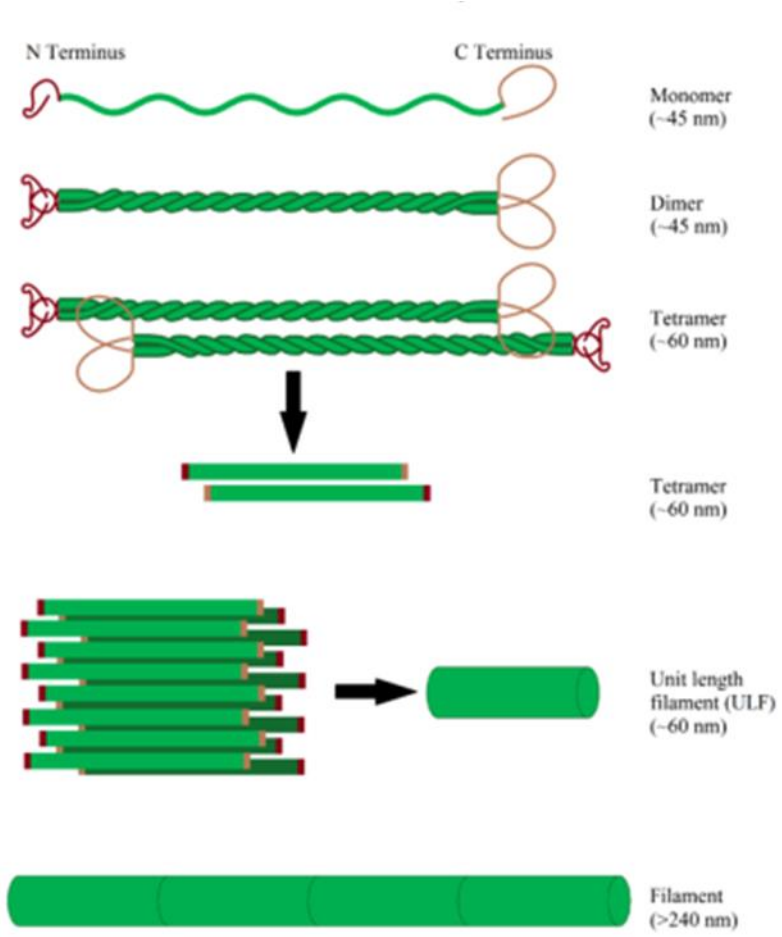

Figure 2.10 Vimentin structure and its assembly.

Vimentin monomer with N- and C- terminals (red and brown respectively) and a central α-helical rod (green). Two parallel monomers form a dimer and two antiparallel dimers assemble laterally and form a tetramer. Eight tetramers assemble laterally and form the unit length of filament (ULF). ULFs elongation in both ends form mature vimentin filaments. (Adapted from [87].)

Vimentin IFs are introduced as a marker of the epithelial to mesenchymal transition (EMT) [88, 89] and affect the cell shape, cell motility, and cell adhesion during this transition [90]. Vimentin filaments play an important role to regulate the position of the organelles in cells and fix the organelles in the cytoplasm [91].Vimentin associates directly and indirectly to other proteins such as actin filaments, MTs, myosin and focal adhesions via protein cross-linkers (e.g. plectin) [92].

The interaction of vimentin and other proteins and its effects on cell function is explained here briefly. Vimentin filaments contribute to the intracellular mechanism and slightly affect the stiffness of the cell cortex [93], while its presence and its amount highly affect the stiffness of the cytoplasm [93]. Vimentin interacts with actin arcs which modify actin flow. In the literature, it has been shown that vimentin either slows down actin retrograde flow [94] or promotes actin retrograde flow [95]. Earlier the direct interaction of actin and vimentin in vitro [96] and also an indirect interaction of vimentin and actin via plectin were shown [11].

The intracellular organization of the IFs (vimentin) is regulated by protein kinases (phosphorylation) [97, 98]. Vimentin phosphorylation plays an important role in cell migration and cell adhesion. In the absence of vimentin phosphorylation, the amount of integrin is reduced and the number of migrating cells is decreased [99]. Furthermore, vimentin depletion leads to the activation of RhoA and modulates F-actin stabilization and actomyosin contraction [100]. Vimentin depletion results in the enhancement of myosin light chain phosphorylation, myosin contraction, and actin SFs assembly via activating RhoA and in consequence activating ROCK.

Even though vimentin has no polarity and is binding to no motor molecules, it provides cell migration and cell adhesion [52] and motivated me to investigate its interaction with actin. In the following chapter, the direct and indirect interactions between cytoskeleton elements are described.

2.3 Interaction between cytoskeletal elements

In cells, the interaction of the proteins may potentially affect their configuration and influences their functions. The association between cytoskeleton elements and its interactions with the other cell components enable studying their role in cell mechanisms.

The link between IFs and actin filaments is still largely unknown. In this project, I concentrated on actin-vimentin interactions, even though vimentin associates directly and indirectly (via protein cross-linkers) to other proteins such as MTs, myosin and focal

adhesions [92]. Earlier the direct interaction of actin and vimentin in vitro [96] and also an indirect interaction of vimentin and actin via plectin were shown [11]. Few studies, mainly *in vitro*, have shown an interaction between actin and vimentin [100]. For example, rheological studies showed that a mixture of vimentin and actin is more stiff compared to actin filaments or vimentin filaments alone [96]. Vimentin filaments contribute to the intracellular mechanism and its presence and its amount highly affect the stiffness of the cytoplasm [93]. Also, there is an interaction between vimentin and actin transverse arcs and this interaction results either in an increase of actin retrograde flow in U2OS human osteosarcoma cells [95] or in a slow actin flow in human foreskin fibroblast (HFF) cells [94].

Studies have been shown the interaction of actin and vimentin-ULFs via binding proteins such as filamin A or fimbrin[11] [101]. Filamin A is a multi-domain ABP. Filamin A isoforms are localized in SFs and focal adhesion [102]. The vimentin-filamin A interaction regulates integrin function and consequently regulates cell migration. Recent studies show the cell adhesion is reduced in vimentin depleted cells, suggesting that vimentin, as well as filamin A, plays a main role in cell adhesion [103] and cell spreading [104]. Vimentin binds to filamin A N-terminal while actin binds to the ABD of filamin A [105], suggesting filamin A links actin and vimentin indirectly.

Plectin plays the main role to organize the cytoskeleton structure and influences the mechanical and dynamical properties of the cytoskeleton. It interacts with almost all the IFs such as vimentin. It binds to intermediate filaments via its repeat domains in C-terminal and also via N-terminal. Plectin is required for IFs formation and their directional movement toward [49-52] the cell periphery [53]. Plectin connects IFs to actin filaments, MTs and membrane [11, 106]. Furthermore, it interacts with MT associated proteins, links intermediate filaments and MTs, and associates with focal adhesions. Actin and vimentin filaments interact indirectly by plectin [11, 50, 54]. The ABD in plectin has a multifunctional structure. Plectin binds to actin, integrin, nesprin and vimentin via ABD. Vimentin-plectin interaction modifies vimentin distribution into the cell by crosslinking vimentin to focal adhesions [46, 95], moreover, plectin is required for the interaction of transverse arcs and vimentin [95].

[11] Fimbrin is a cross linking protein and forms filopodia.

Indicating the direct and indirect interaction between vimentin and actin filaments might help to better understand the cell migration process, and in consequence, investigating how vimentin and actin filaments interplay to carry out cell migration might help to find a solution to prevent metastasis. Reduction of the expression of vimentin in living cells enables studying its interactions with the other cell components.

2.4 Techniques

2.4.1 Transfection

Knock out (KO) or knock down (KD) the expression of an individual protein in living cells enables studying its role in cell mechanisms and its interactions with the other cell components. To knock down a protein, a specific gene is transferred into the cell and silenced the expression of the protein. There are various methods to transfer a gene into the cells but in general can be divided into two methods: non-viral and viral. Non-viral methods are known as transfections and include the use of physical or chemical methods to transfer the gene into the cells. These methods are microinjection, lipofection and electroporation. Viral methods include the use of viruses to deliver the gene into the cells. This method is known as transduction. Common transfection methods can be used to deliver plasmid DNA, small (short) interfering RNAs (siRNA), and RNA into eukaryotic cells. A plasmid is a small DNA molecule that comes from bacteria and is used to transfer genetic information from bacteria to mammalian cells. Plasmid transfection is a method to transfer a complex of plasmid DNA using lipid reagents (lipofection method) into the cells to label a specific protein. siRNA transfection is a common transfection method to silence or knockdown a specific gene expression in cells to investigate its specific function, especially in the case of diseases. There are two important categories of small double-strand RNAs: micro-RNAs (miRNAs) and siRNA. miRNA regulates endogenous genes and siRNA protects the genomes in response to viruses and transgenes. Single-strand forms of miRNA and siRNA are known as gene-specific (RNA) silencers. The siRNA is designed against the messenger RNA (mRNA) of a target gene. It is delivered into the cells usually via physical or chemical methods. In cells siRNA forms single-strand RNA. Single-strand RNA binds to the target mRNA and cut it. The cut mRNA does not convert to the amino acid and protein and silences the target mRNA. To ensure that the effect of a specific siRNA transfection is due to its specificity, a sample as control is needed. A scrambled siRNA whose sequence is different from the siRNA of interest and is randomly rearranged in the nucleotide sequence is taken as a control. A scramble

siRNA will have the same nucleotide components as the siRNA of interest. In a scramble siRNA transfection, one doesn't want to observe any effect due to the silencing of a specific target. It is not contributed to the gene silencing and has no known target in the cell. A scrambled siRNA is not expected to specifically target any mRNA beyond a background level, and it is known as a negative control.

2.4.2 Real-time quantitative polymerase chain reaction

The polymerase chain reaction (PCR) amplifies specific sequences within a DNA (single strand or double strand) or RNA templates. RNA has to be transcribed into complementary DNA (cDNA) before the quantification. PCR makes many copies of the specific sequences of short DNA molecules (Oligonucleotides). In PCR, also called traditional or endpoint PCR, the amplified sequence is not quantified, however, the PCR product is applied on an agarose gel, then it is electrophoresed, and the bands are visualized. If the amplified sequence is quantified at each cycle it is called real-time quantitative PCR (qPCR). In qPCR, a reference gene or a known standard DNA is needed for quantification. To amplify the sequence 15 to 40 thermal cycles are performed. In qPCR, each reaction is monitoring, and the initial quantity of the target is precisely detected as it occurs in real time. Then the initial quantity of the target will be calculated by comparing it with a known standard. In qPCR, the cycle threshold (C_t) is defined as the cycle number that fluorescence signals cross the fluorescence threshold. The fluorescence threshold is calculating by the level of the signal that increased significantly compared to the base of the fluorescence signal (background signal). C_t value and the amount of starting templet are related reversely, the lower C_t value, the higher the amount of starting templet in a reaction.

2.4.3 Fluorescence recovery after photobleaching

In cells as a crowded confined environment, proteins interact with each other individually (with each specific protein) and this interaction may potentially influence their arrangement and configuration. The localization of a protein in a domain and its turnover depend on the fraction of proteins that bind to the domain and the reaction rate factor of the proteins. In a cell, two populations of proteins can be distinguished: the proteins that are linked and bonded together to shape a structure, and proteins that diffuse freely inside the cell. The reaction rate of the proteins is the result of both, association and dissociation of the binding proteins and diffusion of the free proteins. The turnover of the binding proteins may include several proteins. Several studies indicated the precise reaction rate

for many individual purified proteins in *in vitro* or *in vivo* assays [107-109]. However, the protein reaction rate in a pool of proteins in a confined environment (such as in living cells) could be more complicated than *in vitro* and requires accurate settings and methods [110]. Various techniques such as fluorescence recovery after photobleaching [110-114] (FRAP), fluorescence correlation spectroscopy (FCS) [115], fluorescence loss after photoactivation (FLAP) or inverse FRAP (iFRAP) [116], fluorescence loss in photobleaching (FLIP) [116] and single-molecule imaging [117] are existing to indicate the protein kinetics in living cells. FRAP is the most common method to probe protein kinetics and diffusion in living cells, the exchange speed of molecules within the cell, the ratio of immobilization of proteins that are confined within large structures such as cytoskeleton filaments, and nuclear envelope. Moreover, the influence of inhibitors on proteins can be studied via FRAP. In this project, FRAP experiments are performed to indicate the F-actin turnover rate in the cellular environment.

Fluorescent molecules conjugated to specific biological macromolecules (e.g. proteins) allow their visualization via fluorescence microscopy. In a FRAP experiment, a high laser intensity is illuminated to a region of interest (ROI) and bleached permanently the fluorescence of the proteins localized in the ROI. The high laser power applied to the fluorescent molecules damages irreversibly the fluorochromes combined with these molecules. These molecules then have no contribution to the fluorescence turnover in the bleached ROI. The bleached fluorophores (i.e. fluorochromes connected to monomers) are exchanged with nonbleached proteins over time. The fluorescence exchange in the bleached ROI is then monitored over time at low laser power to evaluate the fluorescence recovery. FRAP can be described in three steps: 1) before bleaching, the fluorescence is maximal; 2) the time just after bleaching, the fluorescence is minimal; 3) the post-bleaching time, the fluorescence recovers over time. Figure 2.11 (a) represents a scheme of a cell in which an SF is bleached in the ROI (orange circle), and (b) represents an actin SF labeled in green in a living cell. FRAP analysis consists of measuring three parameters: (i) the recovery time, (ii) the mobile fraction and (iii) the immobile fraction. The recovery time is defined as the time needed for the fluorescence intensity to reach a plateau. The mobile fraction corresponds to the fraction of the molecules contributing to the recovery. The immobile fraction corresponds to the proportion of immobilized molecules after photobleaching that avoids a full recovery.

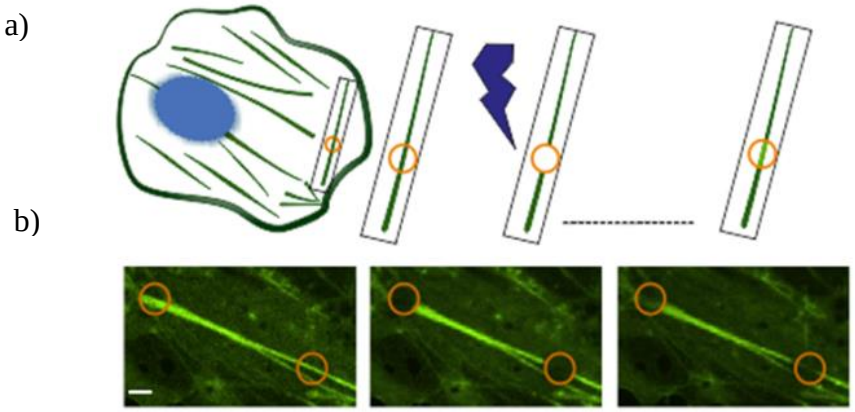

Figure 2.11 Measuring actin dynamics in SFs with FRAP.

a) Schematic representation of a cell with SF bundles in green and the nucleus in blue. Insets show a scheme of one actin SF bundle before (left), directly after (middle) and at a post (right) bleaching time. b) Fluorescence images of an actin bundle. The orange circles in a) and b) on actin bundles represent the bleaching ROIs. Scale bar: 2 µm.

In this project, the appropriate monitoring time for actin proteins is taken from the literature. Figure 2.12 displays a simple example of fluorescence recovery over time for different recovery profiles: highly mobile, intermediate mobility and immobile recovery.

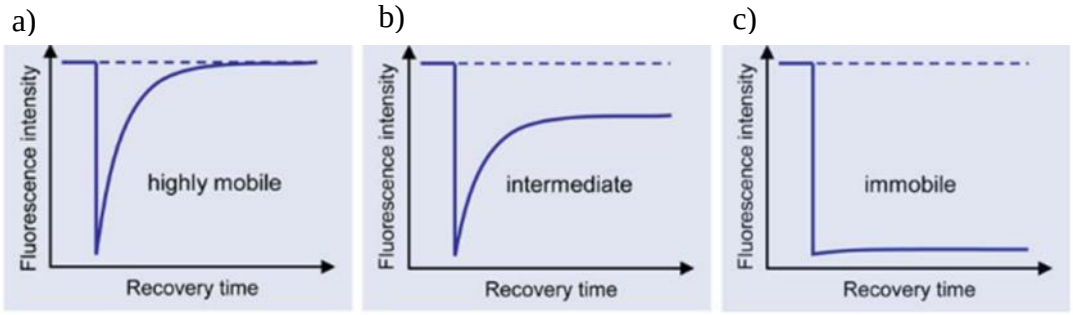

Figure 2.12 Classification of the protein mobility

Three different fluorescence recovery profiles a) highly mobile, full recovery after a certain time, b) intermediate mobile, incomplete recovery and c) immobile, no fluorescence recovery (From [110]).

The total turnover is the sum of the free diffusion of actin monomers in the ROI region (diffusive recovery) and the association and dissociation of the monomers with the actin filaments (reactive recovery) [118]. The dynamics of actin monomers (G-actin) are fast, e.g. its diffusive halftime recovery in the cortex is about 50 ms [119] and about 40 ms

[120] in the cytoplasm even though the density of free monomers is similar in both localizations [119].

In the cytoplasm, the halftime recovery refers only to the diffusive recovery while in the cortex it is a combination of diffusive and reactive recoveries. When the diffusive and reactive recoveries are in different timescales they can be measured and analyzed independently.

The characteristic diffusion time (τ) is the time needed for a monomer to travel a distance (r, the radius of the ROI) with a certain diffusion constant (D) [121, 122]:

$$\tau_{diffusion} \approx r^2/\gamma D$$

where γ is the diffusive process, γ=2 for a 1D diffusion, γ=4 for a 2D region, and γ=6 for 3D diffusion [120]. On the contrary, the reactive recovery time is an intrinsic property of the cell and does not depend on the radius of the ROI [120]. Because characteristics diffusive time is fast (40 ms and 50 ms, in cytoplasm and cortex, respectively) compare to the acquisition time (≥ 200 ms), it will be completed by the first postbleached frame. Therefore, when measuring the recovery time in actin SFs and cortex, the diffusion recovery is negligible compared to the reactive recovery (association/dissociation dynamics).

2.4.3.1 G-actin association and dissociation rates

In the reactive process, the dissociation rate constant k_{off} and the association rate constant k_{on} of G-actin to the filaments describe respectively actin depolymerization and actin polymerization. Dissociation and association rates are defined as exchange rates (or reaction rates) and the turnover rate (ω) in a network or an organelle is the mean value of the exchange rate of the proteins on a binding domain. Characteristics time $\tau = 1/\omega$ and halftime $t_{1/2}$=Ln (2)/ω are two parameters that are obtained from the turnover rate.

2.4.3.2 FRAP recovery curve

From the FRAP recovery curve the fluorescence recovery time, the mobile and immobile fractions are displayed. Figure 2.13 shows a corrected and normalized FRAP recovery curve (black). In phase I, before photobleaching the fluorescence intensity is maximal, normalized as 1. Phase II corresponds to the bleaching time, the intensity in the ROI is normalized as 0. Phase III corresponds to actin fluorescence recovery. The curve reaches a plateau i.e. a maximal fluorescence recovery. The mobile fraction is then measured as the plateau value while the immobile fraction is the difference between the initial maximum intensity and the plateau value.

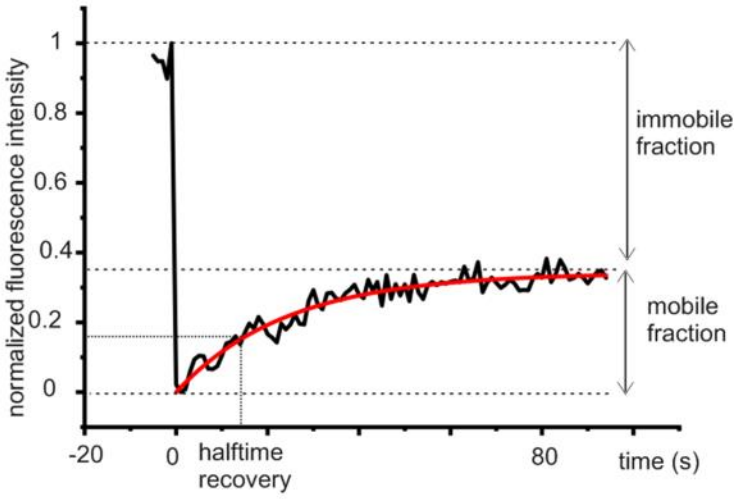

Figure 2.13 FRAP recovery curve

Example of an actin fluorescence intensity curve during the FRAP experiment. Normalized (black) curve represents actin fluorescence intensity before bleaching (time -5 s to 0 s) normalized to 1 and directly after bleaching (time 0 s) normalized to 0. Post bleaching (time 0 s to 94 s) shows the fluorescence recovery i.e. the actin turnover. Halftime and mobile fraction are measured on the fitted (red) curve.

To quantify the turnover and dynamics of the proteins a mono-exponential or multi-exponential fitting was applied. Mono-exponential fitting was applied when only one specific population of filaments is attending to the turnover rate. For example: in actin SFs the first-order reaction kinetics (below) was used to indicate the turnover of fluorescence intensity for reactive recovery (Figure 2.13 (red)),

$$F(t) = a*(1-\exp(-\omega*t))$$

where "a" is the plateau value and "ω" corresponds to the turnover rate. ($t_{1/2} = \mathrm{Ln}(2)/\omega$, is the corresponding halftime recovery). Plateau value represents the fraction of the proteins that are participating in the fluorescence recovery.

Multi-exponential fitting (not shown here) is applied when two distinct populations of filaments are participating in the turnover rate. For example: in the cortex, ARP2/3 and formin result in two distinct polymerizations and nucleation. A fast turnover is the result of the nucleation of actin filaments initiated by ARP2/3, and a slow turnover is the result of formin-mediated filament growth [119, 120]. When two or more than two populations of proteins participate in the fluorescence recovery a multiple of the first-order reaction kinetics will be applied.

$$F(t) = a*(1-\exp(-\omega_1*t)) + b*(1-\exp(-\omega_2*t))$$

where “a” and “b” signify mobile fraction of slow and fast components respectively, and ω_1 and ω_2 correspond to the turnover rate of slow and fast populations ($\omega_i = Ln(2)/\tau_i$, where τ_i corresponds to the halftime recovery). There are many various analytical methods to extract the dynamics of proteins from FRAP curves. References [114, 122] provide an overview of the analytical methods to analyze FRAP data.

2.4.3.3 Confocal microscope

Figure 2.14 presents the light path in a wildfield microscope and a confocal microscope. In an epifluorescence (widefield) microscope due to light excitation, not only the focal plane will be excited but also planes above and below the focal plane (out-of-plane objects) will consider during the excitation, and the resulted images are including an unfocused background. Epifluorescence microscope is applicable for imaging thick (over 10µm) samples.

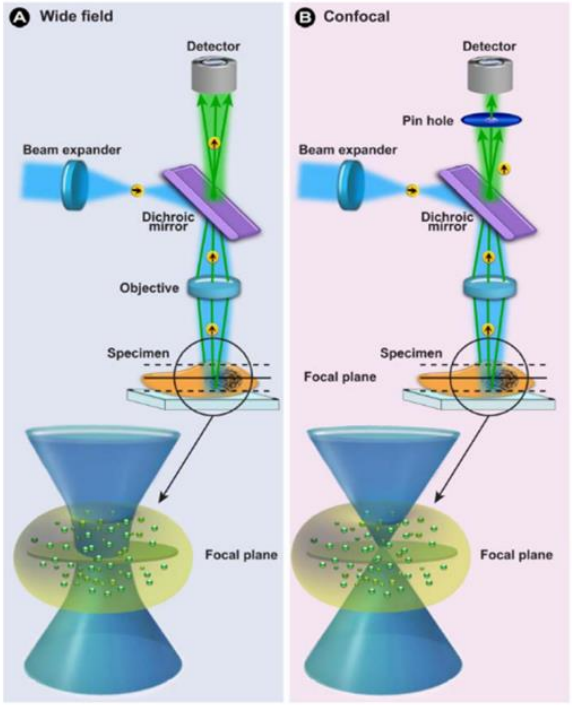

Figure 2.14 A light path in the widefield microscope and confocal microscope

The blue light shows the excitation light and the green light indicates the emitting light in both epifluorescence microscope (a) and confocal microscope (b). (a) The light beam pass through a dichroic mirror through the objective excites the sample which then emits fluorescence that passes through the dichroic mirror and is detected by the camera. (b) The excitation path is similar to the one for epifluorescence, but before being detected the emitted beam passes through a pinhole to block the out-of-plane signals (From [110]).

The confocal microscopy technique overcomes some limitations of the fluorescence imaging resolution. Confocal laser scanning microscopy (CLSM) or (LSM), by adding a pinhole after the dichroic beam splitter (Figure 2.15) between the detector tube and the focusing lenses eliminate out-of-plane signals. It provides a physical barrier and out of focus light is blocked. The pinhole only let the light from the focal plane to pass and be detected.

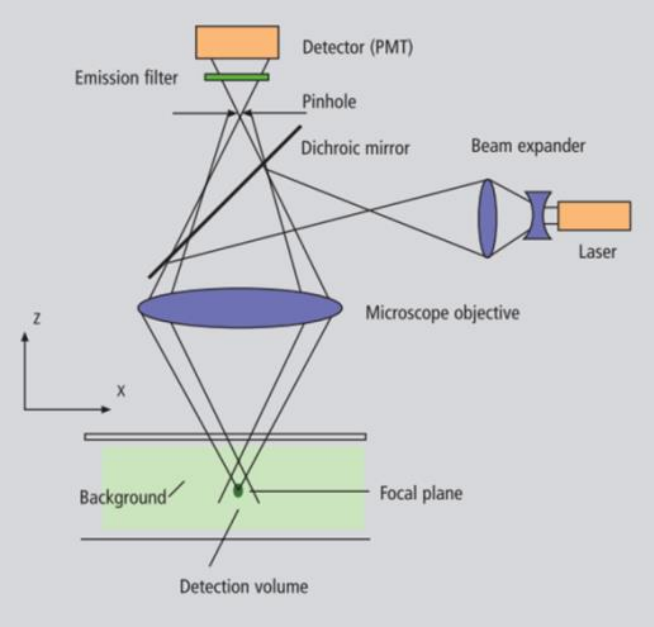

Figure 2.15 A beam path on an LSM

In an LSM a laser beam is focused onto the specimen (light green) via passing through an objective. The fluorescence excited from the specimen is collected via objective. The interesting wavelength of the fluorescence excited light is selected by an emission filter. Between the emission filter and Dichroic mirror, there is a pinhole to block the light coming from planes below and above the focal plane. (From Operating Manual of LSM microscopy (ZEN 2010).)

Via confocal microscope, the reconstruction of a 3D image is feasible by imaging consecutive two-dimensional images in different focal planes. Based on the Rayleigh criterion ($d=\lambda/2NA$) the minimal distance (d) to distinguish between two light spots is defined as the ratio of the optical wavelength (λ) over the numerical aperture (NA) of the objective. The largest value for numerical aperture in highly corrected microscope objectives is between 1.3 to 1.6; which leads to a minimum distance of 200 nm to distinguish two different visible light spots. Compared to widefield microscopy (common fluorescence microscopy), confocal microscopy is capable to record only in-focus or in-plane signals with the option of depth selectivity and improve the signal-to-noise ratio (SNR). In this project two different confocal microscopes are applicable. Laser scanning

confocal microscope (LSM 880, ZEISS) and spinning disc confocal inverted microscopes (Ti-Eclipse, Nikon). The advantage of a spinning disc confocal microscope is that it has a disc with a series of pinholes and instead of having only one pinhole detecting the light (as in LSM), a series of pinholes scan the light over a specific region. The pinholes move parallel over a small area for a longer time to scan the light illumination from the sample during taking fluorescence images and prevent photo-toxicity.

2.4.3.4 Fluorescence labeling of the cell cytoskeleton

The challenge to study cytoskeleton structures is to visualize them without altering their function. Depending on the aim of the research different approaches are available for visualization. The most commonly used approaches are live cell transfection and immunofluorescence [123] in fixed cells. Several traditional fluorescent protein transfection techniques have been employed to deliver a gene into living cells to label specific proteins. Non-antibody fluorescent reagents to label a specific structure in living cells have been limited to few structures such as nucleus labeled with 4′,6-diamidino-2-phenylindole (DAPI) and cell membrane labeled with Wheat Germ Agglutinin (WGA). In this work, I focused on actin fluorescence imaging in living cells in order to understand and study actin dynamics. Actin visualization is achievable with actin probes such as phalloidin (in fixed cells), LifeAct, SiR-actin, tagged actin, green fluorescence protein (GFP)-actin. Despite, Riedl et al. in 2008 suggested LifeAct as a universal marker for actin imaging, [124] there are several limitations to use it as a marker to measure actin dynamics via FRAP. LifeAct labels actin filaments [124], furthermore, LifeAct components can inhibit actin assembly and actin filament elongation, and it can also promote actin filament nucleation [125]. Therefore, LifeAct fusion proteins may modify the initial structure of actin and are not applicable to label actin to measure actin dynamics. Phalloidin in living cells affects actin filaments depolymerization and results in actin stabilization. Furthermore, it is only used to labeled actin filaments in fixed cells. As actin has to be labeled with a FRAP-compatible molecule, I excluded LifeAct and phalloidin to label actin, with an emphasis on use for FRAP measurement. A convenient reagent to probe actin should have a minimum effect on actin dynamics; i.e. actin polymerization and depolymerization cycles. By evaluating actin visualization probes [126-128], I found that GFP-actin and BacMam gene delivery systems (a Baculovirus coupled with a Mammalian promoter) are reliable labeling for actin FRAP measurement. CellLight BacMam 2.0 actin GFP labels the N terminus of β-actin in G-actin. BacMam

gene delivery system is a transduction method and is used as a tool for protein production [127, 129]. Recently it was modified for fluorescence microscopy and imaging a wide range of subcellular structures [127, 130, 131]. A recombinant Baculovirus provides efficient GFP gene delivery into mammalian cells to express and produce protein structure. BacMam transduction is an easy-to-use, economical and efficient method. Besides, actin BacMam transduced cells probe sufficient fluorescence density for FRAP measurements and microscopy imaging. Therefore, the BacMam gene delivery system was used as a convenient and reliable method to label actin.

The direct/indirect immunofluorescence staining methods in fixed cells are also explained here briefly. Immunofluorescence is a staining method using antibodies. The fluorescence can be direct or indirect. Direct immunofluorescence uses a single-fluorophore-conjugated antibody recognizing directly the target protein [123]. Indirect immunofluorescence uses a primary and secondary antibody (Figure 2.16). The primary antibody recognizes the target protein and the secondary antibody is conjugated to a fluorophore and recognizes the primary antibody.

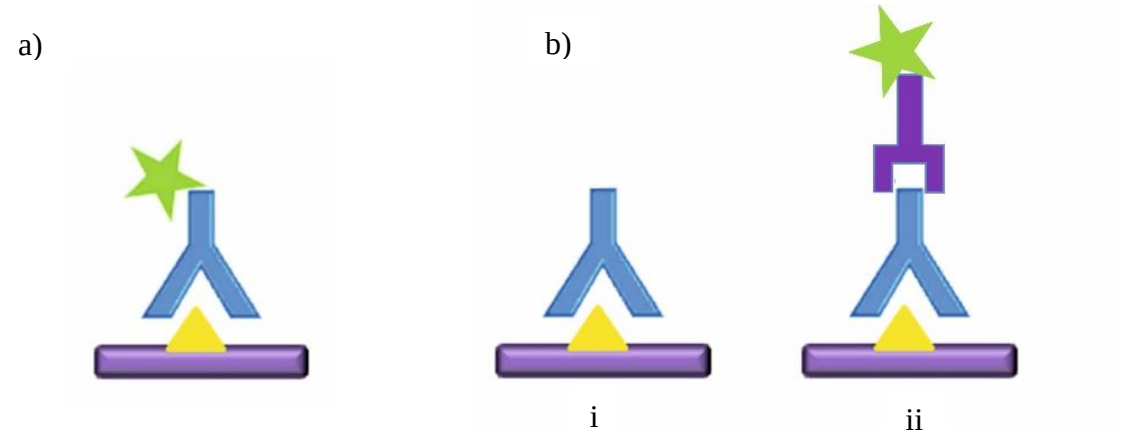

Figure 2.16 Schematic of a direct and an indirect immunofluorescence method

a) Direct immunofluorescence technique, the yellow color indicates the target protein, the primary antibody (in blue) and the fluorophore conjugated to the antibody (in green). b) Indirect immunofluorescence method; (i) a primary antibody (in blue) recognizes the target protein and (ii) one or more secondary antibodies (in purple) conjugated to a fluorophore (green) recognizes the primary antibody (Adapted from [123]).

2.4.4 Traction force microscopy

The principle of traction force microscopy (TFM) technique is based on measuring the force that is applied by an object to a soft surface [132-134]. There are three common methods to determine cell traction force. 1- Embedding cells in a gel disk. 2- Seeding

cells on top of arrays of elastic micropillars. 3- Seeding single cells on the top of a continuous elastic substrate. The third method using continuous elastic substrate is explained here (Figure 2.17). Once cells attach and spread on top of the substrate, they exert traction forces due to actomyosin contraction and retraction, and actin polymerization. Then they transmit those forces to the ECM via focal adhesion (integrin). The surface tension and deformation applied by the cells to the surface are visualized by the displacement of fluorescence beads embedded in the surface. To quantify bead lateral displacements, the particle image velocimetry (PIV) method is used. PIV is based on tracking every single individual bead when cells are adhered and after detachment. PIV is a method commonly used to measure the velocity of fluids. In this method the visible (fluorescence) particles are embedded within the fluid and it is assumed that the motion of the particles indicates the speed and the direction of the fluid.

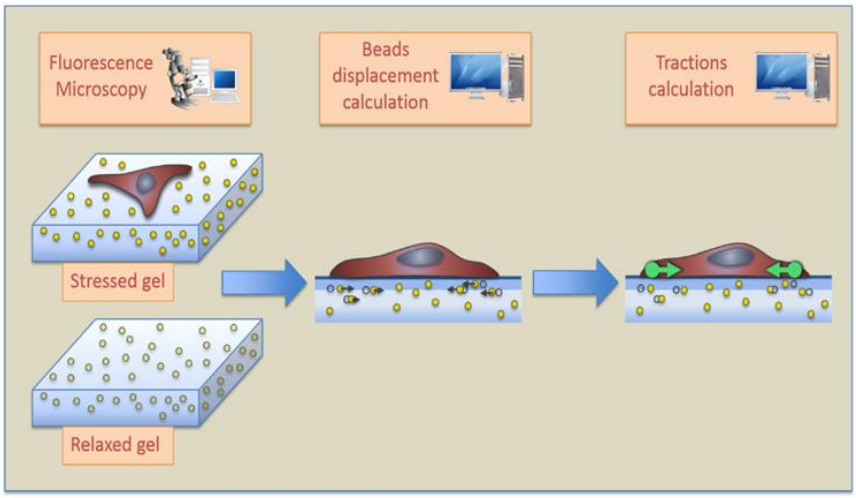

Figure 2.17 TFM technique

A scheme of TFM experiment. The cell exerts traction forces on the surface (stressed gel) and results in fluorescent beads displacement. The traction forces are calculated by monitoring the displacement of the beads from their positions in the stressed and relaxed gel. The yellow circles show fluorescent beads, the black and green arrows show respectively the bead displacements and traction forces (From [135]).

The particles should be sufficiently small (the diameter varies from 10 to 100 nm) to follow the fluid progress continuously and the particle concentration should enable to identify single particle in each image. The particles used to depend on the fluid viscosity and can be in polystyrene, glass, aluminum or oil. The particles will be imaged during the fluid flow. PIV is not limited to fluid velocity analysis and can be applied to TFM by correlating bead displacement to traction force. To obtain traction force, the Fourier

transform traction cytometry (FTTC) model correlates bead displacements to traction force. Traction force is defined as the force vector divided by the unit area (cross-section area) and it has a unit of stress. TFM was originally performed in cell biology but its potential is not only limited to the measurement of cell traction force but is also applicable to soft matter physics.

3 Materials and methods

3.1 Cell culture and cell types

Cell culture and culture conditions such as passage number, cell culture medium, and split scale are specific on cell lines and very important for their growth. The following cell culture recommendations are general for retinal pigmented epithelial cells (RPE1) to promote their suitable reproduction and proliferation.

hTERT RPE-1 cells were obtained as a gift from Dr. Matthieu Piel laboratory in Paris and vimentin mCherry plasmid (obtained as a gift from Prof. Dr. Harald Herrmann-Lerdon laboratory in Heidelberg) was transfected in our lab to label vimentin filaments. RPE1 vimentin mCherry transfected cells from now will be referred to as RPE1 cells. mCherry is a monomeric red fluorescent protein (RFP) that is derived from *Discosoma sea* anemones and transfected to the cells to tag specific proteins into the cells.

3.1.1 Cell culture

Immortalized RPE1 cells were cultured in Dulbecco´s Modified Eagle Medium (DMEM/F-12) (Gibco) supplemented with 10% fetal bovine serum (FBS) (Gibco); 1% GlutaMAX (Gibco) and 1% antibiotics (i.e., penicillin/streptomycin (Gibco)). This mixture will be referred to as complete DMEM/F-12. Flasks (either T25 or T75) and well-plates are the most common growth substrates used for culturing RPE1 cells. In general, there are two ways to grow cells in culture, either a monolayer of cells cultured on an appropriate substrate (adherent culture) or free-floating cells in a culture medium (suspension culture). Many adherent cell lines can be adapted to be in suspension for hours. RPE1 cells grow in monolayer by adhering to the substrate. Cells were incubated in a humid cell culture incubator with 5% CO_2 at 37 °C. Before starting cell culture, the complete DMEM/F-12 and the Trypsin were warmed up at 37 °C in a water bath. RPE1 cells double in a period of time of 19 h to 27 h. When the RPE1 cells were seeded with a 15% confluence, they reach 100% confluence after three days. To dilute the cells the old medium was sucked out and rinsed once with 1 mL Dulbecco's phosphatebuffered saline (DPBS) (Gibco) without calcium and magnesium. The cells were resuspended (detached from the cell culture flask) by using 1 mL prewarmed Trypsin (Ethylenediaminetetraacetic acid) EDTA (0.25%) (Gibco) and the flask was incubated for 5 min. The cells were observed under the microscope to check the detachment and were counted with a counting chamber (e.g. Malassez chamber (BLAU BRAND)) or an

automated cell counter. 15% of the cells were diluted in 5 mL of fresh prewarmed complete DMEM/F-12.

3.1.2 Freezing cells

Cell culture and extraction from the tissue is expensive and time-consuming. Therefore, it is important to conserve and freeze cells for long-term storage. As soon as thawing a new vial of cells, a high concentration of them should be frozen in the low passage and be kept for long-term storage. To freeze the cells, adherent cells were resuspended via Trypsin and centrifuged at 180 g for 5 min and the supernatant was sucked out. The cells were mixed in an appropriate cold freezing medium. The freezing medium for RPE1 cells is complete DMEM/F-12 containing 10% dimethylsulfoxide (DMSO), a cryoprotective agent. The sterile cryogenic storage vials were labeled (i.e., date, cell line, passage rank, number of cells) and 1 mL of cells (containing 5×10^5 cells) was distributed in each vial. The isopropanol chamber containing the cryovials was stored at -80 °C for 24 h. Isopropanol chamber contains isopropyl alcohol that controls the rate of freezing and let the cells freeze slowly (-1 °C.min^{-1}). One of the vials was thawed and cultured for one or two days in parallel with the previous culture. If both batches of cultured cells have the same growth rate and the same cell shape, the rest of the cryovials were transferred into liquid nitrogen for long-term storage.

3.1.3 Thawing cells

As the cell passage number may influence the results of an experiment, it is highly recommended to not use cells with a high passage number. To thaw a new cryovial containing RPE1 cells, a vial from liquid nitrogen was transferred to a water bath at 37 °C for < 1 min. The cells were diluted in prewarmed complete DMEM/F-12 and centrifuged at 180 g for 5 min, to separate the cells from the freezing medium containing DMSO (cytotoxic at high concentration). Cells were mixed gently with 5 mL fresh complete DMEM/F-12, were transferred in a cell culture flask and were incubated at 37 °C, 5% CO_2.

3.2 Transfection

3.2.1 Vimentin siRNA

Vimentin filaments were knocked down using the siRNA transfection technique. To generate vimentin knock down RPE1 cells, 10^5 cells per well were distributed in a six-well plate with 200 µL of master mix. The master mix is defined as the mixture of 10 µM vimentin siRNA (life technologies, Ambion, s14799) diluted in 100 µL serum-free

DMEM/F-12 and 4 µL Lipofectamine RNAiMAX Reagent (13778-075 Invitrogen) diluted in 100 µL non-complete DMEM/F-12. The master mix was incubated for 10 min to 15 min at room temperature before being added to the cells. The wells were filled with DMEM/F12 to reach a final volume per well of 2 mL and they were incubated for 24 h. On the second day of transfection (after 24 h), the spent medium was exchanged with fresh complete DMEM/F-12 and was incubated for 48 h. The transfection steps were repeated on day 4 (three days after the 1st transfection). The spent medium was exchanged again with fresh complete DMEM/F-12 on day 6. The transfected cells were ready for measurements on day 7. Control cells were transfected simultaneously with scrambled siRNA (Silencer Select Negative Control #1 siRNA (life technologies, Ambion)). The scrambled negative control siRNA cells are called negative control cells in the following sections.

3.2.2 Plectin siRNA

To silence the plectin gene in RPE1 cells several siRNA concentrations and incubation times were investigated. Plectin siRNA transfection protocol was similar to vimentin siRNA transfection except that plectin was silenced only once.

To produce plectin knock down cells, RPE1 cells were resuspended with 0.25% trypsin EDTA and distributed in a six-well plate on day 1. 10^5 cells were seeded in each well and were transfected with 10 µM plectin SiRNA (life technologies, Ambion, Pre-designed siRNA ID: 144451). 10 µM plectin siRNA were diluted in 100 µL serum-free (non-complete) DMEM/F-12 in a sterile Eppendorf with a capacity of 1.5 mL (falcon A). In another sterile Eppendorf, 4 µL Lipofectamine RNAiMAX Reagent was diluted in 100 µL serum-free DMEM/F-12 (falcon B). Then falcon A and B were mixed and incubated for 10 min to 15 min at room temperature. Next, the mixture of vimentin siRNA and Lipofectamine was added to the cells and incubated for 48 h. On day 2, plectin siRNA transfected cells were incubated with the fresh complete DMEM/F-12 for 24 h. Control cells were transfected simultaneously with scrambled siRNA (Silencer Select Negative Control #1 siRNA (life technologies, Ambion)).

3.3 BacMam gene delivery system

The volume of CellLight BacMam (V_{BacMam})is defined as:

$$V_{BacMam} = n \times PPC/10^8$$

where n is the number of cells, PPC is the number of particles per cell, and 10^8 is the number of particles per mL of reagent.

The cells were rinsed with 1 mL of DPBS and were detached from the surface with 1 mL of Trypsin_EDTA 0.25%. 10^4 cells were counted and seeded in a glass-bottom dish. The cells were incubated for 4 h to 6 h to let them attach to the surface. Then the spent medium was sucked out, the cells were rinsed with 500 µL DPBS and were diluted with 2 mL complete DMEM/F-12. The CellLight Reagents BacMam 2.0 GFP (Thermofisher (C10582)) were mixed gently (do not vortex) into the vials and the appropriate volume of CellLight BacMam was then added to the cells and the cells were incubated for 40 h.
For example, I considered 10^4 cells with a PPC of 40, the appropriate volume of CellLight BacMam was 4 µL.

3.4 Cell fixation and immunofluorescence staining

The cells were rinsed with 1 mL of DPBS and were detached from the surface with 1 mL Trypsin_EDTA 0.25%. Next, the cells were counted and 10^5 RPE1 cells were seeded overnight on top of a coverslip (of 22 mm in diameter and 0.16-0.19 mm in thickness, (#1.5)) in a six-well plate. The number of cells seeded depends on the size of the coverslip, the cell growth factor, and the incubation time. The medium was then sucked out and the cells on the coverslip were rinsed three times with DPBS. It is recommended to transfer the coverslip to a new well (the side with cells should be top). Under the chemical hood, 500 µL Paraformaldehyde (PFA 4%) (Alfa Aesar (ThermoFischer (Kandel) GmbH,43368)) diluted in DPBS was added on top of the coverslip and was incubated for 10 min at room temperature under the chemical hood. All the incubation times should be considered precisely to avoid damaging the cell membrane and to keep the structure intact. The fixed cells on the coverslip were washed out three times (for 5 min) with DPBS. Pipet tips contaminated with PFA should be discarded in a separate trash bin. The wasted PFA should be sucked out and transferred to a separate container for hazardous liquids. 500 µL of 0.5% Triton X-100 (SIGMA (93426)) diluted in DPBS was added on top of the coverslip and incubated for 5 min at room temperature to permeabilize the cell membrane. The coverslip was washed out 3 times (for 5 min) with DPBS. The unspecific binding-site was blocked with 1 mL of 3% Bovine Serum Albumin Fraction V (BSA) (PanReacAppliChem (A1391)) diluted in DPBS at least for 60 min at room temperature. The antibody was diluted in 3% BSA. The optimal antibody concentration is a parameter that is achieved by practice. For a first trial the datasheet recommendation should be followed. The inner part of the lid of a petri dish was covered with parafilm and the whole petri dish was covered with aluminum foil. A drop of 50 µL

to 80 µL of the diluted antibody was put on the parafilm and the coverslip containing fixed cells was put upside down on the diluted antibody. The coverslip was incubated overnight with the primary antibody at 4 °C. The next day, the coverslip was washed out 3 times for 5 min with distilled water to avoid crystallization of DPBS which will interfere with the imaging in the case of direct immunofluorescence. In the case of indirect immunofluorescence, the primary antibody was washed 3 times with DPBS, and the cells were put into contact with the secondary antibody for at least 2 h before being rinsed 3 times with distilled water. In both direct and indirect immunofluorescence, after rinsing with distilled water, the coverslip was mounted with a mounting medium with/without DAPI (Fluormount-G^{TM} Invitrogen) on a microscopy slide (MENZEL-GLÄSER). Before imaging, the mounting medium dries overnight at room temperature.

List of the antibodies and reagents and their respective concentrations:

- Alexa Fluor®647, dilution 1:200, for plectin staining,
- Phalloidin-iFluor 488 Reagent/ 594 Reagent, dilution 1:1000, for actin staining,

Fluorescence images were indicated by using a fluorescence microscope with the proper filters. Immunofluorescence images were analyzed using the image processing software ImageJ (Fiji).

3.5 Gel staining and Western blot

3.5.1 Protein extraction

Cells were detached from the surface with Trypsin EDTA 0.25%., diluted with DMEM/F12, and counted. 10^6 cells were centrifuged at 180 g for 3 min.

All medium was sucked out and rinsed 3 times with DPBS. The cells were lysed, under a chemical hood, in 100 µL of 4X Laemmli buffer, which contains β-mercaptoethanol, considered as toxic. The lysed cells were incubated at -20 °C for long-term storage or used directly for WB.

3.5.2 SDS gel electrophoresis and protein transfer

The preparation of the gel was performed in two steps. First, the preparation of the separating gel (12% concentration) and the preparation of the stacking gel (5% concentration).

3.5.2.1 Separating gel

The amount of the gel solution and the gel concentration were respectively 10 mL separating (resolving) gel with 12% concentration (see Table 10.7). The gel concentration depends on the molecular weight of the protein of interest. The smaller the protein the

higher the gel concentration. For detecting and separating actin, myosin, vimentin, and Glyceraldehyde 3-phosphate dehydrogenase (GAPDH) proteins with molecular weights ranging from 20 kDa to 70 kDa, 12% gel concentration is required. In the literature, it has been shown that for plectin of a molecular weight of 500 kDa, a 6% gel concentration is required. To separate proteins with a large difference in their molecular weights, it might be necessary to prepare a gel with a gradient of concentrations. The gel is completely polymerized after 15 min therefore, it is required to prepare all the reagents before preparing the gel solution. The gel cast was adjusted and was filled with water to verify whether it is not leaking. The water was removed by turning the cast upside down. It is recommended to prepare two gels in parallel one to transfer the proteins from the gel to the blotting membrane and another one to stain the gel with Bio-safe Coomassie G-250 Stain after the electrophoresis as a control for protein separation. The components following the order presented in Table 10.7 were mixed and vortexed for 10 s. The separating gel solution was pipetted into the gel cast. Two centimeters of the top of the cast were left empty to add the stacking gel solution. The gel cast was filled up with ethanol to avoid ruffles on the edge of the gel. During gel polymerization the cast was left in a smooth place. After polymerization, ethanol was removed, and the stacking gel was added. To know when the gel is polymerized, the rest of the gel solution in the falcon tube was checked.

3.5.2.2 Stacking gel

See Table 10.8 for the actual volume of the components.

The components were mixed and vortexed for a few seconds. A sufficient amount of stacking gel solution (3 mL) was added into the cast on top of the polymerized separating gel; a 10-well gel comb was immediately placed into the cast containing the stacking gel solution.

3.5.2.3 Electrophoresis

Following the gel polymerization, the cast containing the gel and the comb was transferred from the polymerization chamber to the electrophoresis chamber. In this step, it is possible to wrap the cast and its component in a wet paper and cover it with cellophane to avoid drying and incubate it overnight at 4 °C. The cast containing gel and comb was installed in the electrophoresis chamber and the chamber was filled with running buffer up to the marked point. Running buffer was added between 2 packed glasses to fill it entirely. Next, the gel comb was removed. Proteins (the cells lysed with

Laemmli buffer) were denatured for 5 min to10 min at 100 °C in a dry bath. 10 µL of molecular weight marker (PageRuler Prestained Protein Ladder) was pipetted to the first lane. 20 µL/lane of the proteins were loaded into the gel. PowerPacTM HC was connected to the electrophoresis chamber and was run at 70 V/ 300 mA to make the proteins pass through the stacking gel. Then the voltage was raised to 150-200 V/ 300 mA. The electrophoresis was followed by the height of the molecular weight marker and the bromophenol blue. The experiment was running until the bromophenol blue reached the bottom of the chamber. During the electrophoresis, 1 L to 2 L of transfer buffer was prepared and cooled down at 4 °C.

3.5.2.4 Gel staining

Bio-safe Coomassie G-250 Stain is a protein that stains the system to determine the protein concentration in an SDS gel or a solution. The Coomassie dye contains sulfonic acid that binds to proteins in the SDS gel via Van der Waals's attraction and creates ionic interactions between amine groups of the proteins and the sulfonic acid. The Coomassie staining is used to detect proteins whose amount is > 0.5 µg. Following the electrophoresis, the cast was displaced, and the gel was transferred to a plastic or a glass dish. The gel was washed out 3 times with water for 5 min each time, was soaked in Bio-safe Coomassie G-250 Stain and was incubated at room temperature for 1 h. After staining, the gel was washed out with water for 1 h. After destaining the gel with water, all the protein bands were detectable using a WB imaging system (FlourChem Q).

3.5.2.5 Transferring

A transfer system, including a transfer cassette and a transfer chamber, is required to transfer the proteins from the gel to the nitrocellulose blotting membrane. To prepare the transfer cassette (positive pole, filter paper, membrane, gel, filter paper, negative pole) the nitrocellulose membrane was cut in the size of the gel. It was then immersed in 100% methanol or ethanol was soaked in ultrapure water and was plunged into the transfer buffer. The filter papers and sponge support pad were submerged in the transfer buffer. The gel cast was opened carefully and soaked in the transfer buffer to easily remove the gel. A sponge support pad was placed onto the positive pole of the transfer cassette, the blotting paper, the membrane and gel were placed over the sponge respectively. The second blotting paper was placed on the top of the gel and the second sponge support was placed over the blotting paper. The air bubbles of the system were removed, the cassette

was closed, and placed in the transfer chamber. Figure 3.1 displays the order of the transfer cassette.

Figure 3.1 The order of the transfer cassette in WB.

The cathode (-) and anode (+) plates are placed in the sides and the sponge support pads, filter (blotting) papers, nitrocellular membrane and the SDS- PAGE gel is placed in between, in the order shown in the figure. (From [136])

The transfer chamber was filled with an appropriate transfer buffer to cover the transfer cassette completely. PowerPacTM HC was connected to the transfer chamber and run at 100 V for 1 h at 4 °C. This system is called wet transfer and is used to transfer proteins with a size of 20 kDa to 100 kDa. To transfer the proteins with a bigger size such as plectin (≈ 500 kDa) the system is run at 37 V for 12 h at 4 °C.

3.5.3 Western blot

Membrane blocking

To avoid the non-specific binding of antibodies to the membrane, the membrane was incubated in a blocking solution including 3-5% BSA diluted in 50 mL TBST (TBS 1X +Tween 20 0.1%) for 1 h to 2 h at room temperature on the shaker (neoLab).

Incubating with antibodies

Following the blocking procedure, the membrane was transferred to a box covered with aluminum foil. Appropriate antibody diluted in 3-5% BSA was added in a box and incubated at 4 °C overnight. The membrane was washed out with TBST 3 times for 10 min. If the secondary antibody is necessary, then it was added and the membrane was incubated overnight with a control antibody such as GAPDH at 4 °C. It is necessary to wash out the membrane with TBST 3 times for 10 min after incubation with any antibody.

List of the antibodies and their concentrations:

- Vimentin V9 AlexaFluor®647 (sc-6260, Santa Cruz Biotechnology), dilution 1:500,
- Plectin (10F6) Alexa Fluor®647 (sc-33649, Santa Cruz Biotechnology), dilution 1:200,
- GAPDH (0411) Alexa Flour®488 (sc-47724, Santa Cruz Biotechnology), dilution 1:500, control staining.

3.5.4 Data analysis

The WB imaging system (FlourChem Q) was used to take images of the blot or the gel. To acquire the images the membrane or the stained gel was loaded and a preprogrammed protocol was selected (depending on the fluorophore, and on the wavelength of the antibodies). After scanning the membrane or the stained gel via the WB imaging system, direct analysis using the AlphaView program or with Fiji was performed (See 11.2 for data analysis in Fiji).

3.6 Real-time quantitative polymerase chain reaction

To quantify plectin mRNA by qPCR, $5*10^5$ RPE1 cells were transferred to the RNase-free centrifuge tube. The spent medium was discarded, and lysis buffer was added to lyse the cells. A rotor-stator homogenizer was used to homogenize the lysed cells. In order to isolate and purify the RNA, the PureLink RNA Mini Kit (Life technologies, 12183018A) was used. Following the RNA purification, the Rnase-Free Dnase Set (50) Kit (Rneasy/QIAamp Columns) QIAGEN Kit was used for digesting and removing genomic DNA (gDNA) in RNA solution. To clean up the RNA, the PureLink RNA Mini Kit was employed. To synthesize efficiently the first strand of cDNA from RNA the RevertAid First Strand cDNA Synthesis Kit (Thermo Scientific, K1621) was used. This kit can be directly used as a template in qPCR. The amount of RNA was quantified and speculated 100% of RNA was transcribed to cDNA. cDNA Forward primer and reverse primer sequences were designed using the tool called Primer BLAST for finding specific primers, for plectin 1b isoform are introduced below (for more details see 11.3.1):

Forward primer CACCAAGTGGGTCAACAAGC
Reverse primer CCAGCAGGGAGATGAGGTTG

qPCR was running with 216.3ng/µL and 61.5ng/µL cDNA concentrations purified from two different experiments, the 1 µM, 2 µM and 5 µM concentration of each gene-specific primer. GAPDH forward and reverse primers were used as an internal control and a standard or reference gene in order to quantify the specific genes. GAPDH plays a role as a housekeeping gene. Housekeeping genes (such as actin or GAPDH) are genes that are expressed in all cells under a normal condition. GAPDH primers were supplied at Leibniz institute for new material (INM) from Dr. Annette Kraegeloh Laboratory in Saarbrücken Germany. iTaq Universal SYBR Green Supermix (Bio-RAD, 172-5121) was employed to run qPCR. The qPCR reaction protocol was run at a standard ramp speed with thermal cycling conditions cited in Table 3.1. Data were analyzed with the Bio-Rad CFX Manager software.

Table 3.1 qPCR thermal cycling conditions

Stage	Order	Temperature (°C)	Time
Holding	1	95	30 min
Cycling (40 cycles)	2	95	5 s
	3	60	30 min
	4	Plate read and go to 2	
Melting curve	5	65 to 95	5 s
	6	Plate read	
	End		

3.7 Evaluation of actin SF bundle thickness

To evaluate the actin bundles thickness the images taken from FRAP measurements were imported to the Fiji software. A line with a length of 3 µm was drawn perpendicularly to the actin SF in the bleached ROI (Figure 3.2 (a)). Under *Analyze/ Plot Profile* the fluorescence intensity of the SF was measured before bleaching, and the data were imported to the OriginLab Software. The fluorescence intensity profile was plotted (Figure 3.2 (b)) and the curve (black) was fitted with a normal Gaussian function (red), the pink arrow shows the distance of the perpendicular line in the image (a), the purple arrow is the Gaussian full width at a tenth of the maximum (FWTM) grey value and corresponds to the thickness of the actin SF bundle.

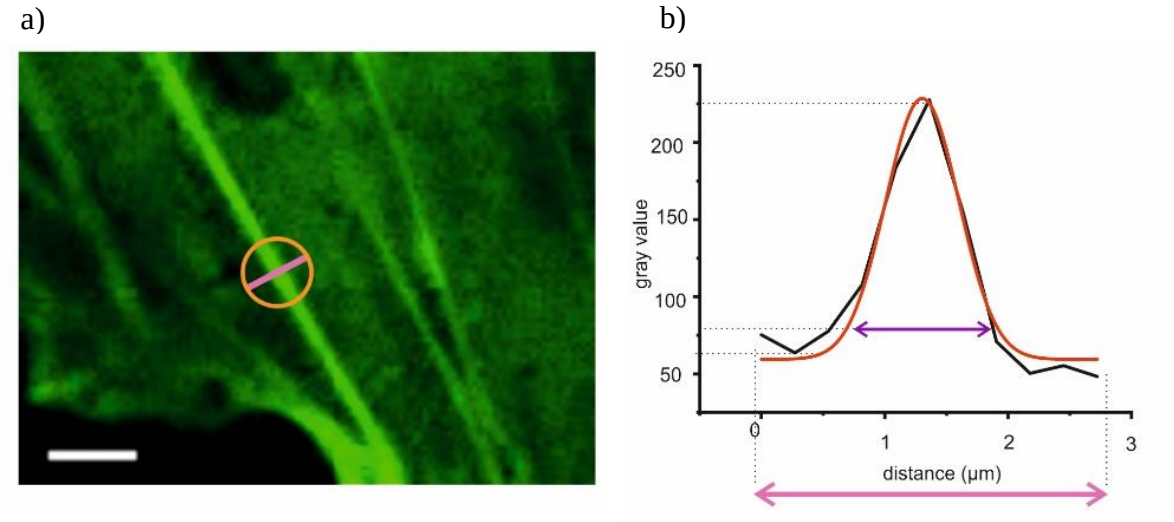

Figure 3.2 Evaluation of actin bundles thickness.

a) Actin SF fluorescence image. The SF is bleached in the ROI whose shape is a circle of diameter 3 µm. The fluorescence intensity is measured along the line perpendicular to the actin SF. b) Actin SF fluorescence intensity curve (black) fitted by Gaussian function (red), pink arrow shows the length of the perpendicular line in the image (a), the purple arrow is the Gaussian FWTM parameter corresponding to the actin SF bundles thickness. Scale bar: 5µm.

3.8 Fluorescence recovery after photobleaching

FRAP method is mainly appropriate to any experiment in which proteins bind to any cellular organelles such as membrane, cytoskeleton, and nucleus. The FRAP measurement was used here to measure F-actin dynamics in SFs and cortex and cytoplasmic actin dynamics, in vimentin depleted, plectin depleted and negative control cells. The method explained here is the same for the preparation of the control samples and the siRNA transfected samples.

3.8.1 FRAP measurements in stress fibers

Two confocal microscopes were used during this project to apply FRAP on actin SFs. 1- Confocal spinning disk inverted microscope (Ti-Eclipse, Nikon) 2- Laser scanning microscope (LSM 880, ZEISS). The Table 11.1 and Table 11.2 present the microscopy setting for the LSM and the spinning disc respectively. The majority of the FRAP measurements were performed with the LSM whose settings are explained in detail here.

A 63x oil immersion objective with a numerical aperture (NA) of 1.4 was used to avoid scattering of the laser line and keep its cylindrical shape. A frame of 128*128 pixels in size with a pixel size of 0.20 µm and 8 µs pixel dwell time was employed for image acquisition. The pixel dwell time (dwell time per pixel) is the time that the laser will illuminate a single pixel. Before bleaching 5 images were acquired with a frame rate of 1 s. Images were taken with 2% of the maximum power of the laser line of Argon Laser

(wavelength 488 nm). A circular ROI of 2 µm in diameter was chosen as a bleached ROI. 100% of maximum power (30 mW) of the laser line of a diode laser (405 nm) was applied to the bleached ROI with 5 to 10 iterations and 20 µs to 60 µs pixel dwell time. I acquired 80, 94 and 240 post bleaching images for a time interval of 1 s. The recovery curve reaches its plateau value after approximately 80 images. I excluded the data obtained after 94 postbleaching images and applied the analysis and the mean value calculation and statistical test to all data including data from either spinning disk microscope or LSM. As mentioned in (3.1 Cell culture and cell types) for all FRAP experiments and measurements I used RPE1 vimentin mCherry transfected cells. In vimentin silenced cells before applying FRAP measurements; the level of silencing was evaluated. To examine vimentin fluorescence an image was taken with 2% of the maximum power (2mW) laser line of HeNe 594 nm Laser.

Due to the slight cell migration in most of the FRAP measurements, after 90 s imaging during the postbleaching, the bleached area moves according to the cell movement in any direction. It was not always feasible to take images of the SF bleached area for 3 min during the postbleaching recovery. But the few images that were taken successfully to the end of 240 postbleaching images with a time interval of 1 s (3 min in total) indicated the equal plateau value the same as 94 postbleaching images (Figure 3.3). Data processing was performed by using the fluorescence intensity of the 94 postbleaching images.

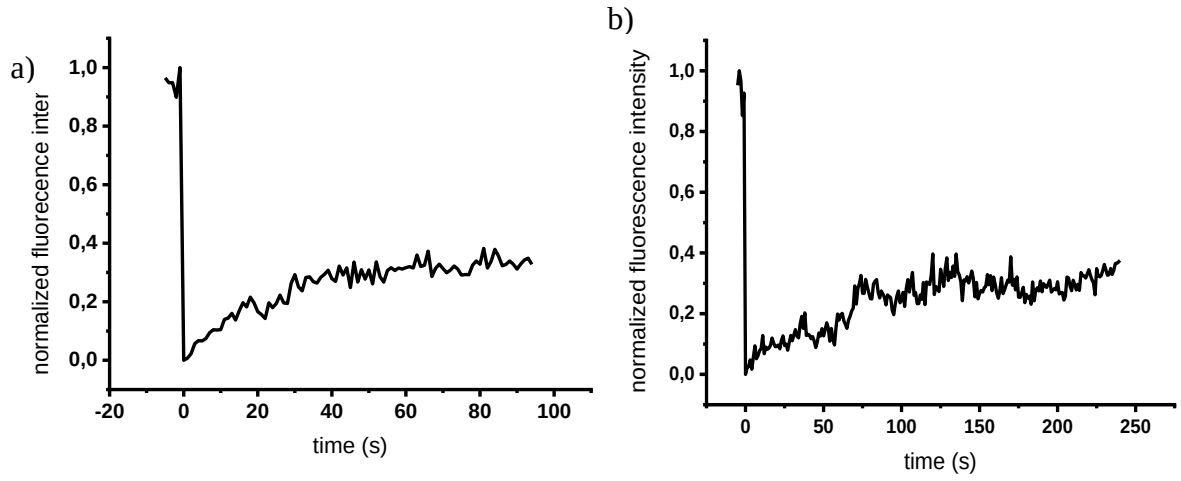

Figure 3.3 Fluorescence recovery of actin GFP in 94 s and 240 s.

The fluorescence recovery was monitored for 94 s (a) and 240 s (b) after bleaching. Both curves reach the plateau value after about 60 s.

3.8.2 Measurements of cytoplasmic actin dynamics via FRAP

To investigate the cytoplasmic actin dynamics, the FRAP technique was applied on a circular ROI in the cytoplasm**.** FRAP experiment on cytoplasm is affected by measurement limitation due to greater bleaching time than actin monomer diffusion time in the cytoplasm. Furthermore, by modifying the microscopy settings and experimental design I attempted to reach a bleaching time equal to or less than actin monomer diffusion time. The modified microscopy setting lets us reach a short-duration bleached time of around 50 ms to avoid the cytoplasmic actin turnover occurs before the end of photobleaching. All the procedures of the sample preparation are as same as FRAP measurements of actin dynamics on SFs. In order to obtain a high SNR (>2), and a bleaching time lower than the diffusive time of G-actin, I chose the smallest possible image size.

The smallest possible image size to reach the shortest bleached time was 27 * 27 µm with a pixel size of 0.27 µm with a total pixel dwell time of 6 µs. Images were taken using a 63X oil immersion objective and a 488 nm wavelength laser with a pinhole of 1.58 Airy units. To expose FRAP on actin cytoplasm a higher laser power (50 mW) with a 405 nm in wavelength and 3 iterations and 2 µs pixel dwell time was applied to a circular ROI with 2 µm in diameter on actin cytoplasm of control and vimentin silenced cells. ROI fluorescent recovery was obtained for 60 postbleaching images with a time interval of 30 ms.

3.8.3 FRAP measurements of actin dynamics in cortex in suspended cells

FRAP was applied to the actin cortex according to [120] by fluorescent recovery after photobleaching and photoactivation (FRAPPA, Andor Technology) tool using an inverted microscope (Ti-Eclipse, Nikon). The microscope is equipped with a Yokogawa spinning disc head (CSU-W1; Andor Technology). One to three circular ROIs with 2 µm in diameter were selected in the actin cortex, far from the nucleus. The cells moving out from the selected ROIs during the acquisition were excluded. The ROIs were exposed to 30% of maximum laser power (50mW) with the 488 nm wavelength for imaging and 100% of maximum laser power with 488 nm wavelength for bleaching. Fluorescent recovery of bleached ROIs was acquired 80 to 100 times with a 1 s frame rate.

3.8.4 FRAP data processing

The fluorescence intensity extraction was analyzed with the image processing software ImageJ (Fiji). OriginLab was used for the correction, normalization, and curve fitting.

Halftime recovery and the mobile fraction of actin dynamics in SFs and the cytoplasm in both populations (vimentin depleted and negative control cells) were statistically tested by the *t*-test for independent samples. Halftime recovery and the mobile fraction of actin dynamics in cortex in both populations were statistically tested for the magnitude of the effect using the Hedges'g test. In the Hedges´g test the value of > 0.2 shows a small effect, > 0.5 shows a medium effect and > 0.8 shows a large effect.

3.9 Micro-Patterning

Crossbow micropatterns were printed on glass coverslips. First, the coverslips were washed with 70% ethanol and were activated in a plasma cleaner (UV ozone oven 185 nm, UVO CLEANER, 342-220, Jelight Company Inc.) for 3 min. The activated side was placed on a drop of 50 µL of poly(L-lysine)-grafted-poly(ethylene glycol) (PLL-g-PEG) solution at a concentration of 100 µg/mL and was incubated at room temperature for 1 h. PLL-g-PEG is a hydrophilic molecule used to avoid protein binding at the surface. It was also used to avoid cell attachment to the surface in the suspension phase of evaluating cell volume and measuring actin dynamics in the cortex. The photomask was washed with acetone and rinsed with pure water. A photomask or an optic mask is a plate with a quartz side and a chrome side with transparent patterns designed on it to allow the light to shine through the pattern shapes and expose the PEG layer to the UV light and destroy it. Damaging the PEG chains on the coverslip let the coating proteins bind to the coverslip substrate only on patterns.

The quartz side of the photomask was cleaned by UV light for 5 min. The PEG-side of the coverslip was faced down on the quartz side of the photomask. 5 µL of pure water between the coverslip and the photomask is essential to keep the coverslip tight to the photomask. To destroy the PEG layer on the coverslip and print the specific pattern on it, UV light was illuminated on the chrome side of the photomask for 6 min. Here crossbow patterns with 40 µm, 39 µm, and 5 µm in length, width, and thickness respectively were printed. The coverslip was coated with fibronectin (F1141, Sigma) at a concentration of 25 µg/mL at room temperature at least for 1 h. The coated coverslip was transferred to the sterile hood and was rinsed with DPBS and put in a six-well dish with the patterned side up. Cells were seeded on top of the coverslip and incubated for 4 h to 6 h to let the cells spread completely on top of the patterns.

3.10 Traction force microscopy

A silane solution was prepared fresh (See 11.4.1) and a glass-bottom six-well plate (No. 0 uncoated, P06G-0-20-F, MatTek Corporation) was coated with the silane solution and incubated overnight at room temperature. Measurement has proceeded with PAAm gel with a Young`s modulus of 5.2 kPa. The PAAm gel solution contains 600 mg acrylamide diluted in 5 mL phosphate-buffered saline (PBS), 30 µL acrylic acid, and 2.5 mg N, N'-methylene-bis-acrylamide. Sodium hydroxide (NaOH) was used to adjust the PH of the gel solution at 7.5-8. Fluorescent polystyrene beads (0.25 µL, 1.25: 1000 volume ratio of the gel solution) and ammonium persulfate APS (10% solution, 1:100 volume ratio) and Tetramethylethylnediamine TEMED (1:1000 volume ratio) were added quickly to the gel solution. The gel solution (8 µL/well) was filled in the six-well glass-bottom plate with a coverslip on top to obtain a hydrogel thickness of 70-80 µm. Coverslip was removed after the gel polymerization at room temperature after 10 min. The hydrogel was activated with a solution of 39 mg Dimethylaminopropyl-3-ethylcarbodiimide hydrochloride (EDC) and 12 mg N-Hydroxysuccinimide (NHS) in 1 mL MES buffer for 15 min at room temperature. The PAAm gel was functionalized with RGDFK (Arg-Gly-Asp-D-Phe-Lys) (0.5 mg in 1 mL PBS) overnight at room temperature to promote cell adhesion. Hydrogels were washed twice with PBS and cells were seeded on top of them and were incubated overnight. Fluorescent bead images of the same frame of the under stress and relaxed hydrogel were taken before and after cell detachment respectively. All images were acquired using an inverted microscope (Nikon) with the Intensilight Epi-Fluorescence illuminator light source. A 60X oil immersion objective was used. The microscope is equipped with a chamber (Okolab) that provides a constant temperature at 37 °C, a constant CO_2 level of 5%, and a humidity level of 100%, required for the live-cell imaging. All displacement and traction force calculations, as well as force plots, were performed using the Fiji PIV and FTTC Plugins.

3.11 Measurements of the cell size (suspension and adherent)

To measure the cell volume in adherent cells, 10^5 cells were seeded on a FluoroDish Tissue Culture Dish with Cover Glass Bottom and were incubated for at least 4 h to spread entirely. Cells were transferred to the inverted microscope (Nikon) using the Intensilight Epi-Fluorescence illuminator light source and connected to an Oko-lab incubation chamber adjusted to 37^o C and 5% CO_2. A 60x oil immersion objective with a NA of 1.4 was used. Images were acquired from the bottom to the top of the adherent

cells. The cell area in each acquired image was measured in Fiji by drawing a line around the cell edge. Data was imported in OriginLab. Cell volume was calculated by the mean value of the cell area multiplied by the height.

The suspended cells preparation (the sample preparation) is explained in detail in section 11.1.3 (procedures 1 to 14). After adding suspended cells into the PDMS chambers and covering chambers with the coverslip coated with PLL-g-PEG, the Fluorodish was mounted on the stage of the microscope. The microscopy setting was the same as for adherent cell imaging (above). Bright-field images were taken in a perfect focus condition (high precision focusing, continuously corrected) by imaging the cell from the bottom to the top. Images were saved and imported in Fiji to measure the cell volume. The area of the cell in each Z-stack was measured and the bigger area was selected to measure its diameter. The cell volume was measured using the diameter of the bigger cell area, assuming the cells in suspension have spherical shapes.

The cell volume was plotted in all conditions in separated graphs for suspended cells and adherent cells. All conditions (RPE1 non-transfected (ctrl), RPE1 vimentin mCherry transfected (ctrl mCherry), RPE1 SiRNA scrambled (negative control) (nCtrl), and RPE1 vimentin siRNA transfected (vimentin depleted) (vimSi) cells) were statistically tested with a *t*-test for independent samples.

4 Results and discussion: Actin dynamics

Dynamics is a branch of physics that studies the motion of an object and involves classical mechanics such as force, displacement, velocity, acceleration and momentum. In cells, the polymerization and depolymerization of actin filaments result in actin dynamics. Actin dynamics are important for most cellular activities such as the transition between different structures of actin filaments and have a main role in cell migration and cell division. Therefore, it has been studied for decades using different methods. For example, actin filament motion was studied using time-lapse imaging of actin SFs in living cells during the assembly of actin in SFs to study actin filaments dynamics [64]. Detecting actin filament was also applicable to visualize the conversion of dorsal SFs and transverse arcs to ventral SFs and classify the distinct actin filaments. [64]. They show that actin stress fibers are thinner and fewer in motile cells when compared to nonmotile cells using live-cell image analysis [64]. Thus, tracking the actin filaments is not a proper method for cells to assess the dynamics of actin filament in motile cells. Using FRAP is another technique to study actin filaments dynamics. In the presented project, I studied F-actin dynamics by labeling G-actin and using FRAP to measure the actin turnover rate and the fraction of monomers that are involved in the actin recovery.

4.1 Labeling of G-actin

The challenge to visualize actin structures is to stain the actin proteins without altering their function. Depending on the aim of the study, different approaches are available for visualization. A convenient reagent to probe actin should have a minimum effect on actin dynamics (i.e., actin polymerization and depolymerization cycles). Actin has to be labeled with a FRAP-compatible molecule to study actin dynamics (i.e., BacMam gene delivery system [126-128]). The BacMam gene delivery system is an accurate marker to label β-actin. To achieve an efficient level of actin fluorescence intensity and obtain a high SNR for FRAP measurements, it is important to calculate: (1) the appropriate number of CellLight BacMam particles per cell (PPC); (2) the sufficient incubation time to mix the cells and the BacMam reagent. The proper PPC number avoids a cytopathic effect on cells. 10,000 RPE1 cells were incubated with CellLight BacMam at concentrations of 30 PPC, 40 PPC, and 50 PPC for 24 h, 32 h, 40 h, and 72 h. The evaluation of the fluorescence intensity using *plot profile* in Fiji shows a low SNR for 30 PPC for all the incubated times. A high SNR was obtained in 40 PPC and 50 PPC treated cells after 40 h, but the observation of the cells shows a cytopathic effect on cells treated with 50 PPC and

incubated for 72 h. As a conclusion, the optimal concentration to probe high fluorescence intensity without having a cytopathic effect on RPE1cells is 40 PPC incubated for 40 h.
In order to validate the accuracy of the BacMam staining, cells stained with BacMam were fixed and stained with Phalloidin Red. Phalloidin is a well-known probe to stain actin in fixed cells but is a huge molecule that is not compatible with life experiments. Phalloidin is thus not a candidate to visualize actin during the FRAP experiment. However, it can be used to evaluate its colocalization with the BacMam signal. The merged image of both staining (Fig. 4.1) confirms that BacMam is an accurate marker to label actin on RPE1 cells. In the following section, FRAP experiments were performed on actin stained with BacMam.

a) b) c)

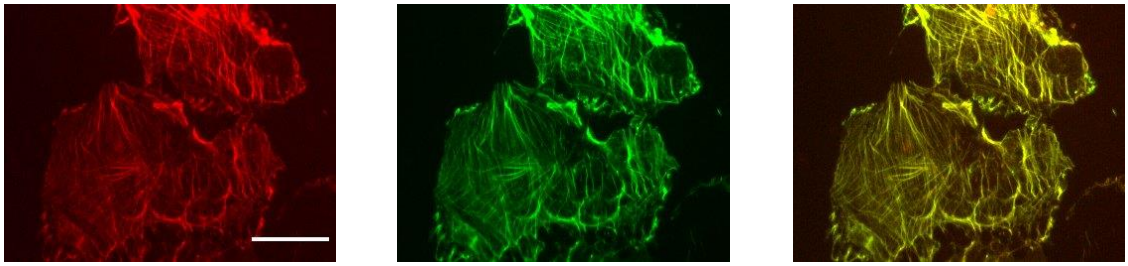

Figure 4.1 Actin labeling

Actin labeled with a) Phalloidin in red and b) BacMam in green. c) The merged image, colocalization of both staining in yellow. Scale:10 µm.

4.2 Actin dynamics in stress fibers

Actin stress fibers are important for the generation of the protrusion and retraction force during cell motility and cell migration in the adherent phase. Polymerization and depolymerization of actin filaments have a critical role in these processes which are influenced by cross-link proteins such as myosin and tropomyosin and other cytoskeleton components. Furthermore, cell migration velocity and cell migration direction are influenced by vimentin deficiency [5] and indicated that vimentin is involved in cell motility and cell migration. Moreover, indicating the interaction between vimentin and actin filaments might help to better understand the cell migration process. Cell geometry is another parameter that is important in cell motility and cell mechanics [137]. Controlling cell geometry using the micropatterning method [138] might be a proper method to have cells in comparable conditions to measure actin dynamics in SFs. Plectin as a cross-linked protein that links IFs to other cytoskeleton components [11] is also involved in cell motility [12], cell stiffness and cell dynamics [139], and it has been

shown that plectin deficiency might affect actin dynamics and impacts cell migration and an overexpression of plectin increases migration and invasion of HNSCC cells [12]. In the presented project, I decided to indicate the contribution of vimentin and also plectin as a vimentin-actin protein cross-linker on actin dynamics in SFs. This would help to understand the interplay between actin and vimentin.

4.2.1 Vimentin contributes to actin dynamics in stress fibers

Several studies revealed the precise turnover rate for many individual purified proteins in *in vitro* and *in vivo* assays [107-109]. However, the protein recovery rate in a confined environment within a pool of proteins (such as in the living cells) is more complicated than *in vitro* assays and requires accurate settings and methods [110]. FRAP measurement is one of the most common methods that overcome the limitation of measuring the biomolecule dynamics in living cells. FRAP measurement probes the exchange speed of biomolecules within the cell and also indicates the ratio of immobilization of proteins that are confined within the large structures such as cytoskeleton filaments [110-114].

In order to investigate the interplay between vimentin and actin filaments, a special focus was put on actin dynamics in SFs in vimentin deficient (knock down, (KD)) cells. Actin monomers were labeled with BacMam gene delivery system (See section 4.1). Vimentin KD cells and negative control cells were produced by transfection technique (See 2.4.1 and 3.2). FRAP experiments were then performed on both vimentin KD and vimentin control cells. FRAP is an appropriate method to measure the F-actin turnover rate and the amount of actin monomers that are involved in the turnover in SFs [140].

4.2.1.1 Measurement of the amount of vimentin in transfected cells

Depleting vimentin in living cells enables us to study its contribution to cellular mechanisms and their interactions with the other cell components, such as actin. In order to determine the implication of vimentin in actin dynamics, vimentin siRNA silenced cells and vimentin scrambled control cells were produced by transfection (See 3.2.1). A first evaluation of the vimentin silencing efficiency was observed with an epifluorescence microscope. The fluorescence images of the vimentin network show a lower fluorescent signal in vimentin KD cells compare to control cells (Figure 4.2). This observation gives a qualitative result of the success of the vimentin siRNA transfection.

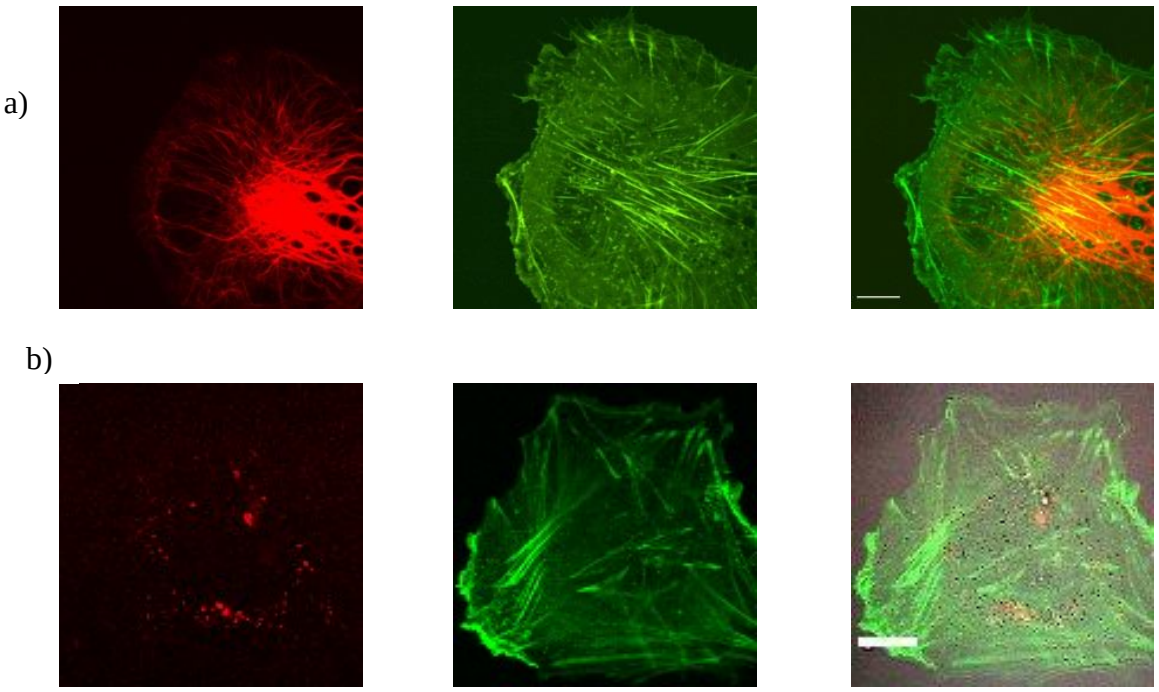

Figure 4.2 Fluorescence imaging of vimentin in negative control and vimentin depleted cells.

a) Vimentin network in a negative control cell (red), actin filaments (green) and an overlay of both vimentin and actin signals. Scale bar: 10 µm. b) Vimentin network in vimentin depleted cell (red), actin filaments (green) and an overlay of vimentin and actin. Scale bar: 20 µm.

The amount of vimentin in vimentin silenced cells and control cells was then measured by using the western blot (WB) technique. Figure 4.3 (a, b) shows WB protein bands, and the relative amount of total vimentin in negative control cells and vimentin depleted cells. Western blot shows that to achieve greater vimentin knock down, one-round of transfection might be insufficient and will require a second round of transfection. The second round of transfection was performed 3 days after the first transfection (on day 4) in the same manner as on day 1. The WB experiments indicate an efficient vimentin silencing on RPE1 cells. The amount of vimentin in vimentin silenced cells was suppressed by 70% compared to the amount of total vimentin in negative control cells after the first round of transfection, and by 95% after the second round. The experiments were always performed directly after the second transfection as the efficiency of silencing will decrease over time because of cell division.

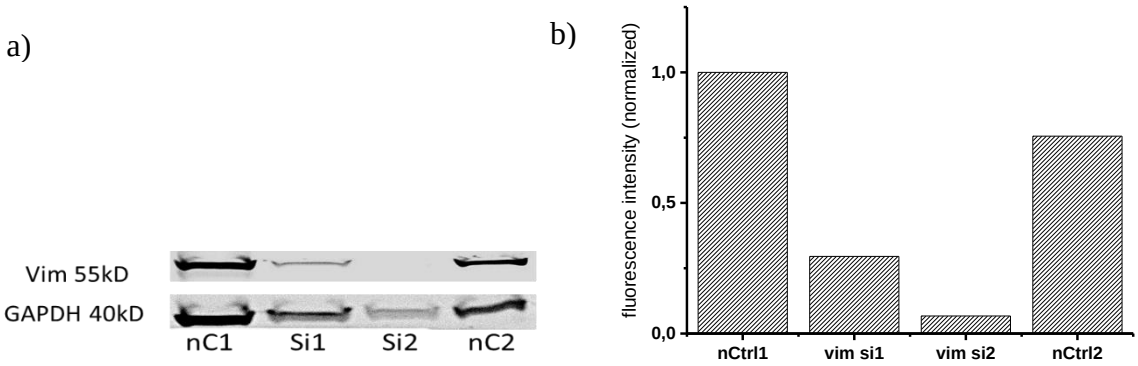

Figure 4.3 Western blot data to measure the amount of vimentin gene silencing.

a) Western blot data to measure the amount of vimentin and GAPDH (as a control) protein, after one round of silencing (nC1 negative control; Si1 vimentin KD) and two rounds of silencing (nC2 negative control; Si2 vimentin KD). b) column chart of the normalized grey values of the first and second rounds of the negative control (nCtrl1 and nCtrl2), and vimentin silencing (vim si1 and vim si2).

Recently it has been shown that vimentin depletion does not affect actin filaments orientation and actin bundles thickness in vimentin KO MEFs cells [141]. In the present study, the amount of actin proteins has not been verified as it was already well documented in the literature that the amount of actin proteins is not impaired in vimentin depleted cells [95, 100, 142].

4.2.1.2 Actin dynamics in stress fibers in nonpatterned cells

Actin dynamics in SFs in scrambled siRNA (negative control cells) and vimentin KD cells was measured by FRAP. From the FRAP recovery curve, actin recovery rate and fraction of actin monomers that are involved in recovery are measured. Figure 4.4 shows examples of corrected and normalized FRAP recovery curves (black) on actin SFs in negative control and vimentin KD cells. Actin SFs halftime recovery and mobile fraction are shown on the fitted (red) curves. While the FRAP curve reached a plateau value that corresponds to the mobile fractions.

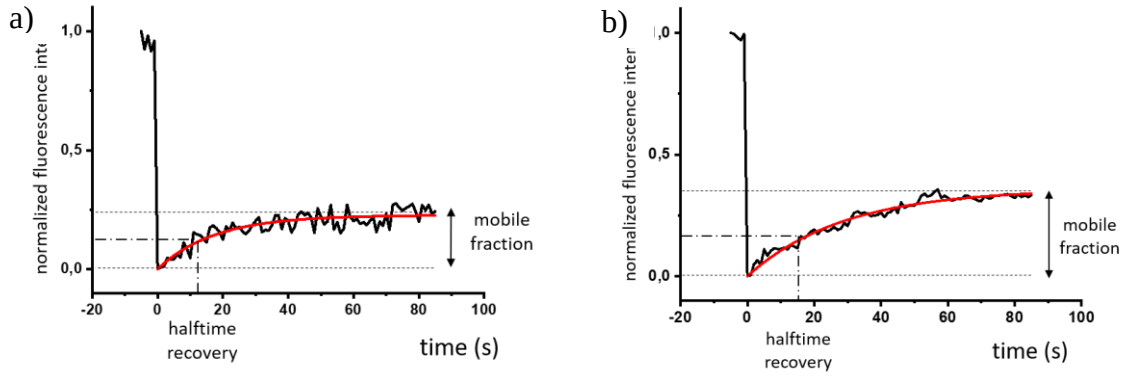

Figure 4.4 FRAP curves of actin SF in control and vimentin KD cells.

The curves of actin stress fiber fluorescence intensity during the FRAP experiment in (a) negative control cell and (b) vimentin KD cell. In both, normalized curves (black) represent actin fluorescence intensity before bleaching (time -5 to 0 second) normalized to 1 and directly after bleaching (time 0 second) normalized to 0. Post bleaching (time 0 to 85 seconds) shows the fluorescence recovery i.e. the actin turnover. Halftime and mobile fraction are shown on the fitted (red) curves.

Actin turnover rate and mobile fraction were measured for every bleached ROI on SFs. The mean value of halftime recovery and the mean value of mobile fractions were calculated for negative control and vimentin KD cells.

The FRAP measurements on SFs were performed either with a spinning disk microscope or an LSM. The results obtained with both microscopes were comparable, therefore the data were pooled together. The actin turnover rate (Figure 4.5 (a)), directly corresponds to the actin halftime recovery and is significantly longer in vimentin silenced cells compared to negative control cells (halftime recovery: 18s and 12s, respectively). The halftime recovery ratio of control cells over vimentin silenced cells is around 0.65, which indicates that actin turnover is 35% slower in the absence of vimentin when compared to negative control cells.

The mobile fraction corresponds to the amount of actin monomers involved in the actin turnover. It shows no significant difference between both conditions with a percentage of 30% of the mobile fraction on average (Figure 4.5 (b)). The 70% that does not recover correspond to the immobile fraction (i.e., the percentage of actin monomers that are staying at their localization after photobleaching.). The lack of vimentin does not impair the amount of actin monomers that participate in fluorescence recovery and are involved in the actin turnover.

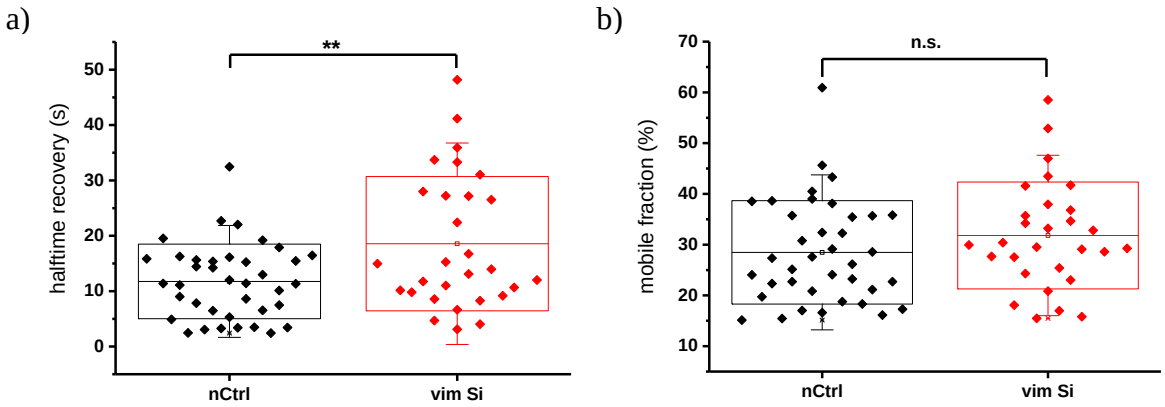

Figure 4.5 Actin dynamics in SFs in negative control and vimentin depleted cells.

a) Half time recovery of actin in SFs in the negative control (nCtrl) and vimentin depleted (vim Si) cells. b) mobile fraction of actin in SFs in negative control and vimentin depleted cells. In all the plot boxes Whiskers on box plots represent standard deviation. The mean value is given by the middle line within the box plot. Significance: *t*-test for independent samples, ** $p < 0.01$, n.s.: not significant. The number of the measured cells and SFs are respectively 29 and 38 in the negative control, and 19 and 29 in vimentin depleted cells.

Taken together, the data show that actin dynamics in SFs are slower in the lack of vimentin even though the amount of actin monomers involved in actin dynamics is not modified. This suggests that vimentin interacts with actin and plays a regulatory role in the dynamics of actin in SFs. To understand if actin bundles thickness is also involved in actin dynamics in SFs, I evaluate the actin bundle thickness and investigate its correlation with actin bundle dynamics.

4.2.1.3 Evaluating actin bundles dynamics correlated to their thickness

Actin SF bundles are composed of 10 to 30 actin filaments [57]. Despite the basic similarities in SF structures, there are main differences (e.g., in their localization, thicknesses, contractility and ABPs that interact with the filaments). The actin bundle thickness varies depending on the number of actin filaments, their interaction with ABPs, cell contractility, and cell motility [64].

In the FRAP measurements, actin dynamics were measured on actin SF bundles of variable thicknesses. Actin bundles thickness was measured using fluorescence microscopy assuming it as a two-dimensional filament. As vimentin has been suggested to promote actin dynamics in SFs [95, 100] I evaluated the thickness of SF to investigate whether the thickness of SFs is modified in the lack of vimentin. Therefore, the thickness of the actin bundles was measured by fitting the fluorescence intensity profile along the

actin fiber bundle section, with a simple Gaussian equation. Actin halftime recovery and mobile fraction in SF bundles were plotted against the actin bundle thickness in scrambled siRNA (negative control) and vimentin depleted (silenced) cells (Figure 4.6). The correlation between the plotted parameters was estimated with the Pearson correlation coefficient. A Person coefficient of [-1, -0.5] and [0.5, 1] means that the two parameters are (negatively and positively, respectively) linearly correlated while a coefficient of [-0.5, 0.5] means that the two parameters are uncorrelated. On the one hand, there is no linear correlation between the half time recovery and the actin SF bundle thickness for negative control cells and vimentin KD cells, (Pearson coefficients: -0.37 and 0.05, respectively) (Fig, 4.5, (a, b)). On the other hand, there is no linear correlation between the mobile fraction and the actin SF bundle thickness for negative control cells and vimentin KD cells, (Pearson coefficients: 0.09 and 0.06, respectively) (Fig, 4.5, (c, d)).

The data show that actin dynamics in SF bundles are not influenced by their thickness in negative control and vimentin silenced cells. However, the opposite effect has been shown recently in the literature, where massive actin SFs were less dynamic than thinner ones [143]. This resulted in impaired migration and motility of the kidney epithelial cells in wound healing assay [143]. In addition, SFs thicknesses vary under tension and become larger and thicker with an increase in applied forces to the surface in plastic or PDMS [70]. This promotes tight adhesion and prevents fibroblast cell migration [70]. For several decades people found that the thickness of actin SFs affects actin filaments' motion but here I study F-actin dynamics in SFs and I showed that the thickness does not have an effect on the polymerization and depolymerization of actin filaments and the rate of F-actin turnover. In the present study, as the FRAP experiments did not show any correlation between actin dynamics and actin SFs thickness on RPE1 cells, I decided to tune actin SFs localization and thickness by seeding the cells on patterns. This would confirm whether cell polarization and organization of SFs affect actin dynamics of control cells and vimentin KD cells.

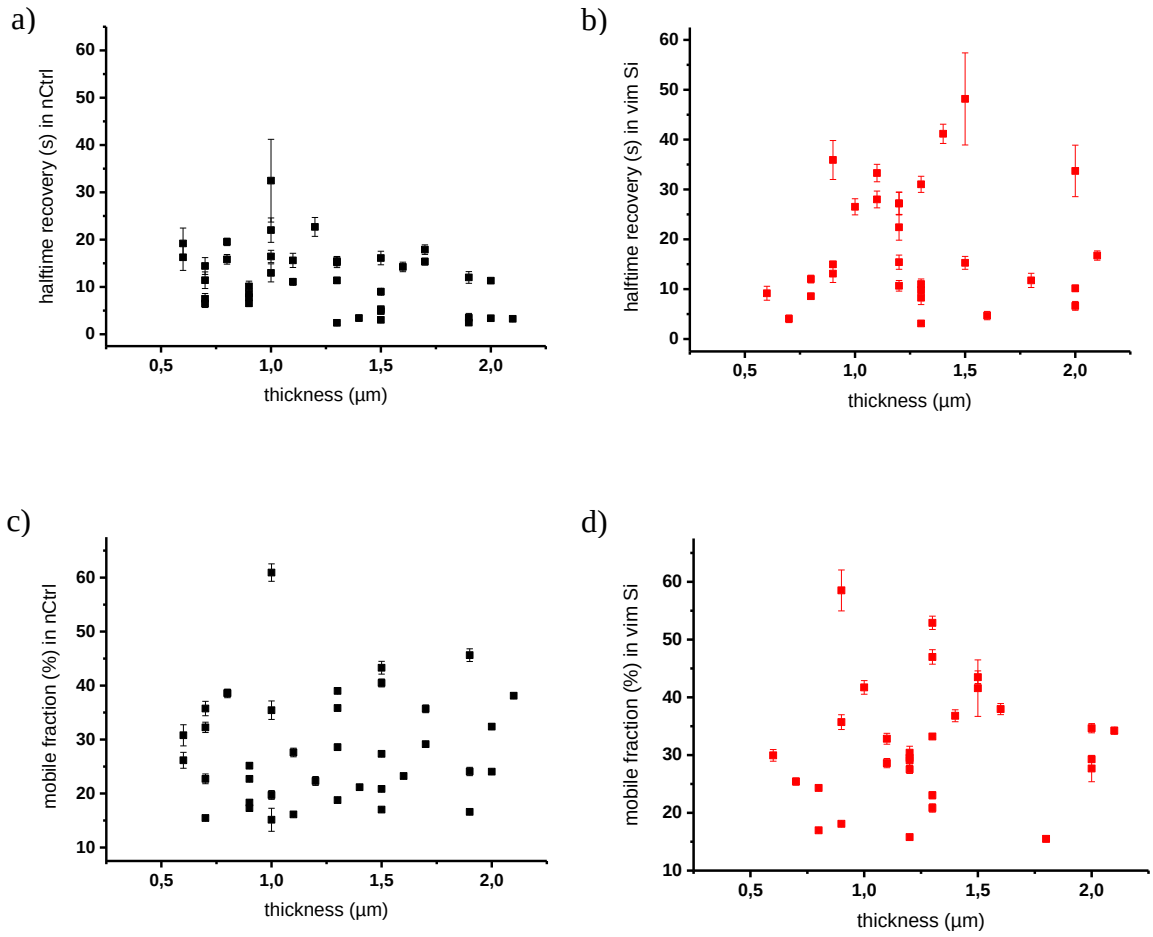

Figure 4.6 Correlation of actin dynamics and bundle thickness.

a, b) Halftime recovery of actin in SF against their thickness in negative control and vimentin depleted cells. c, d) Mobile fraction of actin in SFs against their thickness in negative control and vimentin depleted cells. Error bars show the standard deviation.

4.2.1.4 Actin dynamics in stress fibers in crossbow micropatterned cells

When cells are spreading, their geometry, shape, polarity, and the distribution of their cytoskeleton in the cytoplasm are uncontrollable [144]. Micropatterning is a popular technique to adjust and tune cell geometry in a specific shape. In micropatterned cells, actin SFs are almost in the same position and have comparable sizes in each cell [10].

I hypothesized that the cell shape might influence actin dynamics by modifying the organization of the SFs. This hypothesis motivated me to check a method that controls the shape of the cells, the thickness of SFs and the position and localization of the organelles. I controlled the shape of the cells and the thickness of the SFs using the micropatterning method. Then to determine whether the variation of the organization of SFs and the geometry and polarization of the cell influences actin dynamics in SFs, I measured actin

dynamics in ventral SFs of vimentin KD cells and control cells on crossbow micropatterned cells and compared the results with the nonpatterned cells. Vimentin siRNA transfected and negative control cells were seeded on crossbow micropatterns (Figure 4.7). On this pattern shape, cells have two large actin ventral SFs, one on each cell edge [95].

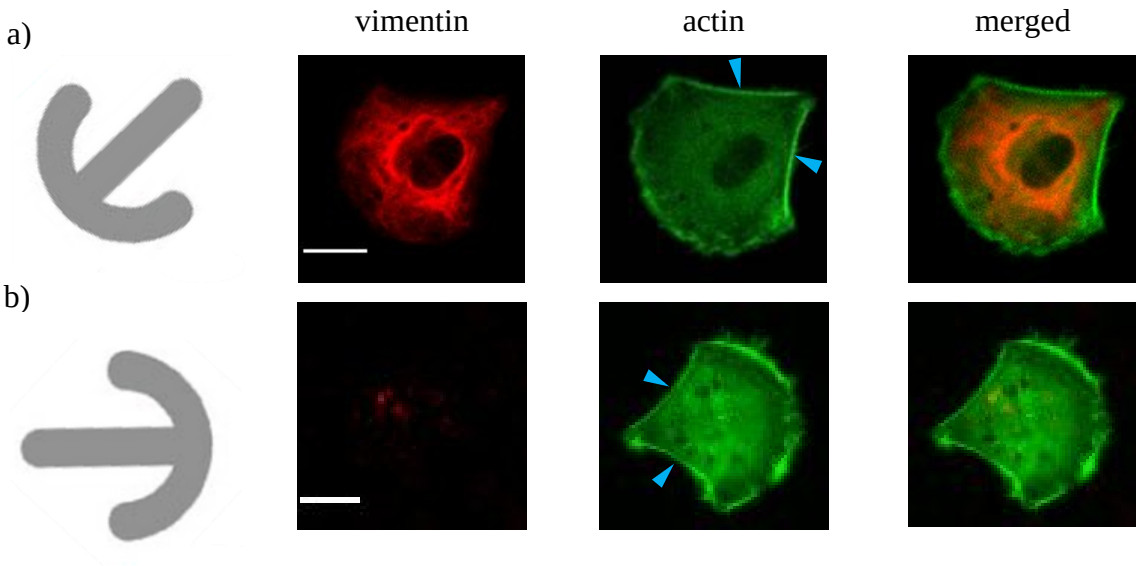

Figure 4.7 Crossbow micro-patterned negative control and vimentin depleted cells.

Fluorescent images of a negative control (a) and vimentin depleted (b) cell on a crossbow micropattern. From left to right: scheme of a crossbow micropattern, vimentin in red, actin in green, and merged image. The blue arrowheads indicate ventral SFs. Scale bar: 20µm.

The FRAP measurements (Figure 4.8 (a)) confirm that actin halftime recovery is longer in vimentin depleted cells than in negative control cells (half time recovery 19 s and 12 s, respectively). The halftime recovery indicates that actin turnover rate is significantly slower in the vimentin KD cells when compared with control cells seeded on crossbow micropatterns. These data are comparable to the ones described for the actin turnover in SFs on nonpatterned cells. The mobile fraction in both patterned and nonpatterned conditions shows no significant differences for control cells and vimentin KD cells (Figure 4.8 (b)). The amount of actin monomers involved in actin recovery stays constant in the lack of vimentin in the micropatterned cells. These data are consistent with the one described for the nonpatterned cells.

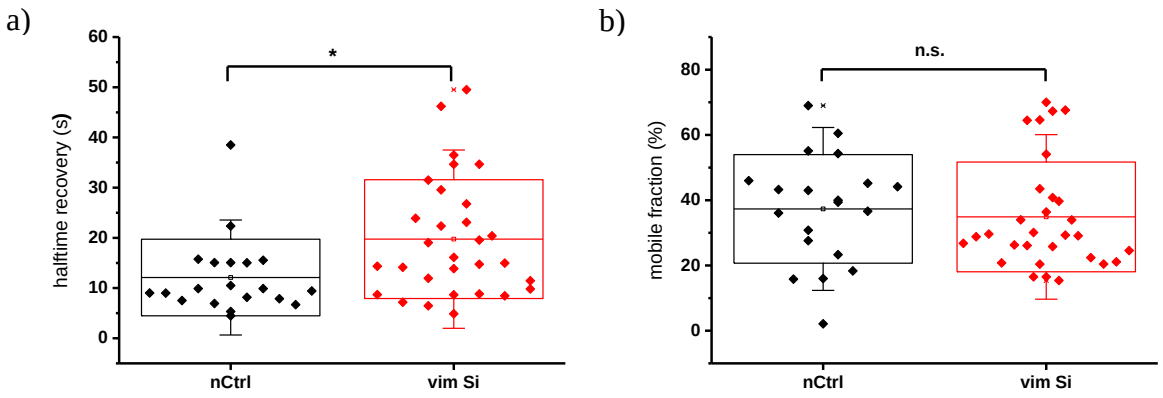

Figure 4.8 Actin dynamics in SFs in crossbow micropatterned cells.

a) Half time recovery of actin in SFs in the negative control (nCtrl) and vimentin depleted (vim Si) crossbow micro-patterned cells. b) Mobile fraction of actin in SFs in negative control and vimentin depleted crossbow micro-patterned cells. Whiskers on box plots represent standard deviation. The mean value is given by the middle line within the box plot. Significance: *t*-test for independent samples, * $p < 0.05$, n.s.: not significant. The number of the measured cells and SFs are respectively 13 and 20 in the negative control, and 18 and 30 in vimentin depleted cells.

The FRAP data (i.e., halftime recovery and mobile fraction) on control cells and vimentin KD cells were similar for patterned and nonpatterned cells. Therefore, cell shape, and the thickness and the position of actin SFs do not affect actin dynamics in SFs. There are no differences in actin dynamics in nonpatterned and patterned cells and I concluded that it is the role of vimentin that affects actin dynamics in SFs. However, it has been shown that actin bundle thickness is correlated with the motion of F-actin using fluorescent images of the cells that migrate [70]. In the current project, the FRAP technique was used to study F-actin dynamics. Moreover, recently actin dynamics have been studied only in nonpatterned cells with instinctive cell geometry, cell shape and cell polarity [140, 145]. Our data show no differences in actin dynamics in SFs in nonpatterned and crossbow micropatterned cells, thus patterned cells are proper in order to make statistics under the same conditions.

4.2.1.5 Discussion on the contribution of vimentin to actin dynamics in stress fibers

The role of actin bundles during cell migration has been studied for decades, however, the interplay between vimentin and actin filaments in cells remains poorly understood. Actin dynamics regulates membrane protrusion, creating new adhesions, contraction and retraction [21]. In particular, vimentin regulates cell contraction and plays a role in cell mechanics and cell signaling in smooth muscle cells [21]. Actin filaments are involved in

cell division and vimentin and plectin control cortical actin network organization [146]. In addition, vimentin itself plays a role in cell migration. A lack of vimentin impairs cell migration [4, 5, 52, 147] while overexpression of vimentin upregulates cell migration [20]. This suggests that vimentin is an important parameter in cell migration progress and invasion [6]. More recently, vimentin overexpression has been shown for metastasis in human lung adenocarcinoma [8], which suggests that vimentin might be a relevant therapeutic target in vimentin-related diseases (e.g., cancer). Until now, the participation of vimentin and actin filaments in cell migration was studied mostly independently. Few studies, mainly *in vitro*, have shown an interaction between actin and vimentin [100]. For example, rheological studies showed that a mixture of vimentin and actin is more stiff compared to actin filaments or vimentin filaments alone [96]. Also, the interaction between vimentin and actin transverse arcs results either in a slow actin flow in HFF cells [94] or in a promotion of actin retrograde flow in U2OS human osteosarcoma cells [95].

Cell migration is a complex mechanism that includes actin assembly and disassembly. In the presented project, I focused on F-actin dynamics in the presence and the lack of vimentin. In the literature, the actin elongation rate is 0.25 µm/min and is similar in dorsal SFs and transverse arcs [64] that is greater than in ventral SFs with the rate of 0.02 µm/min [148]. In the presented project actin halftime recovery in SFs ranges from 12 s in control cells to 18 s in vimentin KD cells; which contrasts with the actin SFs recovery in endothelial cells which range from 3 min to 5 min [149], and 17 s and 202 s for the chondrocyte cell line (H5 strain) [145]. These differences in recovery time measured for actin dynamics can be explained by the different data processing methods used, the different cell lines studied and applying FRAP on actin ventral stress fibers or dorsal SFs and arcs. In the literature, the authors measured actin dynamics in dorsal SFs while I measured actin dynamics in ventral SFs. I considered the photobleaching happening during the acquisition to fit the data which might partially explain the large contrast in actin dynamics compared with the literature.

The presented data show that the lack of vimentin slows down actin dynamics, that actin dynamics is not influenced by SFs thickness but only by the lack of vimentin. This agrees with a recent study where vimentin depletion does not affect actin filaments orientation and thickness [141]. Vimentin filaments interplay with actin filaments to assist actin dynamics. This suggests that vimentin filaments in cooperation with actin filaments facilitate cell migration, but that vimentin does not influence SFs thickness. The regulation of actin dynamics via vimentin confirms the results of studies that have shown

that vimentin KO cells migrate slower than WT cells [5, 52], and that vimentin overexpression enhances cell migration [4]. However, it is important to note that in the presented project vimentin expression was silenced via cell transfection while in the literature vimentin knocked out cells were primary cells arising from genetically modified mice. Moreover, I did not measure the cell migration velocity and relative parameters in vimentin silenced cells, but I focused on actin and vimentin interplay in actin dynamics. Plectin is known to be a cross-linker protein between actin and vimentin. In the following section, I study the role of plectin and measure actin dynamics in plectin KD cells and negative control cells.

4.2.2 Plectin contributes to actin dynamics in stress fibers

In this section, I study the role of plectin-vimentin interaction in actin dynamics. I already described the role of vimentin on actin dynamics, here I hypothesized that not only the presence of vimentin affects actin dynamics but also the interplay of vimentin with actin via plectin. Actin dynamics were assessed in plectin depleted cells and negative control cells. Actin monomers were labeled with BacMam gene delivery system (See section 4.1). Plectin was knocked down in RPE1 cells using the transfection technique (See 2.4.1 and 3.2.2). FRAP experiments were then performed on both plectin KD and negative control cells. I show that the lack of plectin influences the fraction of actin monomers that recovered and is involved in the actin turnover even though actin halftime recovery is comparable in control and plectin silenced cells.

4.2.2.1 Quantification of the amount of plectin in transfected cells

In order to knock down plectin, plectin 1b siRNA was transferred to the cells and silenced plectin 1b isoform expression. Immunofluorescence staining (Figure 4.9) shows a reduction of plectin-derived fluorescence signal after the siRNA transfection (concentration 10 µM, incubation time 40 h). An immunofluorescence staining does not quantify the percentage of plectin-depletion, however, the images (Fig. 4.9) show a weaker fluorescence intensity derived from plectin depleted cells compare to scramble siRNA (negative control) cells and more than 90% of the cells present a reduction of plectin-derived fluorescence intensity (more images of immunofluorescence staining of plectin silenced and negative control cells are presented in appendix, Figure 10.1).

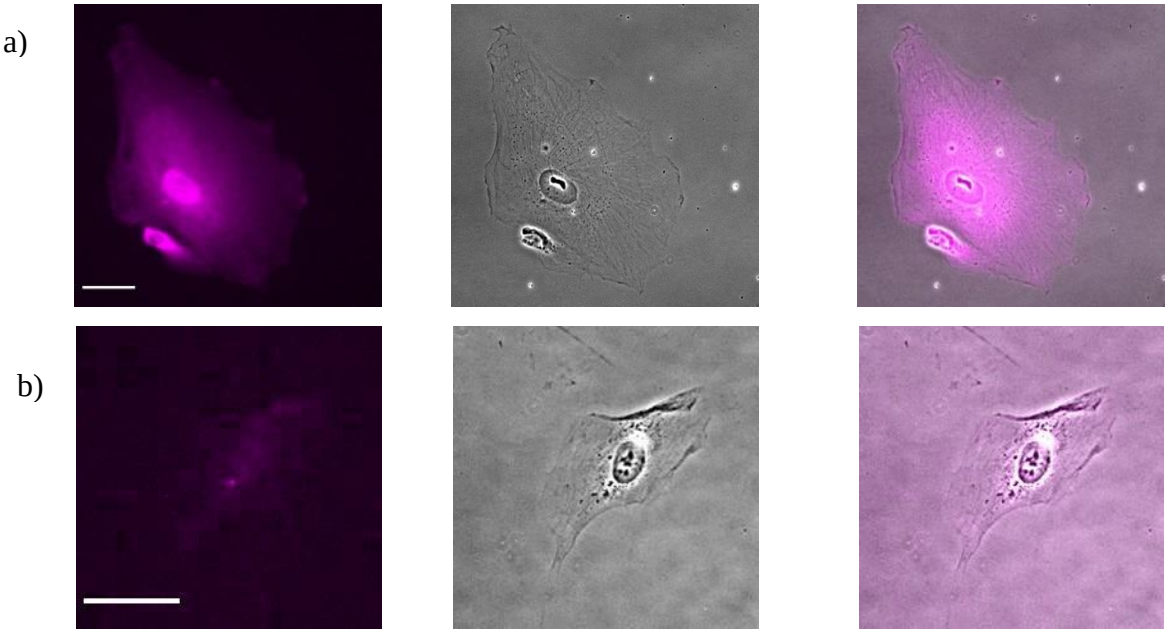

Figure 4.9 Immunofluorescence staining of negative control and plectin depleted cells.

a) Negative control cell. b) Plectin depleted cell. (a, b) from left to right: plectin in purple, phase contrast image of the cell in grey, and overlay image. Scale bar:10 µm.

In the literature, it has been shown that plectin deficiency affects IFs structure (their size, and network distribution) [18, 46], that their deficiency causes the detachment of vimentin filaments from focal adhesions [50, 52], and their distribution to the cell edge. As plectin links vimentin to focal adhesions, the depletion of plectin impairs the link between vimentin and FAs and affects vimentin network localization (i.e., vimentin filaments spread into the cell periphery and lamellipodia protrusions).

In this study plectin silenced cells have a vimentin network distribution toward the cell edge and the cell membrane (Figure 4.10) which reveals the efficiency of the plectin depletion in cells. This has been observed during FRAP measurements on plectin depleted cells (Figure 4.10). Fluorescence imaging of the vimentin network in plectin silenced cells shows an alteration in vimentin network distribution, therefore results in the lack of plectin in cells. Plectin links vimentin to the focal adhesions, thus reducing plectin cuts this link and affects vimentin network localization. Vimentin filaments spread into the cell periphery and lamellipodia protrusions in the lack of plectin.

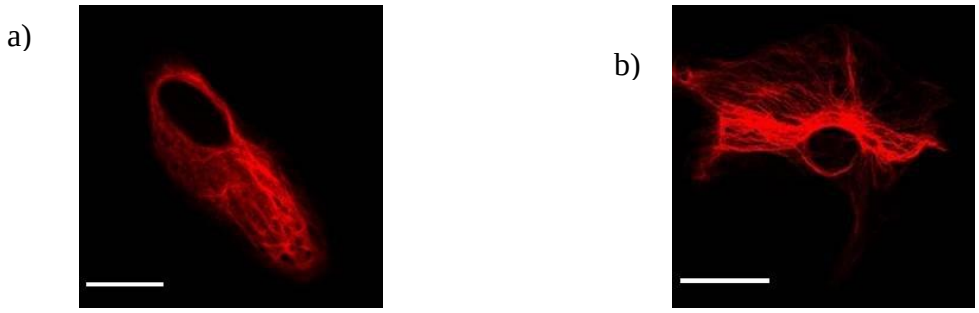

Figure 4.10 Vimentin network in negative control and plectin depleted cells.

Vimentin network (red) in a) negative control cells and b) plectin depleted cells. Only the vimentin network images are shown here as plectin imaging was possible only in fixed cells. Scale bars:10 µm.

Plectin is a huge protein with a molecular weight of 500 kDa that I could not detect with the WB kit available in the laboratory. Therefore, I used the qPCR technique to quantify the amount of plectin mRNA. Plectin 1b isoform binds to vimentin IFs [48]. To silence plectin, cells were transfected with plectin 1b siRNA. Two different template strands for forward and reverse plectin 1b primers were selected based on the mRNA sequence for plectin 1b isoform [48]. The primers were tested first only for control cells to select the proper one. In general, a gene-specific primer is more reliable when it has a low cycle threshold (C_t) value close to the C_t value of the gene normalizer. The C_t value corresponds to the number of cycles that the fluorescence signal crosses the fluorescence threshold. Table 11.9 to Table 11.11 show the results of qPCR using two different sets of primers in different concentrations for control cells. The C_t value for the primers designed in the Primer BLAST tool (will be referred to BLAST) with a concentration of 2 µM was less than the primers with the concentration of 1 µM and 5 µM designed with Primer-3 tool. It indicates that the reactions containing BLAST primers contain a higher amount of the starting templet when compared to the other primers. Moreover, the C_t value for BLAST plectin primers is close to the C_t value in reactions with the GAPDH primer which was used as an internal control. Therefore, BLAST primers with a concentration of 2 µM were chosen to quantify plectin in plectin silenced cells. The C_t value differences between plectin reactions and GAPDH in the other reactions for the untreated samples are higher when compared to the C_t value with BLAST primers. Later in the treated samples, I was not able to verify whether the differences in C_t values were due to the amount of the specific gene expression or the primer. Furthermore, I continued to quantify the plectin mRNA in RPE1 plectin KD cells by using BLAST primers (Table 11.6). Quantifying the

amount of plectin mRNA in plectin depleted cells does not show significant differences in expression of plectin in plectin KD (depleted), siRNA scramble (negative control), and control cells. The qPCR technique is sensitized to several parameters such as the concentration to obtain pure RNA, the designed forward and reverse primer sequences which are also plectin isoform dependent, and even the pipetting skills. That can be explained because of the slight decrease of plectin and I might have performed more experiments of qPCR to amplify the sequence of interest more in order to increase the gap between control and plectin-depleted cells. However, in parallel, I made FRAP experiments on both populations of cells and underlie a significant modification of actin dynamics. Having the exact percentage of depletion would have to be checked in later work but for preliminary studies on plectin role in actin dynamics, I preferred to first focus on the FRAP data.

4.2.2.2 Actin dynamics in stress fibers in plectin silenced cells

Depleting plectin in cells results in distinct biomechanical properties in myoblast and keratinocytes cell lines [18] and mouse skin fibroblast cell line [127] even though this deficiency mostly affects cells when external stress using a cell stretcher is applied to the cell [18]. Plectin deficiency has various effects on cell dynamics and cell motility in different cell types [18]. For example, in general, keratinocyte cells are stiffer than myoblast cells, using magnetic tweezers microrheology. However, the stiffness of plectin KO cells is two times lower than WT myoblast cells, while plectin KO is slightly stiffer than WT keratinocytes [18]. Plectin interacts with almost all the IFs such as vimentin. Vimentin-plectin interaction affects cell migration by positioning the nucleus in the cytoplasm [150]. A deficiency or overexpression of plectin proteins results in abnormal nucleus repositioning in cytoplasm results in various diseases [150]. Nuclear repositioning affects the mechanical properties of the cytoplasm around the nucleus, nucleus signaling pathway and cytoplasmic signaling pathway connection [150].

Vimentin-plectin interaction also modifies vimentin distribution into the cell by crosslinking vimentin to focal adhesions [46, 95], moreover, plectin is required for the interaction of transfected arcs and vimentin [95]. Plectin connects IFs to actin filaments, MTs and membrane [11, 106].

Here, I investigated whether the alteration of actin dynamics in vimentin depleted cells is caused by the presence of vimentin or is due to the interplay between vimentin and actin via plectin. Furthermore, actin dynamics in SFs in scrambled siRNA (negative control)

and plectin deficient cells were measured using FRAP. The halftime recovery is 12 s for both populations (Figure 4.11 (b)), which means that the actin turnover rate is not affected by the lack of plectin. Therefore, the actin turnover rate is comparable to plectin negative control cells and plectin depleted cells. The inhibition of the indirect interaction between vimentin and actin mediated by plectin does not impact the fraction of actin monomers that are participating in the fluorescence recovery in vimentin depleted cells. However, the amount of actin monomers involved in turnover is higher in plectin depleted cells (41% of fluorescent recovery) compare to negative control cells (28% of fluorescent recovery). The ratio of the mobile fractions of plectin depleted cells over the control cells is 1.46 (Figure 4.11 (b)). Taken together these data show that a lack of plectin influences the fraction actin monomers that recovered and are involved in actin turnover but does not influence their halftime recovery.

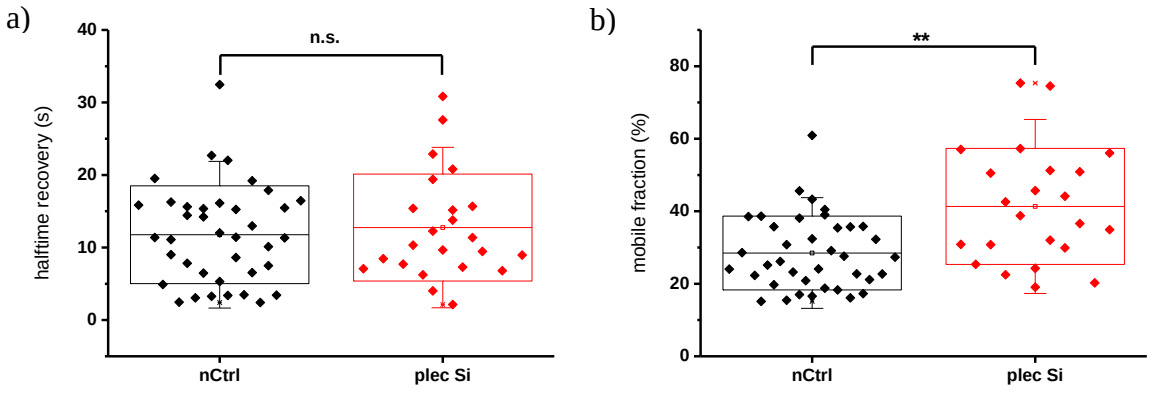

Figure 4.11 Actin dynamics in SFs in negative control and plectin depleted cells.

a) Half time recovery of actin in SFs in the negative control (nCtrl) and plectin depleted (plec Si) cells. b) Mobile fraction of actin in SFs in negative control and plectin depleted cells. In all the box plots Whiskers on box plots represent standard deviation. The mean value is given by the middle line within the box plot. Significance: *t*-test for independent samples, ** $p < 0.01$, n.s.: not significant. The number of the measured cells and SFs are respectively 29 and 38 in the negative control, and 20 and 23 in plectin depleted cells.

4.2.2.3 Discussion on the contribution of plectin to actin dynamics in stress fibers

As mentioned, FRAP is a common technique to study the kinetics of biomolecules *in vitro*. In the presented project FRAP was used as an appropriate method to study F-actin dynamics in SFs in both vimentin depleted and plectin depleted cells. Plectin is known as a vimentin-actin cross-linker [51]. In the presented study, I show the role of vimentin on actin turnover rate (actin halftime recovery in SFs is longer in vimentin KD cells compare to control cells), whereas it is not altered by the lack of plectin. However, the fraction of

actin monomers that are involved in the turnover rate is not altered in vimentin KD cells compared to the control, while this ratio is higher in plectin KD cells than in WT cells. The lack of plectin increased the fraction of actin monomers involved in the actin turnover rate. In the literature, it has been shown that, in the lack of plectin, actin has a weak affiliation in focal adhesions [50, 52] even though the expression of actin is not observed [106] furthermore it might result in an increase in the number of free actin monomers. Plectin maintains the cytoskeleton in a stable shape and plectin deficiency defects the cell formation [151], reposition the nuclear and affects cell migration, even though it does not influence actin polymerization turnover rate.

I already showed that depleting the cross-linker between actin and vimentin changes the amount of actin monomer involved in actin recovery, not only the presence of vimentin is important for actin dynamics but also the interplay of vimentin with actin via plectin. Both the presence of vimentin and also the interaction of vimentin with actin via plectin have an impact on actin dynamics. Plectin deficiency affects intermediate filaments structure (their size, flexibility, stability) [18, 46]. Depleting plectin increased the extractability of vimentin proteins compare to the WT cells [139] in WB. Vimentin is overexpressed in cancer cells and plays a main role in the progression and invasion of the cancer cells. Understanding how plectin affects vimentin is not the goal of this project and the amount of vimentin was not measured in plectin deficient cells; however, plectin might have a role as a mediator in cancer.

4.3 Actin dynamics in the cortex in suspended cells

One of the interests of our lab is to understand the adhered-suspended transition that occurs during diverse steps of cell life. For example, during division the cells detach a little during mitosis, in the case of cancer, metastatic cells detach from the tumor and become suspended to invade other tissues. Two distinctive projects are currently studied in our lab: 1) studying actin dynamics in the cortex during the adhered-suspended transition; 2) studying the role of vimentin in amoeboid cell migration. In an amoebid mode of migration, cells are low-adherent, and due to their minimum adhesion, cells have a cortex similar to a suspension cell. Therefore, I used the expertise I developed for FRAP experiments to study actin dynamics in negative control cells and vimentin depleted cells, in the cortex of cells in suspension.

In the cortex ARP2/3 are nucleator proteins, and formin is a polymerization mediator, which have two distinct turnover rates [119]. A fast turnover that results from the addition

of monomers to free barbed ends (ARP2/3); and a slow turnover that results from formin-mediated filament growth (See section 2.4.3) [119]. It has recently been shown that in mammalian dividing cells the actin cortex turnover rate has a single halftime recovery of 45 s [152].

Here I measured actin dynamics in cortex refereeing to [119] with two turnover rates (one for ARP2/3 contribution and one for formin contribution). Actin recovery rate in vimentin depleted cells is longer (half time recovery: 6.6 s and 79 s for ARP2/3 nucleation and formin mediated polymerization, respectively) compare to control cells (half time recovery: 3.5 s and 65 s for ARP2/3 nucleation and formin mediated polymerization, respectively) (Figure 4.12 (a, b)). FRAP data show that the actin recovery rate in vimentin silenced cells is about 0.5 to 0.2 times slower than in control. The FRAP data also show that the mobile fraction of actin monomers in the lack of vimentin is higher in the fast population compare to control cells (ARP2/3 nucleation: 42% and 30% in vimentin depleted and control cells, respectively), whereas it is lower in the slow population (formin mediated polymerization: 57% and 70% in vimentin depleted and control cells, respectively) (Figure 4.12 (c, d)). This indicates reduced incorporation of exchangeable actin subunits into actin polymers.

In this subproject, I report the effect of vimentin in actin dynamics in the cortex of suspended cells. Actin dynamics in the cortex reveals two separated F-actin populations, ARP2/3 nucleation (fast)) and formin mediated polymerization (slow). FRAP measurements in the cortex show that the reduction of vimentin results in a slower halftime recovery for both populations compared to the control. The presence of vimentin seems to promote the actin turnover rate also at the cellular cortex. These data are in line with what I showed in SFs on adhered nonpatterned cells and crossbow micropatterned cells. Taken together these data show that vimentin influences the actin turnover rate not only in SFs but also in the cortex in suspended cells.

Recently it has been shown that a capping protein (CP) regulator known as CARMIL2 (CP, ARP2/3, myosin I linker 2) localizes in vimentin at the leading edge of the cells and binds to the cell membrane [147]. CARMIL2 forms lamellipodia and assists cell migration in the presence of vimentin. CARMIL2 needs both localization in vimentin and binding to CP to regulate actin assembly during cell migration and membrane protrusion [147]. The actin assembly regulation was studied in adherent cells and also in this subproject I show that the lack of vimentin reduces the actin halftime recovery into the

cortex and reduces the incorporation of exchangeable actin subunits into actin polymers in cells in a suspension state.

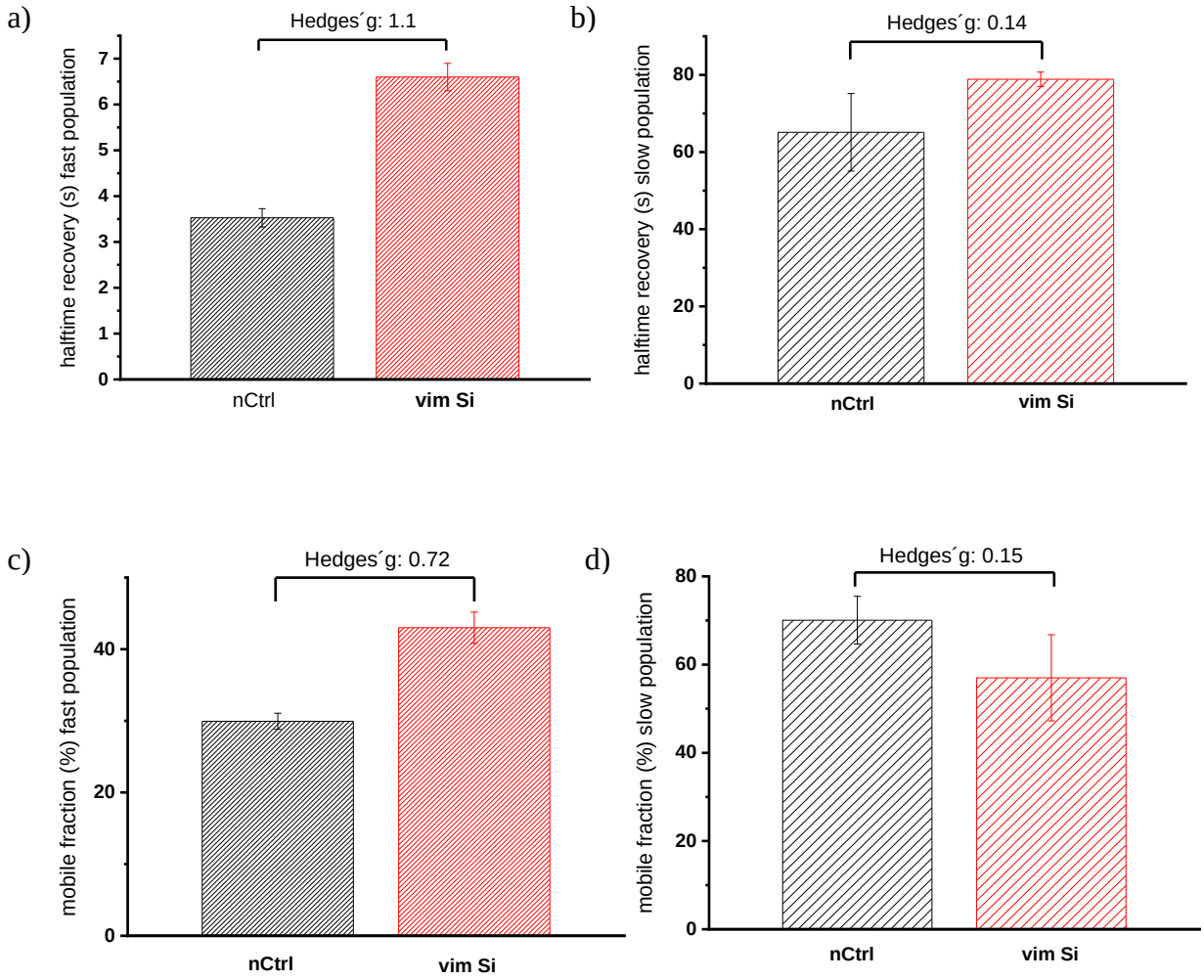

Figure 4.12 Actin dynamics in the cortex in negative control and vimentin depleted cells.

a, b) Halftime recovery of actin in cortex ((a) ARP2/3 nucleation (fast)) and ((b) formin-mediated polymerization (slow)) populations in negative control (nCtrl) and vimentin depleted (vim Si) cells. c, d) Mobile fraction of actin in cortex ((c) ARP2/3 nucleation (fast)) and ((d) formin-mediated polymerization (slow)) populations in negative control and vimentin depleted cells. Whiskers on box plots represent standard errors. Statistics were carried out using a Hedges'g test for the magnitude of the effect. The Hedges´g value of > 0.2 has a small effect, > 0.5 has a medium effect and > 0.8 has a large effect. The numbers of the bleached ROIs are 13 in control and 10 in vimentin siRNA cells.

4.4 The volume of RPE1 negative control and vimentin depleted cells

In the literature, it has been shown that vimentin knock out dendritic cells from genetically modified knock out mice are smaller than the dendritic cells from wild type cells [153]. I showed that actin dynamics in RPE1 SFs are altered in the absence of vimentin and hypothesized that vimentin depleted cells might be smaller than negative

control cells. This might result in fewer free spaces for G-actin to diffuse in the cytoplasm and reach the actin filaments and slow down F-actin recovery. Therefore, I measured the volume of adhered vimentin depleted cells and the volume of adhered control cells. This measurement is challenging on adhered cells because of the lack of accuracy of 3D images I can acquire. For this reason, I also measured the RPE1 cell volume in suspension. The volume of the cells was measured under three conditions as control: RPE1 WT (non-transfected), RPE1 vimentin mCherry transfected and RPE1 vimentin mCherry transfected plus scrambled siRNA cells. By comparing the cell volume in RPE1 WT (non-transfected) and RPE1 vimentin mCherry transfected it will be possible to indicate whether the cell volume is affected by transfection or not.

The volume of vimentin depleted and three types of control cells in adherent and suspension are plotted in the separated graphs (Figure 4.13 (a, b)). The cell volume in RPE1 WT and RPE1 vimentin mCherry transfected in both adherent and suspension conditions have no significant differences, concluding vimentin mCherry transfection itself does not alter the cell volume. Furthermore, RPE1 vimentin depleted cells in both adherent and suspension conditions are significantly larger than control cells. Taken together, the lack of vimentin in RPE1 cells induces a larger cell volume.

There are only a few studies about measuring the cell volume in vimentin depleted cells and most of them were done in vimentin KO cells [141, 153]. Interestingly, it has been recently shown that vimentin KO MEFs cells are slightly larger than control ones [141] but the opposite effect is discussed in the vimentin community as well.

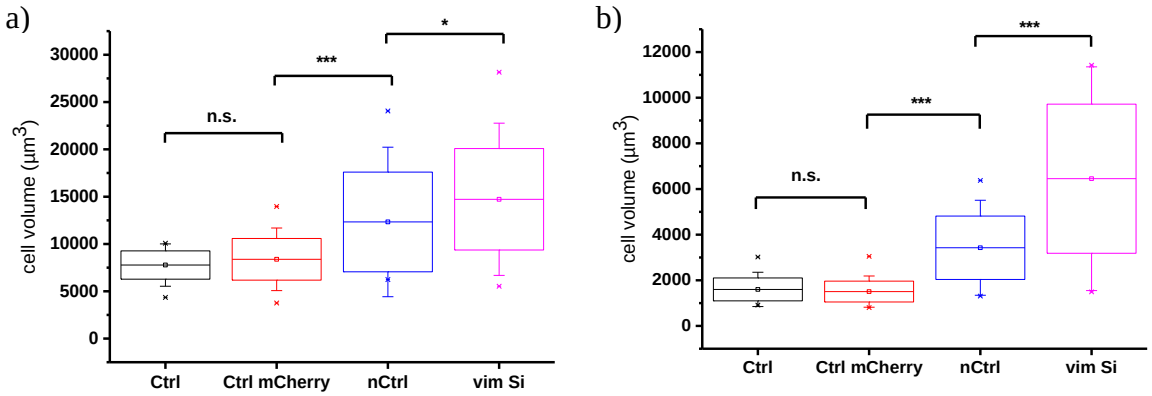

Figure 4.13 The effect of vimentin deficiency on the size of the cells.

a) The cell volume of RPE1 adherent cells and b) RPE1 suspended cells. Measured conditions are: RPE1 non transfected (ctrl), RPE1 cells with vimentin mCherry transfected (ctrl mCherry), RPE1 cells with siRNA scramble (nCtrl), and RPE1 cells with vimentin siRNA transfected (vim Si). Whiskers on box plots represent standard deviation. The mean value is given by the middle line within the box plot. Significance: *t*-test for independent samples, * $p< 0.05$, ** $p< 0.01$, *** $p< 0.001$, n.s.: not significant. The number of the measured adherent cells are respectively 36, 36 ,53 and 36 and 40, 42, 87 and 74 in suspended cells.

The KO cells are genetically different from WT cells. In KO cells the gene is taken out from the cell and does not exist in the genome anymore. Taking out one specific gene could influence the whole genome in an undescribed way. In siRNA transfected cells the gene is not deleted, so the genotype of the cell is not modified and is identical to the WT, this is an important difference between KO cells and KD cells. Furthermore, siRNA transfection method is transient and is specifically affecting the protein level but not the gene expression. These biological differences including the type of cells may lead to opposite effects in cell volume.

Here, vimentin depleted RPE1 cells are significantly larger than control cells, which is in contrast with the hypothesis that the increase of F-actin turnover rate will be the consequence of a reduction of the cell volume. Therefore, I investigated whether there is a significant difference in cytoplasmic actin dynamics and not only in the SFs, in vimentin depleted and control RPE1 cells.

4.5 Cytoplasmic actin dynamics of vimentin KD and control RPE1 cells

Following the evaluation of the cell volume, I investigated the cytoplasmic actin diffusion time [149] in vimentin depleted and control cells via FRAP measurements. Recently it has been shown that in the cytoplasm the G-actin halftime recovery, measured via FRAP, is about 40 ms [120] and it refers only to the diffusive recovery.

In the presented study, the cytoplasmic actin dynamics was measured via FRAP in vimentin depleted and negative control cells. Figure 4.14 (a) presents the cytoplasmic actin halftime recovery in both conditions and indicates that the cytoplasmic actin turnover is comparable in scrambled siRNA (negative control) and vimentin depleted cells. Moreover, the lack of vimentin does not significantly influence the mobile fraction (Figure 4.14 (b)). This suggests that the fraction of cytoplasmic actin is not involved in the actin turnover rate.

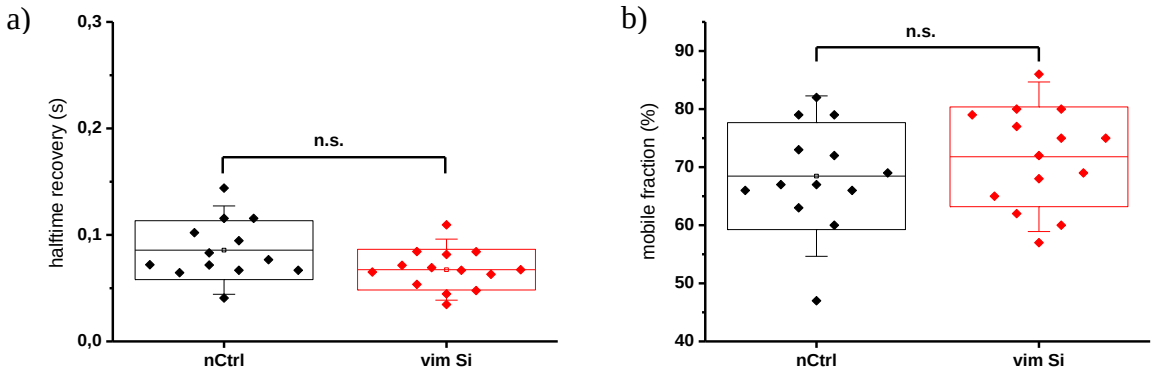

Figure 4.14 Cytoplasmic actin dynamics in negative control and vimentin depleted cells.

a) Half time recovery of cytoplasmic actin in the negative control (nCtrl) and vimentin depleted (vim Si) cells. b) Mobile fraction of cytoplasmic actin in negative control and vimentin depleted cells. In all of the plot boxes, Whiskers on box plots represent standard deviation. The mean value is given by the middle line within the box plot. Significance: *t*-test for independent samples, n.s.: the difference is not significant. The numbers of the bleached ROIs are respectively 13 and 14 in negative control and vimentin depleted cells.

Studying the cytoplasmic actin dynamics via FRAP showed that there are no significant differences in cytoplasmic actin dynamics in vimentin depleted cells as compared to the negative control. In the cytoplasm, the cytoplasmic actin halftime recovery refers only to the diffusive recovery while in the cortex or SFs it is a combination of diffusive and reactive recoveries. Despite the interaction of vimentin and different structures of actin filaments [94, 95], this interaction does not influence cytoplasmic actin diffusive recovery in the presence or the lack of vimentin. As mentioned in 2.4.3 the G-actin characteristic diffusion time (τ) is the time needed for a monomer to travel a distance (r) with a certain diffusion constant (D) [121, 122], where r is the radius of the ROI which was the same in both conditions in all the FRAP measurements. Further, the amount of actin proteins in negative control and vimentin depleted cells is the same [95, 100, 142], moreover, the certain diffusion constant (D) will be the same in both conditions. When all parameters that define the G-actin characteristic diffusion time are equal, in negative control and vimentin depletion cells, and also there are no significant differences in the cytoplasmic actin dynamics in vimentin depleted cells as compared to the control, it is concluded that cytoplasmic actin dynamics is not influenced by the lack of vimentin.

Prior, I hypothesized that vimentin depleted cells might be smaller than negative control cells and the smaller size of the vimentin KD cells compare to the control cells might result in fewer free spaces for G-actin to diffuse in the cytoplasm and reach the actin

filaments and slow down F-actin recovery. Therefore, I measured the volume of adhered vimentin depleted cells and the volume of adhered control cells. Moreover, I showed that vimentin depleted RPE1 cells are significantly larger than control cells, which is in contrast with the hypothesis that the increase of F-actin turnover rate will be the consequence of a reduction of the cell volume. Next, I investigated whether there is a significant difference in the cytoplasmic actin diffusion time in vimentin depleted and control RPE1 cells. I hypothesized that G-actin might have a longer diffusion time to reach the actin filaments in vimentin KD cells compared to the control cells, and that might affect F-actin dynamics. However, I showed that cytoplasmic actin dynamics is not influenced by the lack of vimentin. Furthermore, I hypothesized that even though cytoplasmic actin has the same diffusion time in both vimentin KD and control cells, actin monomers might require a longer time to reach the actin filaments in vimentin KD cells because of the larger size of the vimentin KD cells compared to the control cells. Therefore, suggesting that the cell size might have an effect on actin dynamics in vimentin KD RPE1 cells comparing with the control cells.

5 Results and discussion: Vimentin in actin force generation

Applying stress using atomic force microscopy [81], magnetic twisting cytometry [154], and optical tweezers [91] on vimentin deficient and control cells indicated the contribution of vimentin on the mechanical properties of the cells. Vimentin filaments align traction stresses and are required for the orientation of traction force [94]. This suggests that vimentin is a loadbearing structure in cell motility.

In migrating fibroblast cells, phosphorylated myosin is found to be more concentrated in the tail region (cell rear) compared to the front region (leading edge). The higher concentration of phosphorylated myosin in the tail domain generates the maximum traction force and helps the cell to retract the tail [155]. Moreover, researchers have shown that the absence of vimentin in U2OS cells alters the phosphorylation of myosin II, the amount of phosphorylated myosin is higher [100] and they showed, vimentin KO cells generate greater traction forces than WT cells leading to more stable actin SFs [100]. Furthermore, in my Ph.D. project, I measured the traction force in RPE1 vimentin depleted (vimentin KD) cells. As I already showed that actin turnover rate was faster in negative control RPE1 cells compared to vimentin KD RPE1 cells, I measured the traction forces in both negative control and vimentin KD RPE1 cells.

I hypothesized that vimentin influences actomyosin contraction in cells. Thus, I used traction force microscopy to measure the traction force magnitude and the traction force orientation in control and vimentin KD RPE1 cells.

5.1 Stiffness of hydrogels

Cells generate traction forces when they attach to the surface, migrate and divide. The forces applied by the cells depend on the cell type and can vary from 10 Pa in neuronal growth cones to 1 kPa for platelets [132]. Therefore, the stiffness of the substrate has to be adapted to the traction forces applied by the cells on the substrate. Applying low forces on a stiff gel will not deform it and then will not be measurable; on the other hand with a too soft gel the cell will spread less [156, 157] which may lead to inaccurate measurement of the forces. To find the appropriate gel stiffness to measure the RPE1 traction forces, I seeded the cells on hydrogels with different stiffness (2 kPa, 5.2 kPa, 11.6 kPa, 18.9 kPa, and 50 kPa). The cells are seeded on the hydrogels of different stiffness and observed with an epifluorescence microscope. The attachment and spreading of the cells on the hydrogels are visualized and the acquired images of cells on hydrogels with the different

stiffness (Figure 5.1) show that RPE1 cells are completely spread on gels with Young's modulus of 5.2 kPa. The cells are not completely spread on hydrogels with Young´s modulus of 2 kPa after 12 h or are only spread where the gel is ruffled. Cells are also well spread on hydrogels with Young´s modulus of 11.6 kPa or 18.9 kPa, but when the stiffness of 5.2 kPa can be used, it is not suitable to seed the cells on stiffer substrates. Thus, all the traction force measurements are performed using hydrogels with Young´s modulus of 5.2 kPa.

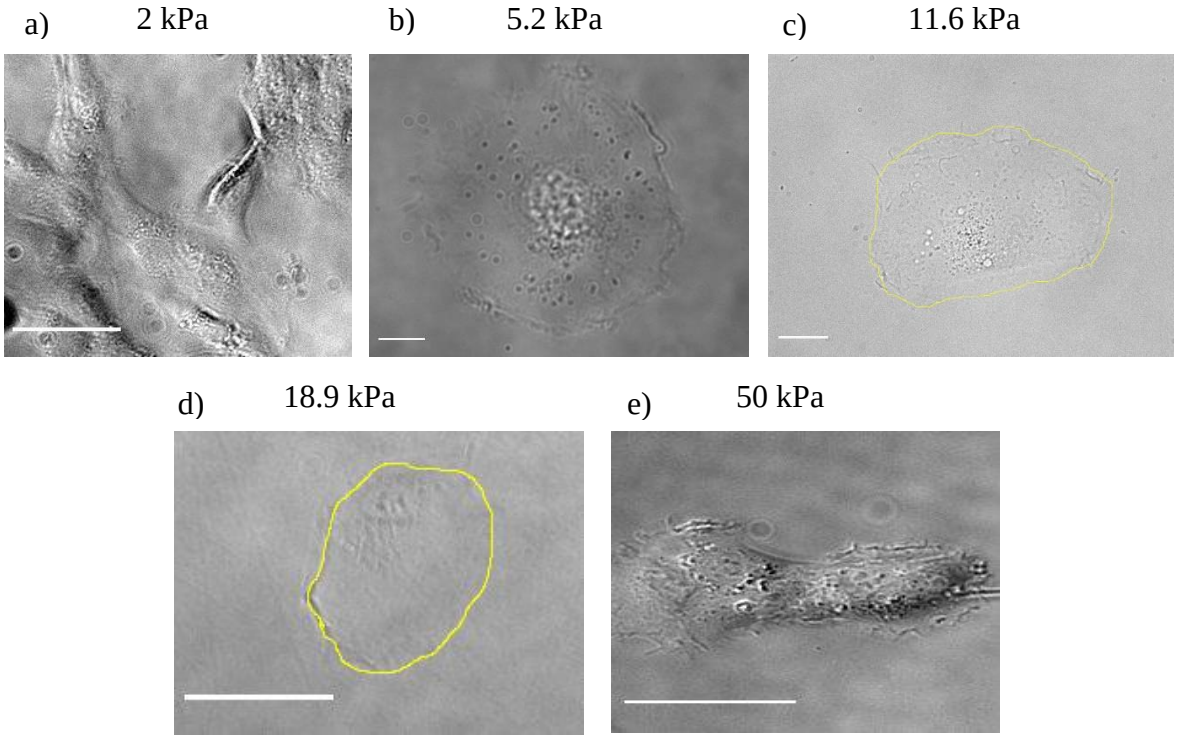

Figure 5.1 Images of the RPE1 cells seeded on hydrogels with different stiffness.

RPE1 cells on PAAm hydrogels with Young´s modulus of a) 2 kPa, b) 5.2 kPa, c) 11.6 kPa, d) 18.9 kPa, and e) 50 kPa. The yellow lines in images c) and d) show the cell edge (border). Scale bar:20 µm.

5.2 Traction force magnitudes in vimentin depleted cells and control cells

Actomyosin contraction in negative control and vimentin depleted cells was measured using traction force microscopy (TFM). Traction forces are applied to the surface via the attachment of the cell on the hydrogel and result in the displacement of the fluorescence beads embedded into the hydrogels. The displacement of the beads is correlated to traction forces using a Fourier transform traction cytometry model. Thus, I obtained the traction forces by calculating the displacement of the beads. Traction force magnitudes were quantified for every cell by summing up all the magnitude of the traction force

vectors. Figure 5.2 shows the quantification of traction force magnitudes in negative control and vimentin KD cells. The mean value of the traction force magnitude in both populations is 300 kPa. These data show there is no significant difference in traction stress in cells with the lack of vimentin compared with control cells. In conclusion, the lack of vimentin does not impair the traction force magnitude of RPE1 cells applied on the hydrogel via actomyosin, and vimentin is not involved in the magnitude of the traction stress.

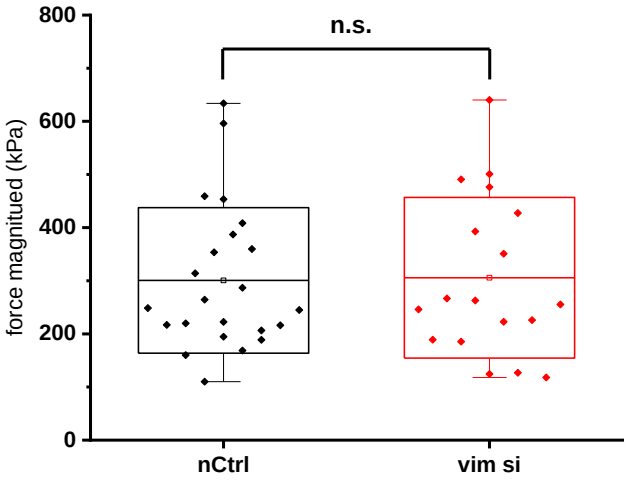

Figure 5.2 Quantification of traction force magnitudes in negative control and vimentin depleted cells.

Traction force magnitudes applied to the surface via negative control (nCtrl) and vimentin depleted (vim Si) cells. Whiskers box plots represent the standard deviation. The mean value is given by the middle line within the box plot. Significance: *t*-test for independent samples, n.s.: not significant. The number of negative control cells and the number of vimentin depleted cells are respectively 23 and 18.

Recently, it has been shown that the orientation of traction stress in vimentin KD HFF cells is not similar to their orientation in control cells [94]. In vimentin KD HFF cells traction stresses are randomly aligned compared to control cells [94]. I also observed the orientation of beads displacements. Figure 5.3 (a) shows the displacement vectors of beads in control cells and vimentin KD cells. The cell edge is drawn with a yellow line. The traction forces are not applied to the surface homogeneously and in the consequence, the displacements of beads are not homogeneous. Figure 5.3 (b) is a sketch of the displacement of the beads. The orientations of the displacement vectors of beads are illustrated with red arrows.

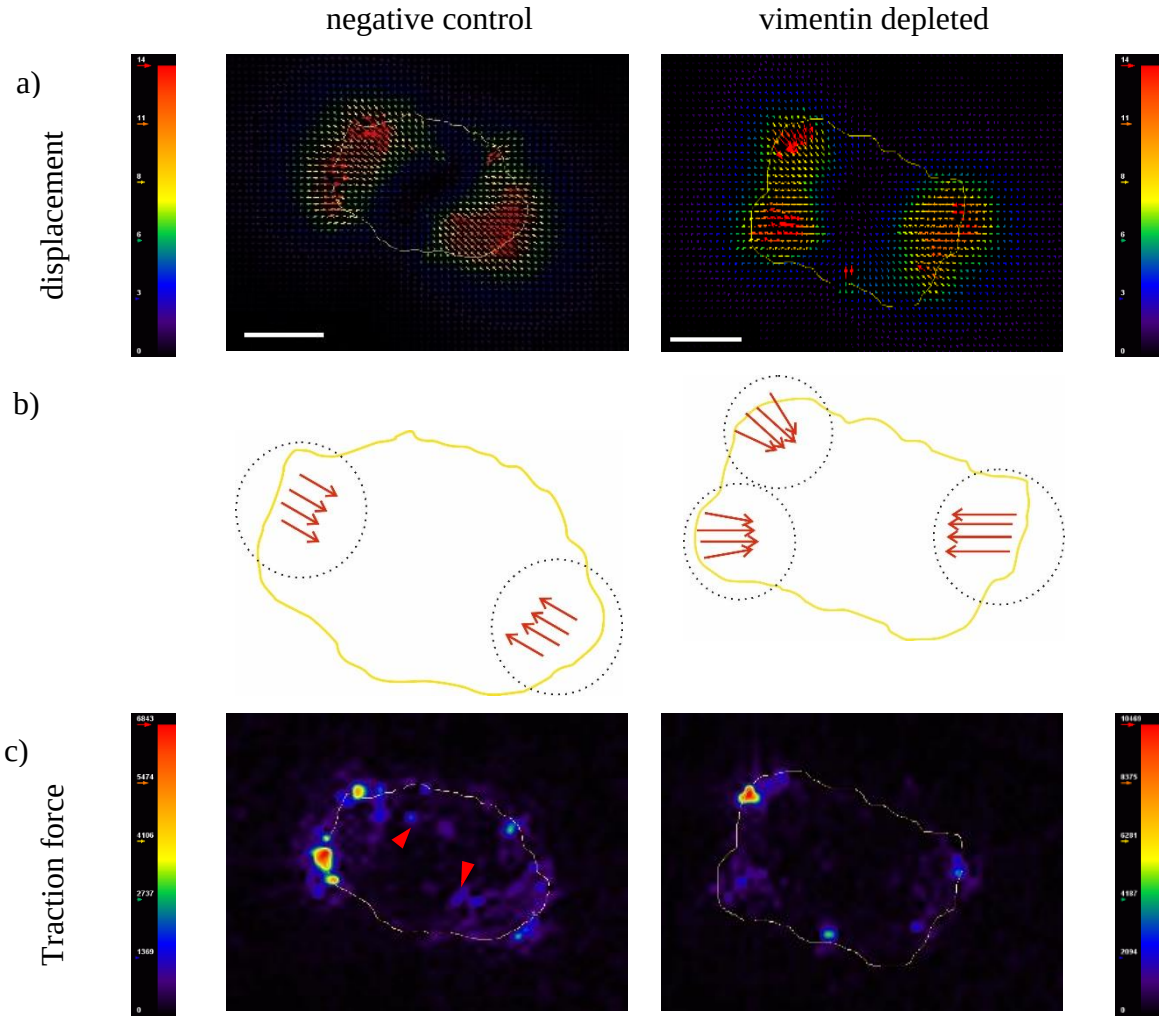

Figure 5.3 Bead displacements and traction forces applied to the surface by negative control cells and vimentin depleted cells.

a) The displacement of the fluorescence beads embedded in the surface under negative control (left) and vimentin KD (right) cells. b) The sketch of the displacement of the beads. The red arrays show the beads displacement vectors and the dot-line circles show traction regions. c) The heating map of traction force magnitudes applied to the surface via the same negative control (left) and vimentin KD (right) cells with the same scale bars in (a). The red arrowheads show traction force not close to the cell edge.

The yellow line in each image shows the cell edge (border). The heat map scales in the left side of the negative control and the right side of the vimentin depleted show the minimum (black) to the maximum (red) values for displacement and traction force magnitudes in pixel and Pascal respectively. Scale bars: 20 µm.

The regions with the higher magnificence of the displacement of beads are shown in Figure 5.3 (b) and are referred to as traction region. My data show that the number of the traction regions in the vimentin KD cells is higher than in control cells (e.g., in Figure 5.3 (b) the number of the traction regions in negative control and vimentin KD cells are

respectively 2 and 3). Therefore, the orientations of the displacement vectors of beads are more randomly distributed in vimentin KD cells when compared to control cells. The orientation of the displacement of beads is correlated with the traction force direction. Therefore, the traction force direction is more random in vimentin KD cells than in control cells, even though the traction force magnitude is comparable in both populations. To conclude, vimentin aligned traction stress in RPE1 cells and the lack of vimentin results in more random orientations of the traction force than in control cells. Figure 5.3 (c) shows the heating map of traction forces in control RPE1 cells and vimentin KD RPE1 cells. The cell edge is drawn with a yellow line. The traction forces applied to the surface are close to the cell periphery for vimentin KD cells while for WT cells, the traction forces applied to the surface are not only at the cell periphery but also close to the cell center (arrowheads in Figure 5.3 (c)). The data show that the lack of vimentin influences traction force distribution in RPE1 cells (one more image of the bead displacement and the heating map of traction forces in vimentin silenced and negative control cells are shown in appendix, Figure 10.2). Taken together, our findings show that the lack of vimentin does not affect the magnitude of the traction forces in RPE1 cells however, it influences traction force magnitude distribution and the direction of traction forces.

5.3 Discussion on the contribution of vimentin to actin force generation

Previous studies suggested that the contraction generated by SFs promotes cell migration [68]. Alternatively, other researchers suggested that SFs are inhibiting cell migration via generating contraction forces [70]. Thus, contractility would either inhibit cell migration or promote cell migration. Therefore, an optimal balance for contractility is required for efficient motility and this balance might be different for different cell types depending on their role in the body.

Moreover, there are distinct findings of the influence of vimentin on traction force generation and cell contractility. In the literature, it has been shown that SFs organization and orientation are unchanged in vimentin KO MEFs cells compare to vimentin WT MEFs cells [141]. However, higher traction forces have been measured when generated by vimentin KO MEFs cells than when generated by vimentin WT MEFs cells [141]. In vimentin KO MEFs cells the resistance against SF contraction decreased, which resulted in an increase in the stress generation [141]. However, it has been recently shown that the absence of vimentin decreases the ratio of actin SFs assembly and disassembly in focal

adhesions [100]. There is evidence that vimentin KD cells migrate slower than WT cells [5, 52]. This suggests that the lack of vimentin leads to less [158] and weaker traction forces [159, 160], and finally slows down cell migration. In the presented project, I show that the lack of vimentin in RPE1 cells has no significant effect on traction force magnitude applied by cells to the surface as compared with negative control cells. However, my findings show that the numbers of the traction regions are more in the vimentin KD cells than in control cells. I also show that in the vimentin KD cells the orientation of the traction forces is more randomly oriented than in control cells. In conclusion, the lack of vimentin might influence actin SFs distribution and in consequence the cell adhesion sites.The effect of vimentin deficiency in actin dynamics in SFs might result from an unknown role of vimentin in cell signalling. Recently, it was shown that ROCK inhibition reduces the expression of vimentin in the human aortic vascular smooth muscle cells (HA-VSMCs) that results in inhibition of migration [161]. It is already commonly accepted that the activation of ROCK via the activation of RhoA stimulates F-actin stabilization and actomyosin contraction. Moreover, it has been shown that the depletion of vimentin activates RhoA [100]. As a consequence, ROCK is activated and increases F-actin stabilization and actomyosin contraction. Thus the activation of RhoA (consequently the activation of ROCK) is vimentin dependent [100] and inhibition of ROCK might affect the expression of vimentin [161]. In the presented project, my data do not show that the lack of vimentin activates or inhibits the ROCK pathway however, our findings show that the lack of vimentin influences the traction force distribution and accordingly it might affect cell adhesion sites. Figure 5.4 shows a small part of Rho pathway that leads to actin filament stabilization and actomyosin contraction.

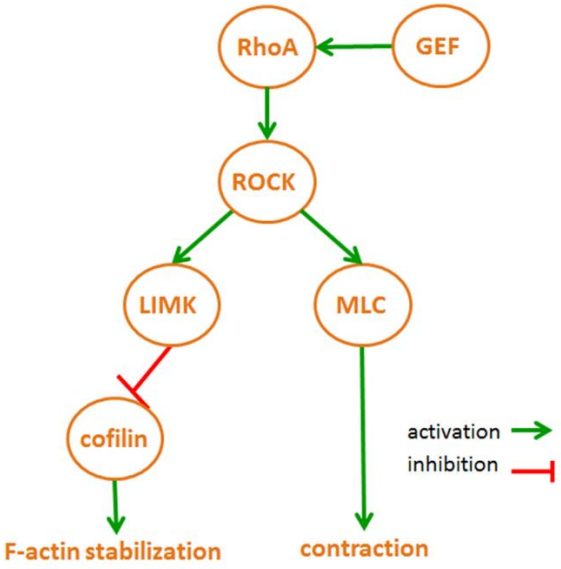

Figure 5.4 Scheme of a part of the RhoA pathway

RhoA is activated through the Guanine nucleotide exchange factor (GEF) that activates ROCK. ROCK activation, actives MLC and Lim Kinase (LIMK). Activation of MLS stimulates actomyosin contraction, and activation of LIMK inhibits cofilin and stimulates F-actin stabilization.

Furthermore, recent studies have shown that the activation of mDia (as a member of formin proteins family that plays a key role in actin filaments elongation and SFs formation) and ROCK together is required to stabilize actin SFs and suggested that a defect in the balance between mDia and ROCK influence actin filaments formation [64, 162]. Activation of mDia results in the fast growth of actin nucleation and elongation [163]. Thus, a lack of vimentin may activate ROCK but not activate mDia spontaneously, to increase the actomyosin contraction. To understand the role of vimentin in cell signaling I would suggest future work to study the influence of vimentin on ROCK and mDia expression simultaneously and independently.

6 Conclusion

The aim of this study was to identify the effects of vimentin IFs on actin dynamics in SFs. I revealed that there is interplay between vimentin IFs and actin SFs in living RPE1 cells. I measured the actin turnover rate and the fraction of the actin monomers that are involved in actin turnover by using FRAP analysis. I concluded that vimentin is an important factor to consider when targeting actin dynamics in SFs. My findings show that vimentin affects actin turnover rate, while the mobile fraction is comparable in vimentin KD and control cells. My data demonstrated that there is no linear correlation between actin dynamics in SFs and the thickness of the bundles in negative control and vimentin silenced cells. Thus, actin dynamics in SFs are not modified by their thickness. I found that actin dynamics, in ventral SFs, in micropatterned cells were comparable to actin dynamics in SFs in nonpatterned cells and moreover, actin dynamics in vimentin KD cells in micropatterned and nonpatterned cells are respectively comparable. From these results, I concluded that the cell geometry is not involved in actin dynamics in ventral SFs. I also showed that the cytoplasmic actin dynamics is not modified by the depletion of vimentin. Thus, vimentin does not affect the diffusion recovery of the cytoplasmic actin.

In the presented study, actin turnover rate in SFs in the absence of plectin is comparable with the control cells however, the fraction of actin monomers involved in actin recovery is higher in plectin KD cells compared with control cells. Our findings show that the inhibition of the indirect interplay of vimentin and actin does not affect actin halftime recovery in SFs; while the mobile fraction of actin monomers recovered was increased in plectin depleted cells.

By measuring the traction forces applied to hydrogel surfaces via vimentin KD and control cells using traction force microscopy, I found that the lack of vimentin does not affect traction force magnitude but the traction force orientation and organization. My findings show that the lack of vimentin influences the traction force distribution and accordingly suggested the influence of vimentin on cell adhesion sites.

In conclusion, by quantifying the actin dynamics in SFs using FRAP, I showed that actin turnover rate in SFs in the lack of vimentin is slower than in control cells. This alteration is neither due to the thickness of SF bundles nor cell geometry. Plectin as a cross-linker protein influences the amount of actin monomers that are involved in actin recovery. In conclusion, not only the lack of vimentin but also cutting the link between actin and

vimentin influences actin dynamics. The lack of vimentin does not influence traction force magnitude, but it influences the distribution of traction stress applied to the surface. Thus, there will be a link between the effects of the lack of vimentin on traction force distribution and actin dynamics. This suggests that the lack of vimentin influences the distribution of adhesion and accordingly influences cell migration.

7 Outlook

Considering the data of my Ph.D., I can confirm the interplay between vimentin and actin filaments, specifically on actin dynamics in SFs. To better understand the mechanisms behind the vimentin-actin interplay, future studies might be performed on SFs distribution in vimentin KD cells.

Moreover, actin dynamics in SFs might be studied in vimentin overexpressed cells or cancer cells in order to better explain the migration progresses and the involvement of vimentin in cancer cells.

Finally, future simulation on actin dynamics in SFs in the presence or absence of vimentin could be performed to enhance our understanding of the mechanisms and models behind the experiment.

8 Publications

1- I.N. Dahmke, P. Trampert, F. Weinberg, Z. Mostajeran, F. Lautenschläger, and N. de Jonge. *Correlative Fluorescence- and Electron Microscopy of Whole Breast Cancer Cells Reveals Different Distribution of ErbB2 Dependent on Underlying Actin*, 30th June 2020, Frontiers in Cell and Developmental Biology Journal.

9 Bibliography

1. Battaglia, R.A., et al., *Vimentin on the move: new developments in cell migration.* F1000Research, 2018. **7**: p. 1-10.
2. Raftopoulou, M. and A. Hall, *Cell migration: Rho GTPases lead the way.* Developmental Biology, 2004. **265**(1): p. 23-32.
3. Lees, J.G., C.T. Bach, and G.M. O'Neill, *Interior decoration: tropomyosin in actin dynamics and cell migration.* Cell Adhesion and Migration, 2011. **5**(2): p. 181-6.
4. Leduc, C. and S. Etienne-Manneville, *Intermediate filaments in cell migration and invasion: the unusual suspects.* Curr Opin Cell Biol, 2015. **32**: p. 102-12.
5. Beate Eckes, D.D., Emma Colucci-Guyon, Ning Wang, Andrew Maniotis, Donald Ingber, Alexandra Merckling, Francina Langa, Monique Aumailley, Annie Delouvée6, Victor Koteliansky, Charles Babinet and Thomas Krieg, *Impaired mechanical stability, migration and contractile capacity in vimentindeficient fibroblasts.* Journal of Cell Science, 1998. **111**: p. 1897-1907.
6. Kidd, M.E., D.K. Shumaker, and K.M. Ridge, *The role of vimentin intermediate filaments in the progression of lung cancer.* Am J Respir Cell Mol Biol, 2014. **50**(1): p. 1-6.
7. Satelli, A. and S. Li, *Vimentin in cancer and its potential as a molecular target for cancer therapy.* Cell Mol Life Sci, 2011. **68**(18): p. 3033-46.
8. Richardson, A.M., et al., *Vimentin Is Required for Lung Adenocarcinoma Metastasis via Heterotypic Tumor Cell-Cancer-Associated Fibroblast Interactions during Collective Invasion.* Clin Cancer Res, 2018. **24**(2): p. 420-32.
9. Ching-Yi Liu, H.-H.L., Ming-Jer Tang, and Yang-Kao Wang, *Vimentin contributes to epithelial-mesenchymal transition cancer cell mechanics by mediating cytoskeletal organization and focal adhesion maturation.* Oncotarget, 2015. **6**(18): p. 15966-83.
10. Thery, M., et al., *Cell distribution of stress fibres in response to the geometry of the adhesive environment.* Cell Motil Cytoskeleton, 2006. **63**(6): p. 341-55.
11. Favre, B., et al., *Plectin interacts with the rod domain of type III intermediate filament proteins desmin and vimentin.* Eur J Cell Biol, 2011. **90**(5): p. 390-400.
12. Katada, K., et al., *Plectin promotes migration and invasion of cancer cells and is a novel prognostic marker for head and neck squamous cell carcinoma.* J Proteomics, 2012. **75**(6): p. 1803-15.
13. *"Eukaryotic cell"*. 13.01.2021; Available from: https://www.britannica.com/science/cell-biology/The-structure-of-biological-molecules, 13.01.2021.
14. Fletcher, D.A. and R.D. Mullins, *Cell mechanics and the cytoskeleton.* Nature, 2010. **463**(7280): p. 485-92.
15. Wickstead, B. and K. Gull, *The evolution of the cytoskeleton.* J Cell Biol, 2011. **194**(4): p. 513-25.
16. Wen, Q. and P.A. Janmey, *Polymer physics of the cytoskeleton.* Curr Opin Solid State Mater Sci, 2011. **15**(5): p. 177-82.
17. Lorenz, C., et al., *Lateral Subunit Coupling Determines Intermediate Filament Mechanics.* Physical Review Letters, 2019. **123**(18): p. 1-6.
18. Bonakdar, N., et al., *Determining the mechanical properties of plectin in mouse myoblasts and keratinocytes.* Exp Cell Res, 2015. **331**(2): p. 331-7.
19. Cooper GM, *The Cell: A Molecular Approach*. 2000, USA: Sinauer Associates Inc.
20. Zhuo Gan, L.D., Christoph J. Burckhardt, Jason Lowery, Assaf Zaritsky, Karlyndsay Sitterley, Andressa Mota, Nancy Costigliola, Colby G. Starker, Daniel F. Voytas, Jessica Tytell, Robert D. Goldman, and Gaudenz Danuser, *Vimentin Intermediate Filaments Template Microtubule Networks to Enhance Persistence in Cell Polarity and Directed Migration.* Cell Syst, 2016. **3**(3): p. 252-63.
21. Tang, D.D. and B.D. Gerlach, *The roles and regulation of the actin cytoskeleton, intermediate filaments and microtubules in smooth muscle cell migration.* Respir Res, 2017. **18**(1): p. 1-12.
22. *"Microtobule filament"* Available from: https://fineartamerica.com/featured/structure-of-a-microtubule-kateryna-konscience-photo-library.html, 02.12.2020.

23. W. Kabsch, H.G.M., D. Suckt, E. F. Pai, K. C. Holmes, *Atomic structure of the actin: DNase I complex*. Nature, 1990. **347**: p. 37-44.
24. Grazi, E., *What is the diameter of the actin filament?* FEBS Letters, 1997. **405**(3): p. 249-252.
25. Özer, I.D., *Analyzing the Role of CyFIP2 in the Mouse Brain*. 2020.
26. Simiczyjew, A., et al., *Are non-muscle actin isoforms functionally equivalent?* Histol Histopathol, 2017. **32**(11): p. 1125-39.
27. Skruber, K., T.A. Read, and E.A. Vitriol, *Reconsidering an active role for G-actin in cytoskeletal regulation.* Journal of Cell Science, 2018. **131**(1): p. 1-11.
28. Perrin, B.J. and J.M. Ervasti, *The actin gene family: function follows isoform.* Cytoskeleton, 2010. **67**(10): p. 630-4.
29. Bunnell, T.M., et al., *beta-Actin specifically controls cell growth, migration, and the G-actin pool*. Molecular Biology of the Cell, 2011. **22**(21): p. 4047-58.
30. Pavlyk, I., et al., *Rapid and dynamic arginylation of the leading edge beta-actin is required for cell migration.* Traffic, 2018. **19**(4): p. 263-72.
31. Pasquier, E., et al., *gamma-Actin plays a key role in endothelial cell motility and neovessel maintenance.* Vascular Cell, 2015. **7**(2): p. 1-16.
32. M. A. Hill, P.G., *Beta and Gamma Actin mRNAs Are Differentially Located within Myoblasts*. The Journal of Cell Biology, 1993. **122**: p. 825-32.
33. Shum, M.S., et al., *γ-Actin regulates cell migration and modulates the ROCK signaling pathway*. The FASEB journal, 2011. **25**(12): p. 4423-33.
34. Pollard, T.D., *Actin and Actin-Binding Proteins.* Cold Spring Harb Perspect Biol, 2016. **8**(8): p. 1-18.
35. Broussard, J.A., et al., *Scaling up single-cell mechanics to multicellular tissues - the role of the intermediate filament-desmosome network.* Journal of Cell Science, 2020. **133**(6): p. 1-13.
36. Blanchoin, L., et al., *Actin dynamics, architecture, and mechanics in cell motility.* Physiol Rev, 2014. **94**(1): p. 235-63.
37. Fujiwara, I., et al., *Polymerization and depolymerization of actin with nucleotide states at filament ends.* Biophys Rev, 2018. **10**(6): p. 1513-1519.
38. D. Pantaloni, M.F.C., M. COU, A. Lal, S. Brenner, and E. D. Korn, *The Critical Concentration of Actin in the Presence of ATP Increases with the Number Concentration of Filaments and Approaches the Critical Concentration of Actin *ADP*. The Journal of Biological Chemistry, 1984. **259**: p. 6274-83.
39. Kudryashov, D.S. and E. Reisler, *ATP and ADP actin states.* Biopolymers, 2013. **99**(4): p. 245-56.
40. Fenix, A.M. and D.T. Burnette, *Assembly of myosin II filament arrays: Network Contraction versus Expansion.* Cytoskeleton, 2018. **75**(12): p. 545-549.
41. Vicente-Manzanares, M., et al., *Regulation of protrusion, adhesion dynamics, and polarity by myosins IIA and IIB in migrating cells.* The Journal of Cell Biology, 2007. **176**(5): p. 573-80.
42. Chang, C.W. and S. Kumar, *Differential Contributions of Nonmuscle Myosin II Isoforms and Functional Domains to Stress Fiber Mechanics.* Sci Rep, 2015. **5**: p. 13736.
43. Makowska, K.A., et al., *Specific Myosins Control Actin Organization, Cell Morphology, and Migration in Prostate Cancer Cells.* Cell Reports, 2015. **13**(10): p. 2118-25.
44. Grison, M., et al., *alpha-Actinin/titin interaction: A dynamic and mechanically stable cluster of bonds in the muscle Z-disk.* PNAS, 2017. **114**(5): p. 1015-1020.
45. Hall, A.J.R.a.A., *The Small GTP-Binding Protein rho Regulates the Assembly of Focal Adhesions and Actin Stress Fibers in Response to Growth Factors.* Cell, 1992. **70**: p. 389-399.
46. Wiche, G., S. Osmanagic-Myers, and M.J. Castanon, *Networking and anchoring through plectin: a key to IF functionality and mechanotransduction.* Curr Opin Cell Biol, 2015. **32**: p. 21-9.

47. Winter, L., et al., *Downstream effects of plectin mutations in epidermolysis bullosa simplex with muscular dystrophy.* Acta Neuropathologica Communications, 2016. **4**(1): p. 1-10.
48. Castanon, M.J., et al., *Plectin-intermediate filament partnership in skin, skeletal muscle, and peripheral nerve.* Histochem Cell Biol, 2013. **140**(1): p. 33-53.
49. R. Foisner, E.E.L., H. Herrmann, J. V. Small, D. Lawson,w and G. Wiche, *Cytoskeleton-associated Plectin: In Situ Localization, In Vitro Reconstitution, and Binding to Immobilized Intermediate Filament Proteins.* The Journal of Cell Biology, 1988: p. 723-733.
50. Burgstaller, G., et al., *Keeping the vimentin network under control: cell-matrix adhesion-associated plectin 1f affects cell shape and polarity of fibroblasts.* Molecular Biology of the Cell, 2010. **21**(19): p. 3362-75.
51. Dave, J.M. and K.J. Bayless, *Vimentin as an integral regulator of cell adhesion and endothelial sprouting.* Microcirculation, 2014. **21**(4): p. 333-44.
52. Ivaska, J., et al., *Novel functions of vimentin in cell adhesion, migration, and signaling.* Exp Cell Res, 2007. **313**(10): p. 2050-62.
53. Steinbock, F.A., et al., *Dose-dependent linkage, assembly inhibition and disassembly of vimentin and cytokeratin 5/14 filaments through plectin's intermediate filament-binding domain.* J Cell Sci, 2000. **113 (Pt 3)**: p. 483-91.
54. Foisner, R., et al., *Distribution and ultrastructure of plectin arrays in subclones of rat glioma C6 cells differing in intermediate filament protein (vimentin) expression.* Journal of Structural Biology, 1995. **115**(3): p. 304-17.
55. Tokuraku, K., M. Kuragano, and T.Q.P. Uyeda, *Long-Range and Directional Allostery of Actin Filaments Plays Important Roles in Various Cellular Activities.* Intenational Journal of Molecular Science, 2020. **21**(9): p. 1-16.
56. Charras, G.T., et al., *Reassembly of contractile actin cortex in cell blebs.* The Journal of Cell Biology, 2006. **175**(3): p. 477-490.
57. Deguchi, S. and M. Sato, *Biomechanical properties of actin stress fibers of non-motile cells.* Biorheology, 2009. **46**(2): p. 93-105.
58. Cooper, J.A., *Actin Dynamics: Tropomyosin Provides Stability.* Current Biology, 2002. **12**: p. R523-25.
59. Hotulainen, P., et al., *Actin-depolymerizing factor and cofilin-1 play overlapping roles in promoting rapid F-actin depolymerization in mammalian nonmuscle cells.* Mol Biol Cell, 2005. **16**(2): p. 649-64.
60. S. M. Wang, M.L.G., E. Schultz, J. C. Bulinski, J. J.-C. Lin, and J. L. Lessard, *Studies on Cardiac Myofibrillogenesis with Antibodies to Titin, Actin, Tropomyosin, and Myosin.* The Journal of Cell Biology, 1988. **107**: p. 1075-83.
61. S. B. Khatau, C.M.H., P. J. Stewart-Hutchinson, M. S. Patela, C. L. Stewart, P. C. Searsona, D. Hodzicb, and D. Wirtz, *A perinuclear actin cap regulates nuclear shape.* PNAS, 2009. **106**(45): p. 19017-22.
62. Maninova, M. and T. Vomastek, *Dorsal stress fibers, transverse actin arcs, and perinuclear actin fibers form an interconnected network that induces nuclear movement in polarizing fibroblasts.* FEBS J, 2016. **283**(20): p. 3676-93.
63. Tojkander, S., G. Gateva, and P. Lappalainen, *Actin stress fibers--assembly, dynamics and biological roles.* J Cell Sci, 2012. **125**(Pt 8): p. 1855-64.
64. Hotulainen, P. and P. Lappalainen, *Stress fibers are generated by two distinct actin assembly mechanisms in motile cells.* J Cell Biol, 2006. **173**(3): p. 383-94.
65. Feng, Y., et al., *alpha-actinin1 and 4 tyrosine phosphorylation is critical for stress fiber establishment, maintenance and focal adhesion maturation.* Experimental Cell Research, 2013. **319**(8): p. 1124-35.
66. *"Actin stress fiber bundles"*. Available from: https://www.mechanobio.info/cytoskeleton-dynamics/what-are-contractile-fibers/, 02.12.2020.
67. Pellegrin, S. and H. Mellor, *Actin stress fibres.* Journal of Cell Science, 2007. **120**(Pt 20): p. 3491-9.

68. T. E. Kreis, W.B., *Stress Fiber Sarcomeres of Fibroblasts Are Contractile.* Cell, 1980. **22**: p. 555-61.
69. Kumar, S., et al., *Viscoelastic retraction of single living stress fibers and its impact on cell shape, cytoskeletal organization, and extracellular matrix mechanics.* Biophys J, 2006. **90**(10): p. 3762-73.
70. Burridge, K., *Are stress fibres contractile?* Nature, 1981. **294**: p. 691-692.
71. Rid, R., et al., *The last but not the least: the origin and significance of trailing adhesions in fibroblastic cells.* Cell Motility and the Cytoskeleton, 2005. **61**(3): p. 161-71.
72. Chesarone, M.A., A.G. DuPage, and B.L. Goode, *Unleashing formins to remodel the actin and microtubule cytoskeletons.* Nature Review Molecular Cell Biology, 2010. **11**(1): p. 62-74.
73. R. Kaunas, P.N., S. Usami, and S. Chien, *Cooperative effects of Rho and mechanical stretch on stress fiber organization.* PNAS, 2005. **102**(44): p. 15895-900.
74. Lodish H, B.A., Zipursky SL, et al., *Molecular Cell Biology*. 2000, New York: W. H. Freeman.
75. Gomes, F.C., D. Paulin, and V. Moura Neto, *Glial fibrillary acidic protein (GFAP): modulation by growth factors and its implication in astrocyte differentiation.* Braz J Med Biol Res, 1999. **32**(5): p. 619-31.
76. Mücke, N., et al., *Assessing the flexibility of intermediate filaments by atomic force microscopy*. Journal of Molecular Biology, 2004. **335**(5): p. 1241-50.
77. Herrmann, H., et al., *Intermediate filaments: from cell architecture to nanomechanics.* Nature Reviews Molecular Cell Biology, 2007. **8**(7): p. 562-573.
78. Schopferer, M., et al., *Desmin and vimentin intermediate filament networks: their viscoelastic properties investigated by mechanical rheometry.* J Mol Biol, 2009. **388**(1): p. 133-43.
79. Block, J., et al., *Physical properties of cytoplasmic intermediate filaments.* Biochimica et Biophysica Acta, 2015. **1853**(11 Pt B): p. 3053-64.
80. M. G. L. van den Heuvel, M.P.d.G., C. Dekker,, *Microtubule curvatures under perpendicular electric forces reveal a low persistence length.* PNAS, 2007. **105**(23): p. 7941-46.
81. Mendez, M.G., D. Restle, and P.A. Janmey, *Vimentin enhances cell elastic behavior and protects against compressive stress.* Biophys J, 2014. **107**(2): p. 314-23.
82. Stankevicins, L.D.C., et al., *Vimentin provides the mechanical resilience required for amoeboid migration and protection of the nucleus.* bioRxiv, 2019: p. 720946.
83. Goldfarb, L.G., et al., *Desmin myopathy*. Brain, 2004. **127**(Pt 4): p. 723-34.
84. G. Bonne, M.R.D.B., S. Varnous, H. Bécane, E. Hammouda, L. Merlini, F. Muntoni, C. R. Greenberg, F. Gary, J. Urtizberea, D. Duboc, M. Fardeau, D. Toniolo, K. Schwartz, *Mutations in the gene encoding lamin A/C cause autosomal dominant Emery-Dreifuss muscular dystrophy*. Nature genomic, 1999. **21**: p. 285-288.
85. Jones, J.R., et al., *Mutations in GFAP Disrupt the Distribution and Function of Organelles in Human Astrocytes.* Cell Reports, 2018. **25**(4): p. 947-58.
86. Margiotta, A. and C. Bucci, *Role of Intermediate Filaments in Vesicular Traffic*. Cells, 2016. **5**(2): p. 1-22.
87. Hohmann, T. and F. Dehghani, *The Cytoskeleton-A Complex Interacting Meshwork.* Cells, 2019. **8**(4): p. 1-58.
88. Guo, M., et al., *Probing the stochastic, motor-driven properties of the cytoplasm using force spectrum microscopy*. Cell, 2014. **158**(4): p. 822-832.
89. Koster, S., et al., *Intermediate filament mechanics in vitro and in the cell: from coiled coils to filaments, fibers and networks.* Curr Opin Cell Biol, 2015. **32**: p. 82-91.
90. Mendez, M.G., S. Kojima, and R.D. Goldman, *Vimentin induces changes in cell shape, motility, and adhesion during the epithelial to mesenchymal transition.* Faseb j, 2010. **24**(6): p. 1838-51.
91. Guo, M., et al., *The role of vimentin intermediate filaments in cortical and cytoplasmic mechanics.* Biophys J, 2013. **105**(7): p. 1562-8.

92. Huber, F., et al., *Cytoskeletal crosstalk: when three different personalities team up.* Curr Opin Cell Biol, 2015. **32**: p. 39-47.
93. Buehler, M.J., *Mechanical players-The role of intermediate filaments in cell mechanics and organization.* Biophysical Journal, 2013. **105**(8): p. 1733-4.
94. Costigliola, N., et al., *Vimentin fibers orient traction stress.* PNAS, 2017. **114**(20): p. 5195-5200.
95. Jiu, Y., et al., *Bidirectional Interplay between Vimentin Intermediate Filaments and Contractile Actin Stress Fibers.* Cell Rep, 2015. **11**(10): p. 1511-8.
96. Esue, O., et al., *A direct interaction between actin and vimentin filaments mediated by the tail domain of vimentin.* J Biol Chem, 2006. **281**(41): p. 30393-9.
97. R. M. Evans, L.M.F., *An alteration in the phosphorylation of vimentin-type intermediate filaments is associated with mitosis in cultured mammalian cells.* Cell, 1982. **29**: p. 43-52.
98. Izawa, I. and M. Inagaki, *Regulatory mechanisms and functions of intermediate filaments: a study using site- and phosphorylation state-specific antibodies.* Cancer Sci, 2006. **97**(3): p. 167-74.
99. Ivaska, J., et al., *PKCepsilon-mediated phosphorylation of vimentin controls integrin recycling and motility.* The EMBO Journal, 2005. **24**(22): p. 3834-45.
100. Jiu, Y., et al., *Vimentin intermediate filaments control actin stress fiber assembly through GEF-H1 and RhoA.* J Cell Sci, 2017. **130**(5): p. 892-902.
101. Robert, A., et al., *Microtubule-dependent transport of vimentin filament precursors is regulated by actin and by the concerted action of Rho- and p21-activated kinases.* The FASEB Journal, 2014. **28**(7): p. 2879-90.
102. Campbell, I.D., *Studies of focal adhesion assembly.* Biochemical Society Transactions, 2008. **36**(Pt 2): p. 263-6.
103. Tsuruta, D. and J.C. Jones, *The vimentin cytoskeleton regulates focal contact size and adhesion of endothelial cells subjected to shear stress.* Journal of Cell Science, 2003. **116**(Pt 24): p. 4977-84.
104. Kim, H., et al., *Regulation of cell adhesion to collagen via beta1 integrins is dependent on interactions of filamin A with vimentin and protein kinase C epsilon.* Exp Cell Res, 2010. **316**(11): p. 1829-44.
105. Kim, H. and C.A. McCulloch, *Filamin A mediates interactions between cytoskeletal proteins that control cell adhesion.* FEBS Letters, 2011. **585**(1): p. 18-22.
106. Liu, Y.H., et al., *Plectin deficiency on cytoskeletal disorganization and transformation of human liver cells in vitro.* Med Mol Morphol, 2011. **44**(1): p. 21-6.
107. Houtsmuller, A.B. and W. Vermeulen, *Macromolecular dynamics in living cell nuclei revealed by fluorescence redistribution after photobleaching.* Histochem Cell Biol, 2001. **115**(1): p. 13-21.
108. White, J. and E. Stelzer, *Photobleaching GFP reveals protein dynamics inside live cells.* Trends Cell Biol, 1999. **9**(2): p. 61-5.
109. Kapustina, M., et al., *Modeling capping protein FRAP and CALI experiments reveals in vivo regulation of actin dynamics.* Cytoskeleton (Hoboken), 2010. **67**(8): p. 519-34.
110. Ishikawa-Ankerhold, H.C., R. Ankerhold, and G.P. Drummen, *Advanced fluorescence microscopy techniques--FRAP, FLIP, FLAP, FRET and FLIM.* Molecules, 2012. **17**(4): p. 4047-132.
111. Lewalle, A., et al., *A phenomenological density-scaling approach to lamellipodial actin dynamics.* Interface Focus, 2014. **4**(6): p. 1-15.
112. Sustr, D., et al., *Multi-Fractional Analysis of Molecular Diffusion in Polymer Multilayers by FRAP: A New Simulation-Based Approach.* The Journal of Physical Chemistry B, 2018. **122**(3): p. 1323-33.
113. Koulouras, G., et al., *EasyFRAP-web: a web-based tool for the analysis of fluorescence recovery after photobleaching data.* Nucleic Acids Research, 2018. **46**(W1): p. W467-W472.
114. Sprague, B.L. and J.G. McNally, *FRAP analysis of binding: proper and fitting.* Trends in Cell Biology, 2005. **15**(2): p. 84-91.

115. Takeshi, S., C.G. Pack, and R.D. Goldman, *Analyses of the Dynamic Properties of Nuclear Lamins by Fluorescence Recovery After Photobleaching (FRAP) and Fluorescence Correlation Spectroscopy (FCS).* Methods Mol Biol, 2016. **1411**: p. 99-111.
116. Rabut, G., V. Doye, and J. Ellenberg, *Mapping the dynamic organization of the nuclear pore complex inside single living cells.* Nature Cell Biology, 2004. **6**(11): p. 1114-21.
117. Watanabe, N., *Inside view of cell locomotion through single-molecule: fast F-/G-actin cycle and G-actin regulation of polymer restoration.* Proc Jpn Acad Ser B Phys Biol Sci, 2010. **86**(1): p. 62-83.
118. Sprague, B.L., et al., *Analysis of binding reactions by fluorescence recovery after photobleaching.* Biophys J, 2004. **86**(6): p. 3473-95.
119. Fritzsche, M., et al., *Analysis of turnover dynamics of the submembranous actin cortex.* Mol Biol Cell, 2013. **24**(6): p. 757-67.
120. Fritzsche, M. and G. Charras, *Dissecting protein reaction dynamics in living cells by fluorescence recovery after photobleaching.* Nature Protocols, 2015. **10**(5): p. 660-80.
121. Axelrod, D., et al., *Mobility measurement by analysis of fluorescence photobleaching recovery kinetics.* Biophys J, 1976. **16**(9): p. 1055-69.
122. Soumpasis, D.M., *Theoretical analysis of fluorescence photobleaching recovery experiments.* Biophys J, 1983. **41**(1): p. 95-7.
123. Becheva, Z.R., K.I. Gabrovska, and T.I. Godjevargova, *Comparison between direct and indirect immunofluorescence method for determination of somatic cell count.* Chemical Papers, 2018. **72**(8): p. 1861-1867.
124. Riedl, J., et al., *Lifeact: a versatile marker to visualize F-actin.* Nature Methods, 2008. **5**(7): p. 605-7.
125. Courtemanche, N., T.D. Pollard, and Q. Chen, *Avoiding artefacts when counting polymerized actin in live cells with LifeAct fused to fluorescent proteins.* Nat Cell Biol, 2016. **18**(6): p. 676-83.
126. Melak, M., M. Plessner, and R. Grosse, *Actin visualization at a glance.* J Cell Sci, 2017. **130**(3): p. 525-530.
127. Dolman, N.J., J.A. Kilgore, and M.W. Davidson, *A review of reagents for fluorescence microscopy of cellular compartments and structures, part I: BacMam labeling and reagents for vesicular structures.* Curr Protoc Cytom, 2013. **65**(65): p. Unit 12.30.
128. Kilgore, J.A., N.J. Dolman, and M.W. Davidson, *A review of reagents for fluorescence microscopy of cellular compartments and structures, Part III: reagents for actin, tubulin, cellular membranes, and whole cell and cytoplasm.* Curr Protoc Cytom, 2014. **67**: p. Unit 12.32.
129. Summers, M.D., *Milestones leading to the genetic engineering of baculoviruses as expression vector systems and viral pesticides.* Advances in Virus Research, 2006. **68**: p. 3-73.
130. Ames, R.S., T.A. Kost, and J.P. Condreay, *BacMam technology and its application to drug discovery.* Expert Opin Drug Discov, 2007. **2**(12): p. 1669-81.
131. Nagayama, K., Y. Yahiro, and T. Matsumoto, *Apical and Basal Stress Fibers have Different Roles in Mechanical Regulation of the Nucleus in Smooth Muscle Cells Cultured on a Substrate.* Cellular and Molecular Bioengineering, 2013. **6**(4): p. 473-81.
132. Style, R.W., et al., *Traction force microscopy in physics and biology.* Soft Matter, 2014. **10**(23): p. 4047-55.
133. Hur, S.S., et al., *Traction Force Microscopy for Understanding Cellular Mechanotransduction.* BMB Reports, 2020. **53**(2): p. 74-81.
134. Ladoux, B. and A. Nicolas, *Physically based principles of cell adhesion mechanosensitivity in tissues.* Rep Prog Phys, 2012. **75**(11): p. 1-26.
135. Sune-Aunon, A., et al., *Full L1-regularized Traction Force Microscopy over whole cells.* BMC Bioinformatics, 2017. **18**(1): p. 1-14.
136. *"Western blot technique"*. Available from: https://www.abcam.com/protocols/general-western-blot-protocol, 02.12.2020.

137. Lecuit, T. and P.F. Lenne, *Cell surface mechanics and the control of cell shape, tissue patterns and morphogenesis.* Nature Reviews Molecular Cell Biology, 2007. **8**(8): p. 633-44.
138. Thery, M., *Micropatterning as a tool to decipher cell morphogenesis and functions.* Journal of Cell Science, 2010. **123**(Pt 24): p. 4201-13.
139. Osmanagic-Myers, S., et al., *Plectin reinforces vascular integrity by mediating crosstalk between the vimentin and the actin networks.* Journal of Cell Science, 2015. **128**(22): p. 4138-50.
140. Smith, M.B., et al., *Distributed actin turnover in the lamellipodium and FRAP kinetics.* Biophys J, 2013. **104**(1): p. 247-57.
141. van Loosdregt, I., et al., *The Mechanical Contribution of Vimentin to Cellular Stress Generation.* J Biomech Eng, 2018. **140**(6): p. 1-10.
142. Dmello, C., et al., *Vimentin-mediated regulation of cell motility through modulation of beta4 integrin protein levels in oral tumor derived cells.* Int J Biochem Cell Biol, 2016. **70**: p. 161-72.
143. Kemp, J.P., Jr. and W.M. Brieher, *The actin filament bundling protein alpha-actinin-4 actually suppresses actin stress fibers by permitting actin turnover.* J Biol Chem, 2018. **293**(37): p. 14520-33.
144. Thery, M., *Micropatterning as a tool to decipher cell morphogenesis and functions.* J Cell Sci, 2010. **123**(Pt 24): p. 4201-13.
145. Campbell, J.J. and M.M. Knight, *An improved confocal FRAP technique for the measurement of long-term actin dynamics in individual stress fibers.* Microsc Res Tech, 2007. **70**(12): p. 1034-40.
146. Serres, M.P., et al., *F-Actin Interactome Reveals Vimentin as a Key Regulator of Actin Organization and Cell Mechanics in Mitosis.* Developmental Cell, 2020. **52**(2): p. 210-22.
147. Lanier, M.H., T. Kim, and J.A. Cooper, *CARMIL2 is a novel molecular connection between vimentin and actin essential for cell migration and invadopodia formation.* Mol Biol Cell, 2015. **26**(25): p. 4577-88.
148. Tojkander, S., et al., *Generation of contractile actomyosin bundles depends on mechanosensitive actin filament assembly and disassembly.* Elife, 2015. **4**: p. 1-28.
149. Endlich, N., et al., *Palladin is a dynamic actin-associated protein in podocytes.* Kidney International, 2009. **75**(2): p. 214-26.
150. Gundersen, G.G. and H.J. Worman, *Nuclear positioning.* Cell, 2013. **152**(6): p. 1376-89.
151. Wiche, G. and L. Winter, *Plectin isoforms as organizers of intermediate filament cytoarchitecture.* Bioarchitecture, 2011. **1**(1): p. 14-20.
152. Murthy, K. and P. Wadsworth, *Myosin-II-dependent localization and dynamics of F-actin during cytokinesis.* Curr Biol, 2005. **15**(8): p. 724-31.
153. Wilhelmsson, U., et al., *Vimentin is required for normal accumulation of body fat.* Biol Chem, 2019. **400**(9): p. 1157-62.
154. NING Wang, D.S., *Contribution of intermediate filaments to cell stiffness, stiffening, and growth.* Am J Physiol Cell Physiol, 2000. **279**: p. C188–C194.
155. Penny L. Post, R.L.D., and D. Lansing Taylor, *A Fluorescent Protein Biosensor of Myosin II Regulatory Light Chain Phosphorylation Reports a Gradient of Phosphorylated Myosin II in Migrating Cells.* Molecular Biology of the Cell, 1995. **32**: p. 289-98.
156. Caliari, S.R. and J.A. Burdick, *A practical guide to hydrogels for cell culture.* Nature Methods, 2016. **13**(5): p. 405-14.
157. Schwarz, U.S. and J.R. Soiné, *Traction force microscopy on soft elastic substrates: A guide to recent computational advances.* Biochimica et Biophysica Acta, 2015. **1853**(11 Pt B): p. 3095-104.
158. Pollard, T.D. and G.G. Borisy, *Cellular motility driven by assembly and disassembly of actin filaments.* Cell, 2003. **112**(4): p. 453-65.
159. Tang, D.D., *Intermediate filaments in smooth muscle.* Am J Physiol Cell Physiol, 2008. **294**(4): p. C869-78.

160. Wang, R., et al., *Dissociation of Crk-associated substrate from the vimentin network is regulated by p21-activated kinase on ACh activation of airway smooth muscle.* Am J Physiol Lung Cell Mol Physiol, 2007. **292**(1): p. L240-8.
161. Tang, L., et al., *RhoA/ROCK signaling regulates smooth muscle phenotypic modulation and vascular remodeling via the JNK pathway and vimentin cytoskeleton.* Pharmacological Research, 2018. **133**: p. 201-12.
162. N. Watanabe, T.K., A. Fujita, T. Ishizaki, S. Narumiya, *Cooperation between mDia1 and ROCK in Rho-induced actin reorganization.* Nature Cell Biology, 1999. **1**: p. 136-43.
163. N. Watanabe, P.M., T. Reid, T. Ishizaki, and A.K. G. Watanabe, Y. Saito, K. Nakao, B. M.Jockusch, S. Narumiya,, *p140mDia, a mammalian homolog of Drosophila diaphanous, is a target protein for Rho small GTPase and is a ligand for profilin.* The EMBO Journal, 1997. **16**(11): p. 3044-56.

10 Appendix: Tables of requirements and ingredients

Table 10.1 Cell culture requirements and ingredients

Requirements and ingredients	Manufacturer
Medium DMEM/F-12 (1:1)	Gibco
fetal bovine serum (FBS)	
GlutaMAX (100X)	
penicillin/streptomycin (p/s)	
0.25% Trypsin_EDTA	
phosphate buffered saline (PBS)	
Dulbecco's phosphatebuffered saline (DPBS) (-$CaCl_2$, -$MgCl_2$)	Gibco (14190-094)
Malassez slide (0.200mm depth)	BLAU BRAND
Centrifuge	Eppendorf Centrifuge 5810 R
Incubator	BINDER
Dimethylsulfoxid (DMSO)	Carl Roth GmbH (A994.1)

Generally, variable pipets and pipet tips with the different values and capacities and ethanol cleaning mix (70% ethanol, 30% ultrapure water) are necessary for the cell culture procedure. All the cell culture procedures must be done under a laminar flow hood.

Table 10.2 Transfection requirements and ingredients

Requirements and ingredients	Manufacturer
VIM Silencer Select validated small interfering RNA (siRNA)	Ambion (s14799)
Silencer select Negative Control #1 siRNA	Ambion
PLEC Silencer Pre-disigned siRNA	Ambion (144451)
Lipofectamin RNAiMAX Reagent	Invitrogen (13778-075)
serum free media, Medium DMEM/F-12 (1:1)	Gibco
RNase-free water	Ambion

Table 10.3 BacMam gene delivery system requirements and ingredients

Requirements and ingredients	Manufacturer
CellLight® Reagent *BacMam 2.0* GFP: 485/520 in nm	Thermofisher (C10582)
FluoroDish Tissue Culture Dish with Cover Glass Bottom of 35 mm and 23 mm and Glass thickness of 0.17 mm	World Precision Instruments, Inc (WPI)

Table 10.4 Cell fixation and immunofluorescence requirements and ingredients

Requirements and ingredients	Manufacturer
Microscope slide, cover slip 22mm	MENZEL-GLÄSER
cover slip with a diameter of 22 mm and thickness of 0.16-0.19 mm, thickness No. :#1.5	VWR
4% Paraformaldehyde (PFA)	Alfa Aesar (ThermoFischer (Kandel) GmbH (43368)
Triton X-100 (0.5%)	SIGMA (93426)
3% Bovine Serum Albumin Fraction V (BSA) (pH 7.0)	PanReacAppliChem (A1391)
Mounting medium with/without DAPI	Fluormount-G™ Invitrogen
Vimentin V9 AlexaFluor®647	Santa cruz (IF,WB) (sc-6260)
Plectin (10F6) Alexa Fluor®647	Santa cruz (WB, IF) (sc-33649)
GAPDH (0411) Alexa Flour 488	Santa cruz (WB, IF) (sc-47724)
Actin, Phalloidin-iFluor 488 reagent,	CytoPainter, Abcam (ab1767536)
Actin Phalloidin-iFlour 594 Reagent	(ab176757, Abcam)
DAPI (diamidino phenylindole)	Invitrogen
Hoechst (nucleus staining)	34580 (Sigma Aldrich, St Louis, MO, USA)

Table 10.5 Gel staining and western blot requirements and ingredients

Requirements and ingredients	Manufacturer
30% acrylamide mix	ROTH
1M Tris (PH8.8)	---
1.5M Tris (PH6.8)	---
10% SDS (SDS Pellets)	(8029.2, Carl Roth)
10% ammonium persulfate (APS)	aMReSCO, 0486-100G
Tetramethylethylenediamine (TEMED)	Sigma, T9281
PageRuler Prestained Protein Ladder	Thermo scientific, 26616
running buffer	---
nitrocellulose blotting membrane (Amersham Protein Permium 0,45um NC)	GE Healthcare Life science (10600048)
Tween20 0.1%	Fluka, 93733
Westen Blotting Filter Paper (8cm*10.5cm sheet)	Thermo Scientific (88600)
Bio-safe Coomassie G-250 Stain	BIO-RAD (161-0786)
PowerPac™ HC	BIO-RAD
WB imaging system	FlourChem Q

electrophoreses chamber	BIO-RAD
transfer system (positive pole, filter paper, membrane, gel, filter paper, negative pole)	BIO-RAD
gel cast with the thickness of 1mm and the glasses size of 7.5*10 cm	BIO-RAD
Shaker	neoLab

Table 10.6 List of the Buffers for western blot

Buffer	**Requirements and ingredients**	**Quantity**
Laemmli buffer	150 mM Tris-Cl/pH6.8	2.250 mL (Tris-Cl pH 6.8 /1.5M)
	300mM DTT (β-mercaptoetanol-15%)	---
	6% SDS	0.9 g
	0.3% Bromophenolblue	0.045 g
	30% Glicerol	4.5 mL
Transfer buffer (Transfer buffer for Plectin: 0.1% SDS and 10% Methanol)	39 mM Glicin	2.9 g
	48 mM Tris	5.8 g
	0.037% SDS (sodium…)	0.37 g
	20% Metanol	200 mL
Tris-buffered saline (TBS) 5X for 1 liter	NaCl	40 g
	KCl	1 g
	Tris, pH 7.4 adjust with HCl	15 g

Table 10.7 Solutions for preparing resolving gels

(for Tris-glycine SDS_Polyacrylamide gel electrophoresis (volumes are in mL))

Components	**Gel volume**							
	5 mL	10 mL	15 mL	20 mL	25 mL	30 mL	40 mL	50 mL
6% gel								
H_2O	2.6	5.3	7.9	10.6	13.2	15.9	21.2	26.5
30% acrylamide mix	1.0	2.0	3.0	4.0	5.0	6.0	8.0	10.0
1 M Tris-HCl (pH 8.8)	1.3	2.5	3.8	5.0	6.3	7.5	10.0	12.5
10% SDS	0.05	0.1	0.15	0.2	0.25	0.3	0.4	0.5
10% ammonium persulfate	0.05	0.1	0.15	0.2	0.25	0.3	0.4	0.5
TEMED	0.004	0.008	0.012	0.016	0.02	0.024	0.032	0.04
8% gel								

H_2O	2.3	4.6	6.9	9.3	11.5	13.9	18.5	23.2
30% Acrylamide mix	1.3	2.7	4.0	5.3	6.7	8.0	10.7	13.3
1 M Tris-HCl (pH 8.8)	1.3	2.5	3.8	5.0	6.3	7.5	10.0	12.5
10% SDS	0.05	0.1	0.15	0.2	0.25	0.3	0.4	0.5
10% ammonium persulfate	0.05	0.1	0.15	0.2	0.25	0.3	0.4	0.5
TEMED	0.003	0.006	0.009	0.012	0.015	0.018	0.024	0.03
10% gel								
H_2O	1.9	4.0	5.9	7.9	9.9	11.9	15.9	19.8
30% acrylamide mix	1.7	3.3	5.0	6.7	8.3	10.0	13.3	16.7
1 M Tris-HCl (pH 8.8)	1.3	2.5	3.8	5.0	6.3	7.5	10.0	12.5
10% SDS	0.05	0.1	0.15	0.2	0.25	0.3	0.4	0.5
10% ammonium persulfate	0.05	0.1	0.15	0.2	0.25	0.3	0.4	0.5
TEMED	0.002	0.004	0.006	0.008	0.01	0.012	0.016	0.02
12% gel								
H_2O	1.6	3.3	4.9	6.6	8.2	9.9	13.2	16.5
30% acrylamide mix	2.0	4.0	6.0	8.0	10.0	12.0	16.0	20.0
1 M Tris-HCl (pH 8.8)	1.3	2.5	3.8	5.0	6.3	7.5	10.0	12.5
10% SDS	0.05	0.1	0.15	0.2	0.25	0.3	0.4	0.5
10% ammonium persulfate	005	0.1	0.15	0.2	0.25	0.3	0.4	0.5
TEMED	0.002	0.004	0.006	0.008	0.01	0.012	0.016	0.02
15% gel								
H_2O	1.1	2.3	3.4	4.6	5.7	6.9	9.2	11.5
30% acrylamide mix	2.5	5.0	7.5	10.0	12.5	15.0	20.0	25.0
1 M Tris-HCl (pH 8.8)	1.3	2.5	3.8	5.0	6.3	7.5	10.0	12.5
10% SDS	0.05	0.1	0.15	0.2	0.25	0.3	0.4	0.5
10% ammonium persulfate	0.05	0.1	0.15	0.2	0.25	0.3	0.4	0.5
TEMED	0.002	0.004	0.006	0.008	0.01	0.012	0.016	0.02

Table 10.8 Solutions for preparing 5% stacking gels

(for Tris-glycine SDS_Polyacrylamide gel electrophoresis (Volumes are in mL))

Components (5% gel)	**Gel volume**							
	1 mL	2 mL	3 mL	4 mL	5 mL	6 mL	8 mL	10 mL
H_2O	0.68	1.4	2.1	2.7	3.4	4.1	5.5	6.8
30% Acrylamide mix	0.17	0.33	0.5	0.67	0.83	1.0	1.3	1.7
1.0*M* Tris-HCl (pH 6.8)	0.13	0.25	0.38	0.5	0.63	0.75	1.0	1.25

10% SDS	0.01	0.02	0.03	0.04	0.05	0.06	0.08	0.1
TEMED	0.001	0.002	0.003	0.004	0.005	0.006	0.008	0.01

Table 10.9 Proper antibodies and their applicable concentration

Requirements and their concentration	**Manufacturer**
Vimentin V9 AlexaFluor®647 (dilution 1:500)	Santa Cruz Biotechnology (sc-6260)
Plectin (10F6) Alexa Fluor®647 (dilution 1:200)	Santa Cruz Biotechnology (sc-33649)
GAPDH (0411) Alexa Flour®488 (dilution 1:500)	Santa Cruz Biotechnology (sc-47724)
Anti-rabbit secondary antibody wavelength 594 nm (dilution 1:1000)	(Abcam, Cambridge, UK)

a)

b)

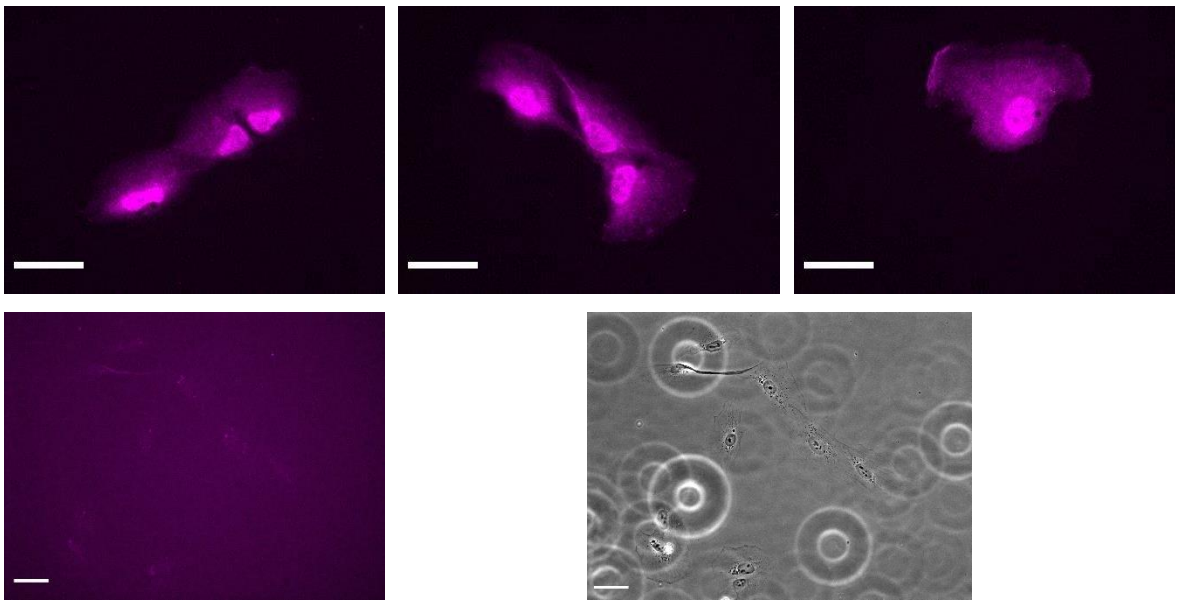

Figure 10.1 Immunofluorescence staining of negative control and plectin depleted cells.

a) Negative control cells. b) Plectin depleted cell. (a) plectin in purple, Scale bar:20 µm. (b) from left to right: plectin in purple, phase contrast image of the cell in grey, Scale bar:40 µm

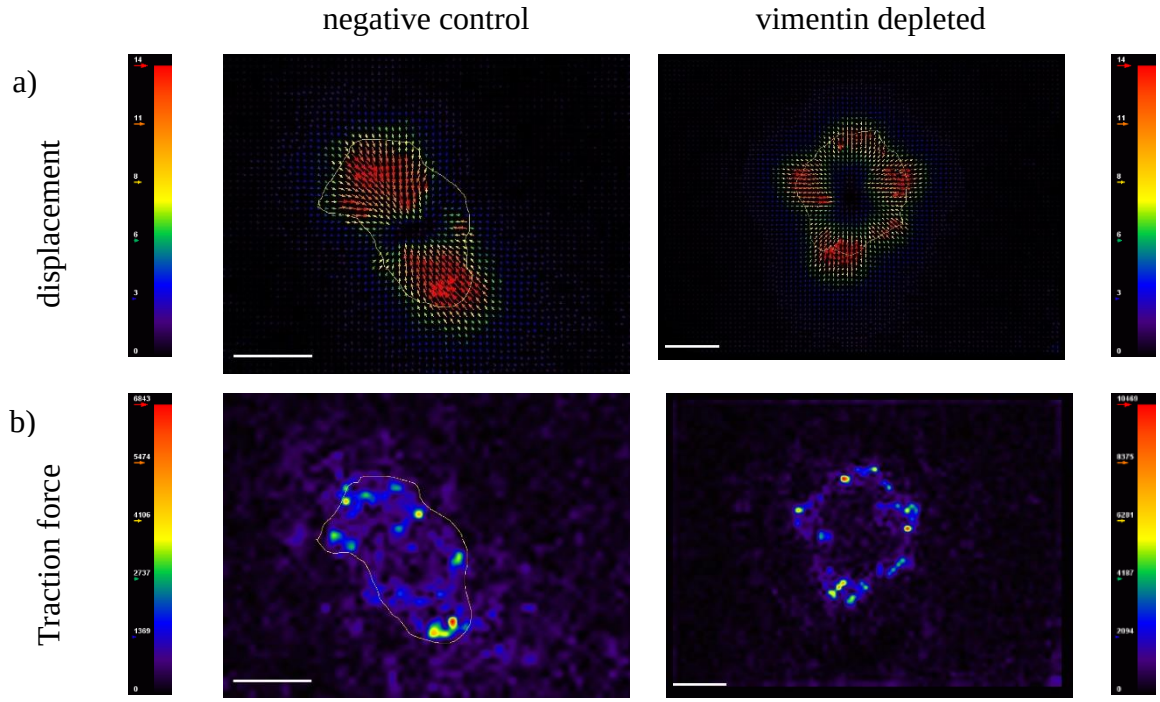

Figure 10.2 Bead displacements and traction forces applied to the surface by negative control cells and vimentin depleted cells.

a) The displacement of the fluorescence beads embedded in the surface under negative control (left) and vimentin KD (right) cells. b) The heating map of traction force magnitudes applied to the surface via the same negative control (left) and vimentin KD (right) cells. The yellow line in each image shows the cell edge (border). The heat map scales in the left side of the negative control and the right side of the vimentin depleted show the minimum (black) to the maximum (red) values for displacement and traction force magnitudes in pixel and Pascal respectively. Scale bars: 20 µm.

11 Protocols

11.1 FRAP measurements

11.1.1 FRAP measurements in stress fibers

Procedures:

1- Under the sterile cell culture hood, open the FluoroDish.

2- Under the sterile cell culture hood aspirate the culture medium from the sample, wash cells with sterile DPBS. Add Trypsin EDTA 25% and incubate the dish for 5 min to detach the cells from the bottom of the six-well plate. Add 1or 2 mL DMEM/F12 and mix it gently, count the cells on a Malassez slide. To avoid cell-cell attachment and avoid too low number of cells for the FRAP measurements, seed 10000 cells in each FluoroDish. Incubate the cells for 4 h in order to let the cells attach and spread on the surface.

3- Considering FRAP measurements in actin SFs, label actin filaments with CellLight Reagents BacMam 2.0 GFP and incubate it for 40 h.

4- 30 min before starting the FRAP experiment turn on the microscope and its incubation system to control the T °C and CO_2 level during the FRAP experiment.

Two confocal microscopes were used during this project to apply FRAP on actin SFs. 1- Confocal spinning disk inverted microscope (Ti-Eclipse, Nikon) 2- Laser scanning microscope (LSM 880, ZEISS). The two tables below present the microscopy setting for LSM and spinning disk accordingly.

Table 11.1 Microscopy setting on spinning disc microscope for actin SFs in adherent cells

Parameters	**Proposed values**
Objective	60x oil immersion objective NA: 1.4
Acquisition wavelength	488 nm
Acquisition intensity	30%
Imaging time interval	1s
Bleaching wavelength	488 nm
Bleaching wavelength intensity	100%
Bleaching time interval	0.17ms
Zoom	1x
Imaging exposure time	400 ms
Pinhole	50 µm
dwell time for acquisition	60 µs
dwell time for bleaching	20 µs
Filters	Turret 2: Beamer Turret1: empty

Table 11.2 Microscopy setting on LSM for actin SFs in adherent cells

Parameters	**Proposed values**
objective	60x oil immersion, 1.4 NA
Acquisition wavelength	488 nm for GFP, 594 nm for mCherry
Acquisition intensity	2%
Bleaching wavelength	405 nm diode laser
Bleaching wavelength intensity	100%
Zoom	5.2
Pixel size	0.2 µm
Number of pixels	128×128
Pixelwise averaging	4×
Pixel dwell time for acquisition	≈ 8µs
Pixel dwell time for bleaching	≈ 20-60µs,
Beam Splitter #1	MBS 488/594
Beam Splitter #2	MBS -405
Beam Splitter #3	Plate
Beam Splitter #4	Rear
Detector Filter	BP 495-550 + LP 570

11.1.2 FRAP measurement in cytoplasm

Table 11.3 Microscopy setting on LSM for actin monomers in cytoplasm

Parameters	Proposed values
objective	60x oil immersion, NA of 1.4
Acquisition wavelength	488 nm for GFP, 594 nm for mCherry
Acquisition intensity for both wavelengths	2%
Bleaching wavelength	405 nm
Bleaching wavelength intensity	100%
Zoom	5.2
Pixel size	≈ 0.27 µm
Number of pixels	128×128
Pixelwise averaging	4×
Pinhole	50
Pixel dwell time for acquisition	≈ 6 µs
Pixel dwell time for bleaching	≈ 2 µs,
Beam Splitter #1	MBS 488/594
Beam Splitter #2	MBS -405
Beam Splitter #3	Plate
Beam Splitter #4	Rear
Detector Filter	BP 495-550 + LP 570

11.1.3 FRAP measurement in cortex in suspended cells

Procedures: (these procedures from 1 to 14 are applicable for sample preparation of the cell size measurement in suspension cells)

1- Cut off a 1cm×1cm of the PF Gel-Film and peel off the protective layers.

2- Place the PF Gel-Film on a folded Parafilm and punch 5 holes with a Harris Uni-Core punch with a diameter of 2.5 mm (figure 4.2) in PF Gel-Film.

3- Take the punched PF Gel-Film and place it in the middle of the FluoroDish tissue/cell culture dish.
4- Put the FluoroDish and coverslip in the plasma cleaner and activate the surface for 2 min to 3 min.
5- Add 10 mL of the PLL-g-PEG solution to each chamber to coat the FlouroDish bottom surface (the function of the PLL-g-PEG is explained in detail in the micro-pattern section). Cover the plate with Parafilm, and incubate it for 1 h at room temperature.
6- Put 50 µL of the PLL-g-PEG on the bottom of a petri dish covered by Parafilm and place the coverslip upside down on PLL-g-PEG.
7- Incubate the FluoroDish and petri dish 1 h at room temperature.
8- Incubate a solution of 3 mL of complete DMEM/F12 and 25 mM of HEPES for 30 min.
9- Aspirate the culture medium from the sample (RPE1vimentin silenced and control cells are actin GFP labeled), wash cells with the sterile DPBS and add Trypsin and incubate it for 5 min to detach the cells from the bottom of the six-well dish.
10- Add 1or 2 mL of complete DMEM/F12 and mix it gently. Transfer suspended cells to a 15 mL falcon tube and centrifuge at 189*g for 3 min.
11- Aspirate the culture medium and add 1 mL of the DMEM/F12 and HEPES solution.
12- Remove Parafilm from the top of the suspension chambers and wash the chambers with sterile DPBS three times.
13- Count the cells on the Malassez slide. Seed 40000 cells/mL to avoid the cell-cell attachment or to low number of cells for the measurements.
14- Wash the coverslip with sterile DPBS and place the PLL-g-PEG covered us side down on top of the chambers.
15- About 30 min before starting the FRAP experiment, turn on the microscope and its heating system to control the T °C and CO_2 level during the FRAP experiment for samples.
16- For FRAP measurements on suspended cells, confocal spinning disk microscope was used.

Table 11.4 Microscopy setting on spinning disc microscope for actin cortex in suspended cells

Parameters	Proposed values
objective	60x oil immersion objective
Acquisition wavelength	488 nm
Acquisition intensity	30%
Imaging time interval	1s
Bleaching wavelength	488 nm
Bleaching wavelength intensity	100%
Bleaching time interval	0.17ms
Zoom	1x
Imaging exposure time	400 ms
Pinhole	50 µm
dwell time for acquisition	60µs
dwell time for bleaching	20µs
Filters	Turret 2: Beamer Turret1: empty

11.1.4 FRAP Data processing

1- Open the FRAP images in Fiji
2- For suspended cells only, correct the cell motion via Plugins/ Registration/ StackReg/ Rigid Body
3- select bleached, reference and background ROI
4- Under *Analyze/ Set Measurements* select Mean gray value.
5- Under *ROI Manager* /*More/ Multi Measure,* measure the mean intensity value of the selected ROIs. (The data will be presented in a table with four columns as a text format: 1-Number of acquired images 2- mean intensity of the bleached region. 3- mean intensity of the Reference region. 4- mean intensity of the Background region.)
6- Import the ROIs intensity values to the OriginLab software.

7- Extract the time from the number of acquired images. The bleaching time is referred as 0 s. The time scale in between two successive images is 1 s or 30 ms for respectively stress fiber recovery and cytoplasm recovery.

8- Calculate the correction factor *Cf:*

$$Cf = (\max (Ref - BG)) / (Ref - BG)$$

Where BG is the background intensity and Ref is the reference intensity.

9- Calculate the corrected bleached intensity named *Correction*:

$$Correction = (Bl - BG) \times Cf$$

Where BG is the background intensity and Bl is the bleached intensity.

10- Normalize the corrected bleached intensity from 0 (bleached intensity at time 0) to 1 (prebleached intensity) with OriginLab under *Analysis/ Mathematics/ Normalize columns/ open dialog/Normalize Methods*:

$$Normalized\ value = (Correction_i - \min Correction) / (Correction_i - \max Correction)$$

Where $Correction_i$ is the correction value at each images *i*.

11- Plot the normalized values over time

12- Fit the curve with the first-order exponential function for SFs and cytoplasm:

$$F(t) = a*(1-\exp(-\omega*t))$$

where *a* signifies the plateau value and ω corresponds to the turnover rate. ($\tau = Ln(2)/\omega$, is the halftime recovery).

Fit the curve with the second-order exponential function for actin fibers in cortex:

$$F(t) = a*(1-\exp(-\omega_1*t))+b*(1-\exp(-\omega_2*t))$$

where *a* and *b* are the mobile fractions of respectively slow and fast components, ω_1 and ω_2 correspond to the recovery times of respectively slow and fast populations. ($\tau_i = Ln(2)/\omega_i$, is the halftime recovery).

11.2 Western blot data analysis

1- Open the images in Fiji. The first column presents the molecular marker with the weights in different colors, the next columns present a specific sample. The bands in each row present the amount of a specific protein in different samples.

2- To measure the amount of specific proteins, under the *analyze* menu select *Set Measurements…* and check in *Grey Mean Value* from the checkboxes. Each row presents the amount of the specific protein.

3- Define a ROI by selecting the rectangle tool and drawing a frame around the largest band on the row.
4- To quantify the gray value of each band with the same frame save the proper frame under *File/Save as/Selection* with the protein name.
5- For each row use the same frame for all the protein bands and measure the gray value under analyze/measure.
6- In a place where there is no band take a background measurement. Measure the gray value of the control in the same way.
7- Save all of the values and export them into OriginLab.
8- Invert the pixel density for all data via:

$$\text{The inverted value (is expressed as)} = 255\text{-}X_i,$$

where X_i is the gray value of each band recorded by Fiji.
9- For protein X calculate inverted protein X and inverted background.
10- Net protein X is defined as an inverted protein X – inverted background.
11- Calculate net loading protein the same as net protein for loading control.
12- The ratio of Net protein X/ Net loading control is the final relative quantification values every specific protein.
13- To compare them in different samples plot them as bar or box plots.

11.3 Real-time quantitative polymerase chain reaction

Protocols are adapted from the original protocols of the kit's companies.
Table 11.5 List of the kits for qPCR

Kit	Manufacturer
PureLink RNA Mini Kit	(ambion by life technologies, 12183020)
Rnase-Free Dnase Set (50) Kit	(Rneasy/QIAamp Columns) QIAGEN Kit, 12183018A
RevertAid First Strand cDNA Synthesis Kit	(Thermo Scientific, K1621)
iTaq Universal SYBR Green Supermix	(Bio-RAD, 172-5121)

11.3.1 Sequence of the Plectin Primers

Table 11.6 List of the primers for plectin qPCR

Based on mRNA sequence for plectin 1b, forward and reverse primers were ordered by two different companies. Later depends on the obtained results, the experiments were continued with BLAST primers.

Primer	Sequence (5'->3')	Length	Start	Tm
Plectin Forward primer (BLAST)	CAC CAA GTG GGT CAA CAA GC	20	239	59.61
Plectin Reverse primer (BLAST)	CCA GCA GGG AGA TGA GGT TG	20	336	60.11
Plectin LEFT PRIMER (Primer-3)	GAT CAC CAT CTC CTC CTC GG	20	12635	59.03
Plectin RIGHT PRIMER (Primer-3)	CGA TGA GGT TCT TGG CGA TG	20	12738	59.07
GAPDH forward primer	CAA ATT CCA TGG CAC CGT CA	20	-	-
GAPDH reverse primer	TGA AGA CGC CAG TGG ACT C	19	-	-

11.3.2 RNA purification

Table 11.7 PureLink RNA Mini Kit

(ambion by life technologies, 12183018A)

Components	Quantity
Lysis Buffer	125 mL
Wash Buffer I	50 mL
Wash Buffer II	15 mL
RNase-Free Water	15.5 mL
Spin Cartridges (with collection tubes)	50
Collection Tubes	50
Recovery Tubes	50

11.3.2.1 Lysis and Homogenization[12]:

1- Transfer cells 1×10^6 to 5×10^6 to a 15-mL tube and add 0.6 mL Lysis Buffer with 2-mercaptoethanol
2- Vortex until the cell pellet is dispersed and the cells appear lysed.
3- Homogenize at room temperature with a rotor-stator homogenizer

11.3.2.2 RNA Purification [13] (Binding, Washing, and Elution of RNA)

1- Add one volume 70% ethanol to each volume of cell homogenate. (first round 700ul) (second round 100% and 30-100ul depends on step 12)
2- Vortex to mix thoroughly and to disperse any visible precipitate that may form after adding ethanol.
3- Transfer up to 700 µL of the sample (including any remaining precipitate) to the spin cartridge (with the collection tube).
4- Centrifuge at 12,000 × g for 30 seconds at room temperature. Discard the flow through and reinsert the spin cartridge into the same collection tube.
5- Repeat steps 3–4 until the entire sample has been processed.
6- Add 700 µL Wash Buffer I to the spin cartridge.
7- Centrifuge at 12,000 × g for 30 seconds at room temperature. Discard the flow-through and the collection tube. Place the spin cartridge into a new collection tube.
8- Add 500 µL Wash Buffer II with ethanol to the spin cartridge.
9- Centrifuge at 12,000 × g for 15 seconds at room temperature. Discard the flow-through.
10- Repeat Steps 8–9 once.
11- Centrifuge the spin cartridge at 12,000 × g for 1–2 min to dry the membrane with bound RNA. Discard the collection tube and insert the spin cartridge into a recovery tube.
12- Add 30–100 µL RNase–free water to the center of the spin cartridge.
13- Incubate at room temperature for 1 min.

---

[12] **Adapted from the original protocols of the kit's companies.**

[13] **Adapted from the original protocols of the kit's companies.**

14- Centrifuge the spin cartridge for 2 min at ≥12,000 × g at room temperature to elute the RNA from the membrane into the recovery tube. Note: If the expected RNA yield is >100 µg, perform 3 sequential elution of 100 µL each. Collect the eluates in a single tube.
15- Store your purified RNA or proceed to downstream application. (Store the purified RNA on ice for immediate use. For long–term storage, keep the purified RNA at –80°C.)
16- Determine the quality and quantity of your RNA by UV absorbance at 260 nm.

After the first round purification proceed to Rnase-Free Dnase Set (50) Kit (10.6.2).

After the second round purification proceed to RevertAid First Strand cDNA Synthesis Kit (Thermo Scientific) (10.6.3).

11.3.3 DNase Digestion of RNA before RNA Cleanup[14]

Rnase-Free Dnase Set (50) Kit (Rneasy/QIAamp Columns) QIAGEN Kit is used. It contains:

RNA solution (contaminated with genomic DNA)
Buffer RDD
DNase I stock solution

1- Mix the following in a micro centrifuge tube:
   _ ≤87.5 µl RNA solution (contaminated with genomic DNA)
   _ 10 µl Buffer RDD
   _ 2.5 µl DNase I stock solution
   Make the volume up to 100 µl with RNase-free water.
   The reaction volumes can be doubled if necessary (to 200 µl final volume).
2- Incubate on the benchtop (20 °C –25 °C) for 10 min.
3- Clean up the RNA according to "Protocol RNA Purification (PureLink RNA Mini Kit).

11.3.4 First Strand cDNA Synthesis[15]

Table 11.8 RevertAid First Strand cDNA Synthesis Kit
(Thermo Scientific, 1621)

[14] **Adapted from the original protocols of the kit's companies.**
[15] **Adapted from the original protocols of the kit's companies.**

Components	Quantity
RevertAid RT (200 U/µL)	25 µL
RiboLock RNase Inhibitor (20 U/µL)	25 µL
5X Reaction Buffer 250 mM Tris-HCl (pH 8.3) 250 mM KCl, 20 mM MgCl2 50 mM DTT	150 µL
10 mM dNTP Mix	50 µL
Oligo(dT)18 Primer,100 µM	25 µL
Random Hexamer Primer,100 µM	25 µL
Forward GAPDH Primer,10 µM	20 µL
Reverse GAPDH Primer,10 µM	20 µL
Control GAPDH RNA, 0.05 µg/µL	20 µL
Water, nuclease-free	2 × 1.25 mL

1- After thawing, mix and briefly centrifuge the components of the kit. Store on ice.

2- Add the following reagents into a sterile, nuclease free tube on ice in the indicated order:

Template RNA	Total RNA	0.1 ng - 5 µg **(11 µL)**
Primer	Oligo (dT)18 primer (1 µL) **or** Random Hexamer primer	(1 µL)
	gene-specific primer	15-20 pmol
Water, nuclease-free	to 12 µL	
Total volume	12 µL	

3- Add the following components in the indicated order:

5X Reaction Buffer	4 µL
RiboLock RNase Inhibitor (20U/µL)	1 µL
10 mM dNTP Mix	2 µL
RevertAid M-MuLV RT (200 U/µL)	1 µL
Total volume	20 µL

4- Mix gently and centrifuge briefly.

5- For oligo(dT)18 or gene-specific primed cDNA synthesis, incubate for 60 min at 42 °C.

For random hexamer primed synthesis, incubate for 5 min at 25 °C followed by 60 min at 42 °C.

6- Terminate the reaction by heating at 70 °C for 5 min.

The reverse transcription reaction product can be directly used in PCR applications or stored at -20 °C for less than one week. For longer storage, -80 °C is recommended

11.3.5 qPCR Reaction Mix Preparation and Thermal Cycling[16]

iTaq Universal SYBR Green Supermix (Bio-RAD, 172-5121) is used.

1- Thaw iTaq Universal SYBR® Green Supermix and other frozen reaction components to room temperature. Mix thoroughly, centrifuge briefly to collect solutions at the bottom of tubes, then store on ice protected from light.

2- Prepare (on ice or at room temperature) enough reaction mix for all qPCR reactions by adding all required components, except the DNA template, according to the recommendations in table below. The primer concentration and cDNA concentration should be in a same range.)

Component	**Volume/20 µL reaction**	**Final concentration**
iTaq SYBR Green Supermix (2X)	10	1x
Forward and reverse primers	Variable	300-500nM each primer
DNA template	Variable	cDNA: 100ng-100fg
Nuclease-free water	To 20 µL	-
Total reaction mix volume	20 µL	-

3- Mix the reaction mix thoroughly to ensure homogeneity and dispense equal aliquots into each qPCR tube or into the wells of a qPCR plate. Good pipetting practice must be employed to ensure assay precision and accuracy.

4- Add DNA samples (and nuclease-free H2O if needed) to the PCR tubes or wells containing reaction mix (Table 1 (above)), seal tubes or wells with flat caps or optically transparent film. Spin the tubes or plate to remove any air bubbles and collect the reaction mixture in the vessel bottom.

5- Program the thermal cycling protocol on a real-time PCR instrument according to Table below (as an image in the figure file).

6- Load the PCR tubes or plate into the real-time PCR instrument and start the PCR run.

7- Perform data analysis according to the instrument-specific instructions.

[16] **Adapted from the original protocols of the kit's companies.**

Table 11.9 Threshold cycle values with the primer concentration of 1 µM

Threshold cycles measured for two different plectin primer sequences and GAPDH primer. The abbreviations presented in the table are listed here: A≡RandomHexamo, B≡Oligo dT from First Strand cDNA Synthesis kit (Table 11.8), Plectin1≡ Plectin Primer BLAST, Plectin2≡ Plectin Primer-3 in the list of the primers (Table 11.6), 1≡216.3 ng/µL and 2≡ 61.5 ng/µL cDNA concentrations purified from two different experiments, NTC≡ no template control, Ct is the amount of threshold.

Content	GAPDH	GAPDH	Plectin1	Plectin1	Plectin2	Plectin2	NTC-13	NTC-14	NTC-15
Sample	1A	2A	1A	2A	1A	2A	GAPDH	Plectin1	Plectin2
Ct	21.32	19.10	24.21	22.83	29.46	28.94			
Content	GAPDH	GAPDH	Plectin1	Plectin1	Plectin2	Plectin2	NTC-13	NTC-14	NTC-15
Sample	1A	2A	1A	2A	1A	2A	GAPDH	Plectin1	Plectin2
Ct	20.31	19.31	23.37	23.13	29.08	28.11			39.06
Content	GAPDH	GAPDH	Plectin1	Plectin1	Plectin2	Plectin2			
Sample	1A	2A	1A	2A	1A	2A			
Ct	20.14	19.20	23.27	22.89	29.23	27.84			
Content	GAPDH	GAPDH	Plectin1	Plectin1	Plectin2	Plectin2		1µM primer concentration	
Sample	1B	2B	1B	2B	1B	2B		1≡216.3 ng/µL cDNA	
Ct	21.66	20.93	29.25	27.10	32.30	28.89		2≡ 61.5 ng/µL cDNA	
Content	GAPDH	GAPDH	Plectin1	Plectin1	Plectin2	Plectin2		A≡RandomHexamo	
Sample	1B	2B	1B	2B	1B	2B		B≡Oligo dT	
Ct	21.67	20.59	29.04	27.05	31.31	33.04			
Content	GAPDH	GAPDH	Plectin1	Plectin1	Plectin2	Plectin2		Plectin1≡ Plectin Primer BLAST	
Sample	1B	2B	1B	2B	1B	2B		Plectin2≡ Plectin Primer-3	
Ct	21,51	20,91	29,34	27,26	31,25	29,11			

Table 11.10 Threshold cycle values with the primer concentration of 5 µM

Threshold cycles measured for two different plectin primer sequences and GAPDH primer. The abbreviations presented in the table are listed here: A≡RandomHexamo, B≡Oligo dT from First Strand cDNA Synthesis kit (Table 11.8), Plectin1≡ Plectin Primer BLAST, Plectin2≡ Plectin Primer-3 in the list of the primers (Table 11.6), 1≡216.3 ng/µL and 2≡ 61.5 ng/µL cDNA concentrations purified from two different experiments, NTC≡ no template control, Ct is the amount of threshold.

Content	GAPDH	GAPDH	Plectin1	Plectin1	Plectin2	Plectin2	NTC-13	NTC-14	NTC-15
Sample	1A	2A	1A	2A	1A	2A	GAPDH	Plectin1	Plectin2
Ct	18.83	17.61	23.94	23.00	24.49	23.36	33.26	32.87	38.03
Content	GAPDH	GAPDH	Plectin1	Plectin1	Plectin2	Plectin2	NTC-13	NTC-14	NTC-15
Sample	1A	2A	1A	2A	1A	2A	GAPDH	Plectin1	Plectin2
Ct	19.33	17.98	24.03	22.74	24.45	23.41	33.04	32.50	36.92
Content	GAPDH	GAPDH	Plectin1	Plectin1	Plectin2	Plectin2			
Sample	1A	2A	1A	2A	1A	2A			
Ct	19.05	17.65	23.81	22.48	24.40	23.19			
Content	GAPDH	GAPDH	Plectin1	Plectin1	Plectin2	Plectin2		5uM primer concentration	
Sample	1B	2B	1B	2B	1B	2B		1≡216.3ng/µL cDNA	
Ct	19.08	18.99	28.49	26.81	24.94	23.91		2≡ 61.5ng/µL cDNA	
Content	GAPDH	GAPDH	Plectin1	Plectin1	Plectin2	Plectin2		A≡RandomHexamo	
Sample	1B	2B	1B	2B	1B	2B		B≡Oligo dT	
Ct	19.05	18.98	28.15	26.82	25.06	23.74			
Content	GAPDH	GAPDH	Plectin1	Plectin1	Plectin2	Plectin2		Plectin1≡ Plectin Primer BLAST	
Sample	1B	2B	1B	2B	1B	2B		Plectin2≡ Plectin Primer-3	
Ct	19.47	18.90	28.50	26.75	25.45	23.80			

Table 11.11 Threshold cycle values with the primer concentration of 2µM

Threshold cycles measured for two different plectin primer sequences and GAPDH primer. The abbreviations presented in the table are listed here: A≡RandomHexamo, from First Strand cDNA Synthesis kit (Table 11.8), Plectin1≡ Plectin Primer BLAST, Plectin2≡ Plectin Primer-3 in the list of the primers (Table 11.6), 1≡216.3 ng/µL and 2≡ 61.5 ng/µL cDNA concentrations purified from two different experiments, NTC≡ no template control, FW ≡ forward primer, RE≡ reverse primer, LE≡ left primer, RI≡ right primer, Ct is the amount of threshold.

Content	GAPDH	GAPDH	Plectin1	Plectin1	Plectin2	Plectin2	GAPDH(NTC)	Plectin1(NTC)	Plectin2(NTC)
Sample	1A	2A	1A	2A	1A	2A		FW	LE
Ct	20.09	17.08	24.56	22.10	28.02	25.08	39.19		
Content	GAPDH	GAPDH	Plectin1	Plectin1	Plectin2	Plectin2	GAPDH(NTC)	Plectin1(NTC)	Plectin2(NTC)
Sample	1A	2A	1A	2A	1A	2A		RE	RI
Ct	20.13	17.20	24.76	22.37	28.29	24.94			
Content	GAPDH	GAPDH	Plectin1	Plectin1	Plectin2	Plectin2			
Sample	1A	2A	1A	2A	1A	2A			
Ct	20.10	17.10	24.32	22.03	28.26	24.68			
Content	GAPDH	GAPDH	Plectin1	Plectin1	Plectin2	Plectin2		2 µM Primer concentration	
Sample	1B	2B	1B	2B	1B	2B		1≡216.3 ng/µL cDNA	
Ct	21.26	18.01	28.31	26.11	28.46	25.72		2≡ 61.5 ng/µL cDNA	
Content	GAPDH	GAPDH	Plectin1	Plectin1	Plectin2	Plectin2		A≡RandomHexamo	
Sample	1B	2B	1B	2B	1B	2B		B≡Oligo dT	
Ct	19.43	18.08	28.52	25.97	28.22	25.18		Plectin1≡ Plectin Primer BLAST	
Content	GAPDH	GAPDH	Plectin1	Plectin1	Plectin2	Plectin2		Plectin2≡ Plectin Primer- 3	
Sample	1B	2B	1B	2B	1B	2B			
Ct	19.29	18.12	29.16	26.26	28.23	26.98			

Table 11.12 Threshold cycle values with the BLAST plectin primer concentration of 2µM

Threshold cycles measured for BLAST plectin primer sequences and GAPDH primer in plectin depleted and control cells, cDNA concentrations = 6.6 ng/µL. WT≡ wild type, Si≡ plectin silenced, nCtrl≡ negative control, NTC≡ no template control, Ct is the amount of threshold.

Content	GAPDH	GAPDH	GAPDH	Plectin	Plectin	Plectin	NTC	NTC
Sample	WT	nCtrl	Si	WT	nCtrl	Si	GAPDH	Plectin
Ct		17.05	18.14	24.07	21.43	25.22	39.10	38.50
Content	GAPDH	GAPDH	GAPDH	Plectin	Plectin	Plectin	NTC	NTC
Sample	WT	nCtrl	Si	WT	nCtrl	Si	GAPDH	Plectin
Ct	19.03	17.13	34.59	24.29	31.32	25.65		38.52
Content	GAPDH	GAPDH	GAPDH	Plectin	Plectin	Plectin	NTC	NTC
Sample	WT	nCtrl	Si	WT	nCtrl	Si	GAPDH	Plectin
Ct	18.85	17.01	21.43	39.26	30.95	25.61	37.73	38.04

Table 11.13 Threshold cycle values with BLAST plectin primer concentration of 2µM

Threshold cycles measured for BLAST plectin primer sequences and GAPDH primer in plectin depleted and control cells, cDNA concentrations = 6.6 ng/µL. WT≡ wild type, Si≡ plectin silenced, nCtrl≡ negative control, NTC≡ no template control, Ct is the amount of threshold.

Content	GAPDH	GAPDH	GAPDH	Plectin	Plectin	Plectin	NTC-7	NTC-8
Sample	WT	nCtrl	Si	WT	nCtrl	Si	GAPDH	Plectin
Ct	19.06		29.10	24.78		24.80	37.88	38.50
Content	GAPDH	GAPDH	GAPDH	Plectin	Plectin	Plectin	NTC-7	NTC-8
Sample	WT	nCtrl	Si	WT	nCtrl	Si	GAPDH	Plectin
Ct	19.39		29.17	39.09	25.14			
Content	GAPDH	GAPDH	GAPDH	Plectin	Plectin	Plectin	NTC-7	NTC-8
Sample	WT	nCtrl	Si	WT	nCtrl	Si	GAPDH	Plectin
Ct	19.43	17.05	38.44	34.39	30.00	26.02		

11.4 Traction force

Table 11.14 Chemical requirements and warnings

Chemical	Warnings when use
Acrylamide (AAm)	Warm up aliquot at RT for 0.5 h-1 h. Refill the Ar (better) or N_2 after using its solution. Storage temperature: 4 °C.
N,N'-methylene-bis-acrylamide (bis-AAm)	Warm up aliquot at RT for 0.5-1h, Refill the Ar (better) or N_2 after using its solution. Storage temperature: 4 °C.
acrylic acid (AA)	Warm up aliquot at RT for 0.5-1 h, Refill the Argon (better) or N_2 after using. Storage temperature: 4 °C.
ammonium persulfate (APS)	Warm up stocking reagent at RT for 1h, always use the very fresh solution. Storage temperature: 4 °C.
Tetramethylethylnediamine (TEMED)	Warm up aliquot at RT for 0.5-1h, Refill the Argon (better) or N_2 after using. Storage temperature: 4 °C.
3-acryloxypropyl-trimethoxysilane	Refill the Ar (better) or N_2 after using. Store it at room temperature.
Sigmacote	Warm up aliquot at RT for 0.5-1h, Refill the Argon (better) or N_2 after using. Keep away from water, reuse your aliquot (3-5 times) (Check to make sure no water went inside before use). Storage temperature: 4 °C.
MES buffer (0.1M, +0.5M NaCl)	Check pH to make sure it is always around 4-5. Storage temperature 4 °C.
Dimethylaminopropyl-3-ethylcarbodiimide hydrochloride (EDC)	Warm up aliquot at RT for 0.5-1h, make sure no aggregates inside. Storage temperature -20 °C.

N-Hydroxysuccinimide (NHS)	Keep dry. Store it at room temperature.
RGDFK (0.5 mg in 1 mL PBS)	Make sure your reacting solution has a pH around 7.5-8.5
fluorescent beads of 200 nm in diameter	Thermofisher G200, fluorescence wavelength of 488 nm
coverslip 13 mm in diameter	VWR (631-0150)

Procedure:

11.4.1 Acryl-sinalize

1- Prepare the silane solution [0.5% (or 1%) 3-acryloxypropyl-trimethoxysilane in ethanol (95%)/ water (4%)] and add 500 µL of the solution on the bottom of the wells in a six-well plate and incubate it at room temperature overnight.

Table 11.15 The value of the gel solution components

The precise value of the gel solution components and the correlated Young´s modulus.

AAm (mg)	bis-AAm (mg)	AA (µL)	bis-AAm/AAm ratio (%)	Young's modulus E (kPa)
300	2	30	0.67	1-2.0
600	2.5	30	0.42	5.2
600	5.5	30	0.92	11.6
600	10	30	1.67	18.9
600	17.5	30	2.92	31.4
600	21	30	3.50	38.0
600	25	30	4.17	50.0

11.4.2 PAAm gel solution

2- a PAAm gel solution containing 600 mg acrylamide diluted in 5 mL PBS, 30 µL acrylic acid, and 5.5 mg N, N'-methylene-bis-acrylamide will have a Young`s modulus of kPa. The solution can be stored at 4 °C for several weeks.

3- Use NaOH to adjust the gel solution pH to 7.5-8.

11.4.3 PAAm gel preparation

4- Rinse the acryl-silanized dish three times with ethanol (99.9%) and let it dry at room temperature.

5- Degas the gel solution with nitrogen flow for 2 min and take 200 µL of the solution in an eppendorf tube. Add 0.25 µL of fluorescence polystyrene beads, APS (10% solution, 1:100 volume ratio) and TEMED (1:1000 volume ratio) to the gel solution and vortex it for 10 seconds.

6- Pipet 8 µL droplets of gel solution onto the acryl-silanized six-well glass-bottom plate and cover it with the coverslip to obtain a 70-80 µm thick hydrogel.

7- Let the gel to polymerize at room temperature for 10 min.

8- Add PBS into the wells after the gel polymerization and incubate the plate at room temperature for at least 30 min and remove the coverslip without damaging the gel.

11.4.4 Hydrogel activation and functionalization

9- Activate the hydrogel with a solution of 39 mg Dimethylaminopropyl-3-ethylcarbodiimide hydrochloride (EDC) and 12 mg N-Hydroxysuccinimide (NHS) in 1 mL MES buffer for 15 min at room temperature.

10- Functionalize PAAm gel with RGDFK (0.5mg in 1 mL PBS) at room temperature for a whole night.

11- Transfer the six-well plate containing the hydrogel under the sterile cell culture hood.

12- Wash Hydrogels twice with PBS and seed 10000 cells/well on top of the hydrogel. Incubate it overnight.

11.4.5 TFM microscopy setting

1- Transfer the six-well plate containing gels and cells into the epifluorescence inverted microscope (Nikon) connected to an Oko-lab incubation chamber adjusted to 37^{o} C and 5% CO2. (Turn on the microscope and its incubation system 30 min before starting the experiment.)

2- A 60x oil immersion objective with a numerical aperture (NA) of 1.4 and laser in 488nm wavelength is used to acquire fluorescent bead images.

3- Acquire the image of the fluorescent beads in a ROI containing a single cell.

4- Save the images of the cells and under stressed fluorescent beads (deformation image).

5- Save all the conditions.
6- Detach the cells with trypsin EDTA (0.25%) from the gel substrate without moving the plate.
7- The same conditions and the same frames are accessible to acquire the relaxed fluorescence beads images (reference image).
8- Save the images of the relaxed fluorescence beads.

11.4.6 Image processing

1- Import images in Fiji to analyze them. The analyzing process was performed in three steps:
2- Register deformation image (acquired with the cells on top of the gel) and reference image (acquired after removing the cell) under *Plugins/ Registration/ Descriptor-based registration (2d/3d).*The registration will align the deformation image to the reference image in order to correct the experimental shift.
3- Calculate the beads displacement in deformation image under *Plugin/ PIV/iterative PIV (cross correlation)/ ok.* At the end of the PIV run, normalize the data by selecting the normalized median test and replace invalid by median, then save the data. In addition, PIV plugin can also provide a plot of the displacements for visualizing.
4- Use the FTTC plugin under *Plugin/ FTTC* and fill the required parameters relevant to the hydrogel properties to reconstruct the force field. It will ask the displacement data acquired in the previous step. Plot FTTC under *Plugin/plot FTTC* to visualize the forces and save it in the same folder. A text file with 5 columns arranged as following will be the output to calculate the traction force absolute value:

x coordinate of the data (in pixel)	y coordinate of the data (in pixel)	x component of the traction force (in Pascal)	y component of the traction force (in Pascal)	force magnitude

The PIV (particle Image Velocimetry) and FTTC (Fourier Transform Traction cytometry) plugins have been downloaded from: **https://sites.google.com/site/qingzongtseng/tfm**.
In the last step, import the output in OriginLab to compute the entire traction force by summing all the force magnitude.